THESIS FOR THE DEGREE OF DOCTOR OF PHILOSOPHY

Electronic paper in color by electrochromic materials and plasmonics

OLIVER OLSSON

Department of Chemistry and Chemical Engineering

CHALMERS UNIVERSITY OF TECHNOLOGY

Gothenburg, Sweden 2023

Electronic paper in color by electrochromic materials and plasmonics
OLIVER OLSSON
ISBN: 978-91-7905-859-3

Doktorsavhandling vid Chalmers Tekniska Högskola
Ny series nr 5325
ISSN 0346-718XX

Department of Chemistry and Chemical Engineering
Chalmers University of Technology
SE-412 96 Gothenburg
Sweden
Telephone + 46 (0)31-772 1000

Cover Image: A vague plan of how to, step-wise, go from an electrochromic material to a graphical display. The first of the two middle steps are to pairing the electrochromic material on a working electrode with a suitable counter electrode. The second is to utilize a gel/solid electrolyte thus making it an electrochromic device. The last step is to make a passive/active matrix.

Printed by Chalmers Digitaltryck

Gothenburg, Sweden, 2023

Electronic paper in color by electrochromic materials and plasmonics

Oliver Olsson
Department of Chemistry and Chemical Engineering
Chalmers University of Technology

Abstract

The most common display today is emissive. It produces its own light and emits it to the viewer's eye. A reflective display, also known as electronic paper, uses ambient light and reflects it to the viewer, just like a newspaper. Electronic paper has some advantages over emissive displays such as: lower power consumption and readability in sunlight. Today, electronic papers in color lack a desirable color gamut - the colors look bad. The purpose of this thesis is to investigate how structural colors, plasmonics and electrochromics can be used to increase the optical performance of electronic paper in color.

By using structural colors (metal-insulator-metal) and plasmonics, we could create highly reflective color pixels. The pixels could be made to turn ON and OFF using electrochromic materials. In this thesis, conjugated polymers (PProDOT-Me_2 and PProDOP) or tungsten oxide were employed. The reflection difference between the ON and OFF states was 60%. This was better than previously reported values for other electrochromic materials.

If the electrochromic material instead was incorporated into the nanostructure (metal-electrochromics-metal), applying a voltage would then alter the color of the pixel. If tungsten oxide was used inside the structure, the color of one pixel could change, but it would not be able to span the whole visible spectra. If, instead, the conjugated polymer (PT34bT) was used inside the structure, the whole visible spectra could be accessed with one pixel.

To create a real display, it is not enough to have one pixel that can change color. Millions of pixels in a grid are necessary. This poses a problem since each pixel needs to be individually contacted. This can be overcome by using a matrix configuration such as a passive matrix (PM) or an active matrix (AM). This thesis investigates both these configurations. PM requires the color change to be strongly non-linear with the applied voltage. It must have memory such as hysteresis. This effect can be incorporated by utilizing an indium-tin-oxide electrode as a counter electrode to a metal working electrode coated with a conjugated polymer as electrochromic material. To avoid crosstalk between pixels, a photo patterned electrolyte was used.

Commercial thin-film transistor arrays were used for AM configuration. The red, green, and blue nanostructures were deposited on the array. The conjugated polymer PProDOT-Me_2 is synthesized directly on individual pixels and switched without crosstalk.

Keywords: reflective display, conjugated polymers, PProDOT-Me_2, plasmonic electronic paper, electrochromism, structural color, plasmonic

List of papers included

I. **High-contrast switching of plasmonic structural colors: inorganic versus organic electrochromism.**
Marika Gugole*, Oliver Olsson*, Kunli Xiong, Jolie C. Blake, José Montero Amenedo, Ilknur Bayrak Pehlivan, Gunnar A. Niklasson, and Andreas Dahlin
ACS Photonics 2020 *7,* 7, 1762-1772
*Contributed equally as first authors

II. **Enhanced electrochromic switching contrast in the blue by 3,4-propylenedioxypyrrole - implementation on structural colors.**
Oliver Olsson, Marika Gugole, Andreas Dahlin.*
Nanophotonics, 2023

III. **Dynamically tuneable reflective structural colouration with electroactive conducting polymer nanocavities.**
Stefano Rossi, Oliver Olsson, Shangzhi Chen, Ravi Shanker, Debashree Banerjee, Andreas Dahlin, and Magnus P. Jonsson*
Advanced Materials 2021, 33 (49), 2105004.

IV. **Comparison of electrodeposited and sputtered tungsten trioxide films for inorganic electrochromic nanostructures.**
Marika Gugole, Oliver Olsson, Vandna K. Gupta, Romain Bordes, Elisabet Ahlberg, Anna Martinelli, and Andreas Dahlin*
ACS Appl. Opt. Mater. 2023, 1, 2, 558–568

V. **Electrochromic Passive Matrix Display Utilizing Diode-Like Redox Reactions on Indium-Tin-Oxide**
Oliver Olsson, Marika Gugole, Jolie C. Blake, Ioannis Petsagkourakis, Peter Andersson Ersman, Andreas Dahlin.*
Manuscript

VI. **Electronic paper by plasmonic electrochromic active matrix**
Oliver Olsson*, Marika Gugole, Jolie C. Blake, Maxim Chukharkin, and Andreas Dahlin.
Manuscript

Contribution to the listed papers

I. Shared first author. Developed methodology for deposition and analysis of organic materials. Conducted all experiments of the organic materials. Contributed to the writing of the manuscript, particularly the sections regarding the polymers.

II. First author. Planned and performed all experiments except fabrication of metasurfaces. Contributed to the writing of the manuscript, particularly the experimental section.

III. Second author. Started the work with the polymer. Purified the monomer and identified which electrolyte would work best for the scope. Traveled to teach the first author how to perform the polymer deposition and testing. I did SPR experiment and analysis and the EQCMD experiments. Contributed to the writing of the manuscript, particularly the sections regarding the polymer.

IV. Initiated the work with electrodeposited tungsten oxide. Taught the first author how to perform the deposition. The first author later developed the deposition recipe. Collected the CVs, EIS-spectra and the lifetime test. Did all work regarding tungsten oxide deposited with sol-gel. Collected FTIR together with the first author. Contributed to the writing of the manuscript.

V. Came up with the idea and developed the hypothesis. Performed all experiments and device fabrication. Wrote the first drafts of the manuscript.

VI. I did all experiments except metasurface deposition and wire bonding. Wrote the full manuscript.

List of papers not included

Video-rate switching of high-reflectivity hybrid cavities spanning all primary colors
Kunli Xiong *, Oliver Olsson, Stefano Rossi, Magnus P. Jonsson, Jeremy J. Baumberg and Andreas Dahlin
Submitted

Stable Trapping of Multiple Proteins at Physiological Conditions Using Nanoscale Chambers with Macromolecular Gates
Justas Svirelis, Zeynep Adali, Gustav Emilsson, John Andersson, Jesper Medin, Radhika Vattikunta, Krzysztof Koloman, Oliver Olsson, Yusuke Sakiyama, Roderick Lim, and Andreas Dahlin*
Submitted

Video Speed Switching of Plasmonic Structural Colors with High Contrast and Superior Lifetime
Kunli Xiong, Oliver Olsson, Justas Svirelis, Chonnipa Palasingh, Jeremy J. Baumberg and Andreas Dahlin
Adv. Mater. **2021**, 2103217

Electrochromic Inorganic Nanostructures with High Chromaticity and Superior Brightness
Marika Gugole, Oliver Olsson, Stefano Rossi, Magnus P. Jonsson, and Andreas Dahlin*
Nano Letters ***2021*** *21 (10), 4343-4350*

All-Printed Multilayers and Blends of Poly(dioxythiophene) Derivatives Patterned into Flexible Electrochromic Displays
Robert Brooke, Ioannis Petsagkourakis, Subimal Majee, Oliver Olsson, Andreas Dahlin, and Peter Andersson Ersman*
Macromol. Mater. Eng. **2023**, 308, 2200453.

Switchable Plasmonic Metasurfaces with High Chromaticity Containing Only Abundant Metals
Kunli Xiong, Daniel Tordera, Gustav Emilsson, Oliver Olsson, Ulrika Linderhed, Magnus P. Jonsson, and Andreas B. Dahlin
Nano Lett. **2017**, 17, 11, 7033–7039

Contents

1 Introduction

My elevator pitch when I am describing what we are working on is: Have you seen Harry Potter? The answer is usually: -Yes. -You know how they have newspapers with moving images? -Yes! -That is what we are working on, but in color.

Every day we use screens to read our emails or watch funny videos. Technological advancement has been very rapid. I remember when flat TVs were introduced, which by today's standards are pretty thick. Before that, TVs were really thick, so thick they required 2 people to move one upstairs to the bedroom when a more recent version was installed downstair in the living room. The thickness wasn't the only dimension that changed. While the screen was getting wider on some devices, it was also getting smaller on other. So small that it would fit in your pocket.

Advancements have not been uniformly distributed across all kinds of screens. One screen has received less attention: the reflective screen. Unless you have actively searched for one, you are probably not carrying around one of those in your pocket. Or, if you have an old calculator that can display black and white - or more towards black and dark green - then you have one.

As the name suggests, a reflective screen reflects ambient light instead of emitting it. In the same way, a newspaper reflects light. This screen also comes by the name of *electronic paper*. There are many advantages to electronic paper over ordinary *emissive screens*. One aspect that is easy to point out is power consumption. If utilizing ambient light, from the sun, or from incandescent lights, no further energy is required to produce the light This has an advantage, not only for our environmentally conscious, energy-saving society, but also for the individual who doesn't continuously have to plug in his, or her, device to recharge it [1].

Less critical for some, but more relevant for others is how the screen is perceived. Some people prefer to read print such as a physical newspaper over reading on a bright tablet or computer. However, they might be a dying breed with the upcoming generation getting more exposed to emissive screens from an early age. Still, there is some research that points toward the benefits of reading print, and electronic papers, instead of reading on a tablet. Adjacent to this is visibility in the sunlight. A tablet on a beach in Greece is something that can be seen pretty frequently, although you usually just see the reflection of the sun – the glare. To be able to watch an image of the screen, the brightness must be high enough to overcome the glare from the sun. Imagine, instead, if you could use the sun's glare [2].

There is not a lack of desire for electronic paper. There are commercial products on the market as this is written. I think most of us should have known by now if there existed a Harry Potter newspaper in color. A fair assumption is that the technology isn't good enough. It is hard to create colors with high reflection that can be modulated. And since emissive screens have technologically leaped so far, and fast, maybe electronic paper has been overlooked. Some existing techniques are shown in Figure 1. This thesis will investigate how to produce colors for electronic paper with higher reflection and higher optical contrast. As a comparison the reflection of a newspaper is around 60% to 10% [3].

The most common technology today is liquid crystal display (LCD). Liquid crystals themselves have a property of "twisting light" - altering the polarization. This twisting can be controlled by an electric field. This by itself has less value for creating a screen. The magic happens when liquid crystals are sandwiched between two polarizers perpendicular to each other. One polarizer transmits 50% of light

with a certain polarization. Schematic of a *twisted nematic* (TN-LCD) can be viewed in Figure 1A. If the liquid crystal is adjusted to "not twist the light", the light will get stuck in the second polarizer and no light will pass through the sandwich. If the liquid crystal instead was set to twist the light the stacking would appear transparent since the light can pass through both polarizers [4]. This is the foundation technique, but many different configurations have been developed to fit various applications. But no configuration suits reflective displays since 50% of the light is already lost to the polarizer. Still, the displays of some old calculators, and one of the first handheld Nintendo, Game Boy, used this technology. Game Boy even came in a color version, Game Boy Color. If you were lucky to own any of these devices, you know the struggle to catch Pokémon on a reflective LCD. The problem is that the LCD screen is very dark. LCDs cannot transmit more than 50% of the light due to the polarizers. This is like reading your newspaper behind light to medium-tinted sunglasses, which would obscure the whole page. Optical measurements on my old GameBoy Color shows a reflection between 20 to 10%. When operating an LCD in emissive mode, this can be overcome by raising the brightness of the lamp behind the stack. As for Nintendo's GameBoy, a hybrid solution was implemented to let the user decide the background brightness in the following generations. Theoretically, the highest achievable reflection for a color device is 50%, but only 33% have been achieved in a device [4].

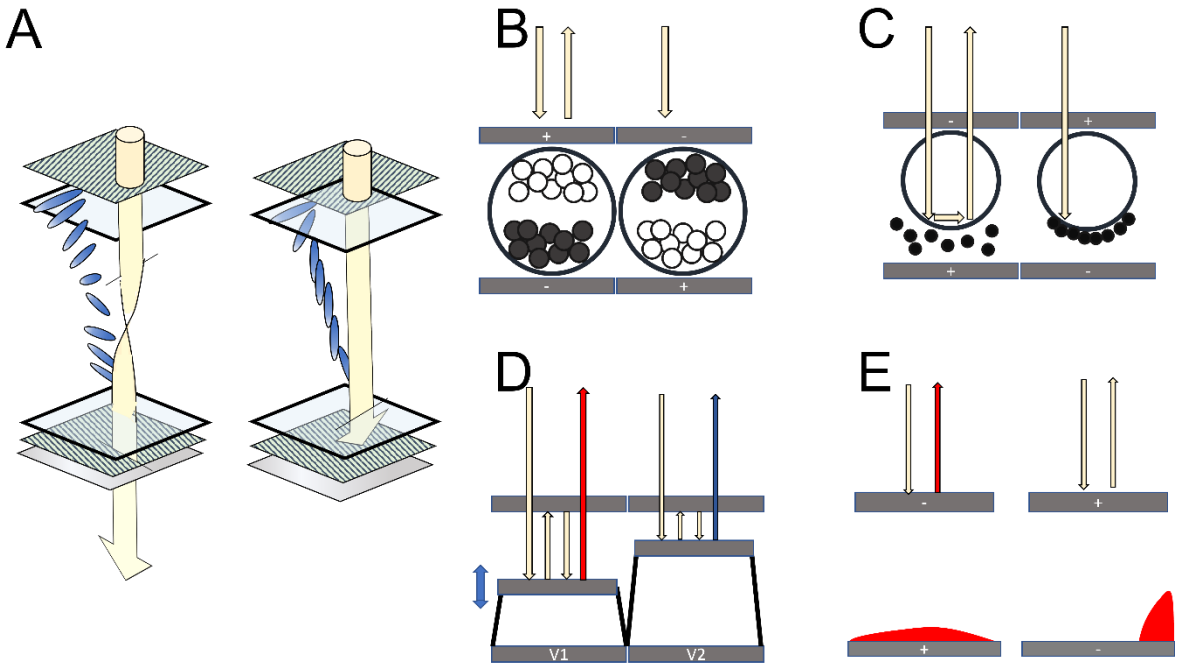

Figure 1 Schematics of different reflective display technologies. A) Liquid crystal display. The liquid crystals twist the light between two polarizers and the transmitted light is modulated. If a mirror is placed on the bottom the modulated light is not transmitted but reflected. This example shows the twisted nematic (TN) configuration, but many other configurations are possible B) Electrophoretic display (EPD). Particles are dragged up and down into visibility. C) ClearInk use particles to shut on and off total internal reflection D) Interferometric display where a mirror can be adjusted to change the air pocket in a cavity. E) Electrowetting use oil and move it in and out of visibility.

Another approach to create electronic paper is to use controllable ink particles (Figure 1B). With the help of electrostatic forces, black and white microparticles can move up and down in a capsule. When the black particle is at the top, the capsule appears dark. This technology is called electrophoretic display (EPD) and is used in the commercial *ebook* Amazon Kindle. The optical reflection of their monochrome device is between 40% to 4%. A great feature of this technology is bistability. This keeps the produced image on the screen without power consumption. Power is only required when the display is updated from one image to another. A drawback is the refresh rate which is more than a

second. To be able to display video, the screen must be updated at least 24 times a second, or every 40 milliseconds. Some color alternatives have been produced, however, the depth and saturation of the color are less than ideal. The reflection of one of these devices is around 25% with a contrast of 10% [5, 6].

New technologies have ushered in the past decade. One of them is branded ClearInk and you could call it a modification of the EPD. Microcups reflect all light to the viewer by means of the phenomenon of *total internal reflection* (Figure 1C). The same principle that applies to "retroreflectors" that warn drivers in the dark of construction workers and pedestrians. Particles are dragged in the vicinity of the cups and the total internal reflection is reduced and the area appears black for the viewer [7].

Another noteworthy technology on the rise is electrowetting. Instead of particles entering the visible part of a capsule as in EPD, a colored fluid is used (Figure 1E). An external electric field makes the fluid wet a surface and stains it with its color. This process is reversible, and the surface staining is removed when the fluid is no longer wetting the surface. This process can be made very rapid and video speed refresh rates have been demonstrated in color [8, 9]. This technology does not exhibit inherent bistability and the reflection for a color device is 27% [4].

A technology that has shown promising results to produce flexible electronic paper in color is the fusion between structural plasmonic colors and electrochromic materials. Electrochromic materials are a class of materials that change their color with an applied voltage, often between a black absorbing state and a transmissive state. The material changes its color by changing its electronic structure by redox reactions in an electrolyte. It works without polarizers and can transmit more than 50% of the light. A famous example is the inorganic tungsten oxide, transmissive in its pristine state, which can be made blue by lithium intercalation. This material has been studied for decades and is commercially incorporated into *smart windows* for both offices and airplanes. Conjugated polymers are another class of electrochromic materials that have recently received a lot of attention due to other possible applications such as antistatic coatings, solar cell materials, or printed electronics [10]. Synthesizing different monomers has made it possible to produce polymers that can change from transparent to any color. Electronic paper in color requires three different polymers. Each switching between transparent and one of the three primary colors, red, green, and blue. Another approach is to have one polymer that switches between transparency and black upon highly reflective color pixels. The electrochromic material can then act as a shutter, turning it ON and OFF [11, 12].

Structural coloration is a phenomenon that occurs when a micro or -nanostructure is reflecting a color even though the material itself is colorless. Many examples can be found in nature such as the blue Morpho butterfly or the peacock. Both have vivid colors, but the color is only produced by the structure of the wings, or feathers. Light bounces off the structure and interacts with itself to reflect only one part of the visible spectrum. Another example is an oil film on water which produces faint colors [13]. This phenomenon has been used to color metal by heating it. The heat creates a colorless metal oxide on top of the reflective metal and the interference produces different colors which vary with the oxide thickness. Colorful patterns have even been made on chocolate, not by adding dyes, but by removing the chocolate to create a nanostructure [14]. Birds and butterflies are also using this technique to create their vivid colors [15].

Another way to create colors is to make nanoparticles out of metals and suspend them in glass. This effect can be viewed in church windows and is known as plasmonics. Light interacts with free electrons in metals and scatters a portion of the light, leaving the remaining light to be observed as a specific

color. This technique has been used together with structural colors to produce replications of famous artworks [14]. A first goal of this thesis is to find an electrochromic material on top of a plasmonic pixel to modulate its reflection with a higher optical contrast than previous reported values.

With one color pixel and its ability to adjust the reflection, only said color can be observed. To create all the colors, three pixels are needed. These subpixels are placed next to each other and are usually the primary colors red, green, and blue. This is a huge drawback for the reflective screen since if one of the primary colors is desired, only one-third of the light can be reflected at best. Actively tuned plasmonic color generation is a field that has emerged to overcome this issue. Similar to electrochromics, other properties of a material, such as size, can be altered. With clever designs, the structural color that is reflected can also be tuned. The need for subpixels and cutbacks in reflection would be alleviated by having one pixel with the ability to alter its color throughout the whole visible spectrum [16]. To create such a structure is the second goal of this thesis. A similar concept, only based on structural coloration, is Qualcomm's Mirasol. A micro mechanical system (MEMS) tuned the distance between two metals to create different colors (Figure 1D). Unfortunately, the project was put to halt [17].

In most laboratories, one pixel is created and controlled, but rarely is a screen created from those pixels. To do that, many pixels, often thousands, must be controlled simultaneously. There are some common techniques to do this, active matrix, and passive matrix. Both require pixels to be laid out in a grid, a matrix. Without this technique, if *m* times *n* pixels are used, *m* times *n* electrodes are required. Sometimes double the amount if two contacts are required for each pixel. The number of electrodes can be reduced to *m* plus *n* if every pixel in each row is connected together. In a similar way, every pixel in each column is connected to another. The active matrix utilizes transistors to open and close rows. A passive matrix utilizes the intrinsic properties of the color-changing device to sensibly design a grid [18].

A quick search in the scientific database Scopus reveals that the number of publications including the word "electrochrom*" is increasing every year. 5 documents were added in 1970, 401 added in the year 2000, and 845 in 2020. Similar for structural colors, in the year 2020 there were around 2000 published publications and two years later it was close to 3000 fresh articles referencing this field. Plasmonic color had zero before the year 2000 but 200 added in the year 2020. All three fields are active, and research are ongoing. However, if we extend the search of electrochromic to include either a passive or active matrix, the total number of articles is 30 and 105, respectively. Most of the publications do not present any matrices. The number of relevant documents could be read in the weekend. So, the question is: are matrix configurations too challenging to make? Or is it trivial? To investigate this, is the third and final goal of the thesis.

1.1 Goals of this thesis

This thesis has three goals which can be summarized into three questions that we want to answer:

1. Which electrochromic material is the most suitable to use with plasmonic pixels?
2. Can electrochromics be used to create a color changing pixel?
3. Is a matrix configuration compatible with electrochromics and plasmonics?

This thesis will begin with theory (2). To lay the foundation of why plasmonic pixels generate highly reflective color pixels. To lay the foundation of electrochemistry and its importance to electrochromics. To lay the foundation of conjugated polymers, the chosen electrochromic material.

To lay the foundation of matrix configurations, and their importance to graphical displays. Theory will be followed by methods (3) where equipment and procedures will be listed. There are three sections in the following results chapter (4). Data will be presented to explain how each goal was achieved or partly achieved. Both major achievements and reflections on failures will be discussed. Concluding remarks (5) will summarize what has been accomplished and I will give my opinion on future prospects in the field.

Hopefully my contributions will have bridged a small gap from the science in the lab, to the magic of Harry Potter paper. Enjoy!

2 Theory

2.1 Optics - structural colors and plasmonics

This theoretical part will deal with light's interaction with materials – optics and photonics. For those of you who have worked with optics or taken a course in optics, you know that it requires a great deal of math. A lot of equations are manipulated back and forth until you have lost all sense and intuition of what is happening. I will try to keep it at a minimum.

Light is a continuous wave, at least in this section. In later sections light will be photons - the quantized quasi particle of the light wave. These are two different models with different applications. Now we use the *classical* – a wave. An electromagnetic wave (EM-wave) consists of two components, one electric and one magnetic. The magnetic field is always perpendicular to the electric field and in this section we only write out the electric component; $E_s = E_{s,0}e^{i(k_0 x - \omega t)}$, which oscillates with a certain frequency, ω, wave vector, $k_0 = \hat{x}\,2\pi/\lambda$, , wavelength, λ, amplitude, E_0, and polarization *s* or *p*. Note that the wave vector is in fact a vector and is directed perpendicular to the electric and magnetic field. One of the most principal property of EM-waves is *superposition*; when two different EM waves are radiated together, they create one resultant wave. In practice there are some conditions for this to occur such as coherence – the waves are not allowed to be spread out too much. The two waves can interfere *destructively* – the resultant wave has a lower amplitude than the two components, or *constructively* when the resultant amplitude is higher than its components [19].

When a charged particle is embedded in an oscillating electromagnetic field the mobile charges in the particle will start to oscillate together with the field. This oscillating charged particle radiates out another electromagnetic wave, it scatters the light. When light impinges on a material that consists of a lot of charged particles – electrons and protons - an electric field is reradiated by the oscillations of electrons. The force between the electrons and the protons acts as an elastic spring and when the electrons are displaced from the nucleus they are dragged back. Since they behave like an oscillating "plus and minus" charge in total, they are known as *dipoles* and are basically a harmonic oscillation. There is also some "friction" which can cause the reradiated light to lag behind - *damping*.

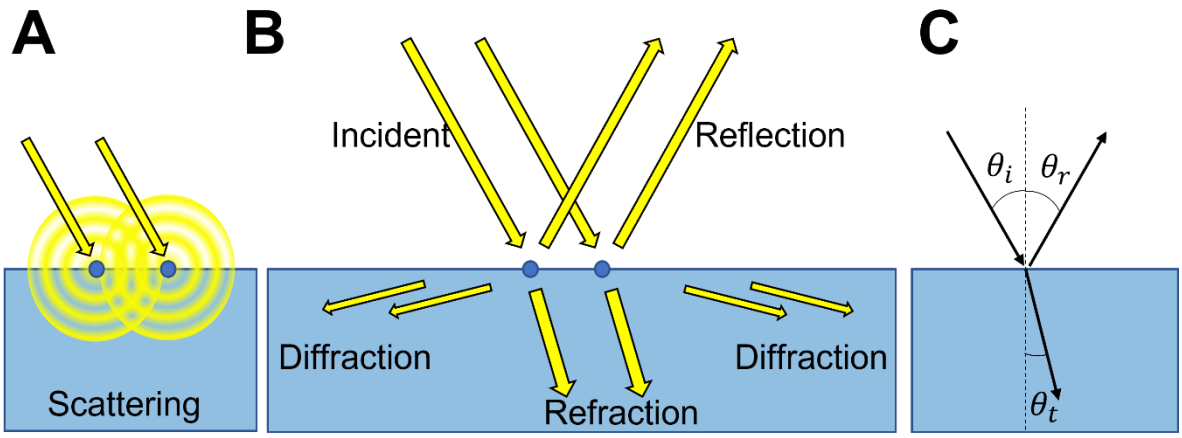

Figure 2 A) Scattering B) constructive interference generates reflection, diffraction, or refraction. C) Angles of reflection and refraction.

The superposition of the impinging and the reradiated light is characterized by a prefactor of the EM-field called the dielectric function or *permittivity*, ϵ. When it is positive the wave propagates through

the material, and it is a *dielectric* material. If the permittivity is negative, it is metal and the light is reflected [19].

The redirection of light from one particle is called scattering (Figure 2A). Bundling together the impinging light and the re-emitted light, constructive interference occurs. This is because the *optical path length difference* between the impinging wave and the reradiated wave differs by an integer of the wavelength. If constructive interference occurs backwards, it is called *reflection*. If it constructively interferes in the forward direction, it is called *refraction,* or *transmission* if the angle of the incident angle is zero. In some cases, constructive interference can occur at other angles than the forward direction (reflection and refraction) and this is known as *diffraction* (Figure 2B). The reflected wave has the same angle as the angle of the incident wave, $\theta_i = \theta_r$ (Figure 2C) and the refracted wave obeys *Snell's law* (Equation *2.1.1*) where "*n*" is the *refractive index* which tells how much the EM-wave slows down in the material. The "slowing down" is a result of the addition of impinging EM waves and the reradiated waves, and it is not a surprise that this is associated with permittivity; $\sqrt{\epsilon} = n$. The refractive index is added into the wavenumber $k = nk_0$. In most materials, if not all, permittivity or refractive index depends on wavelength - *dispersion*. There are many types of dispersion, not just when the permittivity changes with wavelength [19].

$$n_i \sin(\theta_i) = n_t \sin(\theta_t) \qquad 2.1.1$$

The Fresnel coefficients show how much light is reflected and refracted (Equation 2.1.2 & 2.1.3). As the refractive index differences between the two materials increase, so does the reflection. However, it should be noted that what we usually refer to as light is not the value of the electromagnetic wave amplitude – the field strength *E* - but its intensity; $I = |E|^2$. Conservation of energy states that incident intensity equals the sum of reflected, transmitted, scattered, and absorbed light. This is what we measure, both with our eyes and with spectrometers. A common example of when Fresnel's coefficients are relevant in our daily life is the reflection of a glass surface with refractive index $n = 1.5$. form a normal incident $r_s = r_p = \frac{n_i - n_t}{n_i + n_t} = \frac{1-1.5}{1+1.5} = -0.2$. The reflected intensity then becomes $I = |r|^2 = 0.04 = 4\%$.

$$r_{s/p} = \frac{E_r}{E_i} = \frac{n_{i/t}\cos(\theta_i) - n_{t/i}\cos(\theta_t)}{n_{i/t}\cos(\theta_i) + n_{t/i}\cos(\theta_t)} \qquad 2.1.2$$

$$t_{s/p} = \frac{E_r}{E_i} = \frac{2\, n_i \cos(\theta_i)}{n_{i/t}\cos(\theta_i) + n_{t/i}\cos(\theta_t)} \qquad 2.1.3$$

When a *thin film* (thickness of the order of the wavelength of the EM-wave) is used there will be reflection and refraction on both surfaces which interfere with each other. To summarize the reflection and transmission of multiple layers a simulation method called *Transfer Matrix* can be used. This method uses a lot of "mathematical-patience" to go from the Fresnel coefficient of each interface to a final value. An example of a Transfer Matrix simulation of a thin film of glass (*n* = 1.5) can be seen in Figure 3A (schematic of structure in Figure 3B). Thin film interference creates reflection peaks when there is one whole wavelength that fits inside the cavity/film. But it is not that some light is 'lost' just because destructive interference occurs. It is just that it cannot exist at some points when you have

destructive interference [19]. Similar phenomena can be seen with an oil film on water and is one case of *structural coloration*. Other examples of structural coloration can be seen widely in nature. The feathers of pigeons consist of a keratin layer that reflects purple or green light. The blue wings of the Morpho butterfly consist of a periodic nanostructure that reflects blue light [13].

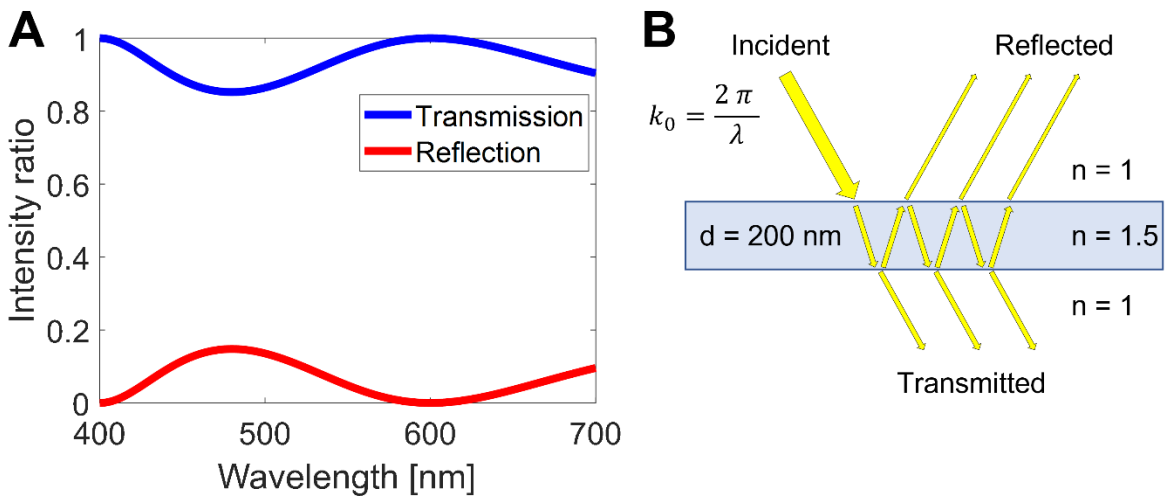

Figure 3 A) simulated spectra of a 200 nm glass film. B) Schematic of the structure. The light comes in with an angle in the schematic just to easier show the reflections. In the simulation the angle is zero.

In the above simulation (Figure 3A) no light is absorbed, if an imaginary component is added to the permittivity or the refractive index, $\bar{n} = n + i\kappa$, the EM-field will decrease exponentially trough the material $E = E_0 e^{-\kappa k_0 x} e^{i(nk_0 x - \omega t)}$. When converted to intensity the transmitted light falls exponentially trough the material; $T = \frac{I_t}{I_i} = e^{-4\kappa k_0 x}$. This is related to the famous *Lambert-Beers law* used frequently in absorbance spectroscopy; $A = -\ln(\epsilon c l)$ where ϵ is the molar extinction c is the concentration, l is the path length, and A is absorbance. Another form which is frequently used is the *optical extinction;* which includes all the processes; absorption, scattering and reflection (Equation 2.1.4). This is usually what is measured.

$$E = \ln\left(\frac{1}{T}\right) \qquad 2.1.4$$

As aforementioned, the real part of the dielectric function does not have to be positive, when it is negative it means that the EM-field in the material is out of phase with the impinging EM-filed and is reflected from the surface. The reason for the 'shininess' of metals is because they have a negative permittivity in the visible part of the electromagnetic spectrum. Metals can be used to create structural colors in *Fabry-Pérot cavities*, where the metal is thin enough to transmit part of the light and also reflect part of it. This configuration creates a reflection dip instead of the desired reflection peak due to sharp transmission and absorption peaks [20]. In this work, the cavity is constructed by using a silver, aluminum, or platinum mirror to reflect nearly all visible light. A layer of dielectric material is then deposited on top, followed by a thin layer of gold. Because thin gold is semitransparent, it reflects some yellow light while transmitting green light. Blue light is normally absorbed by gold.

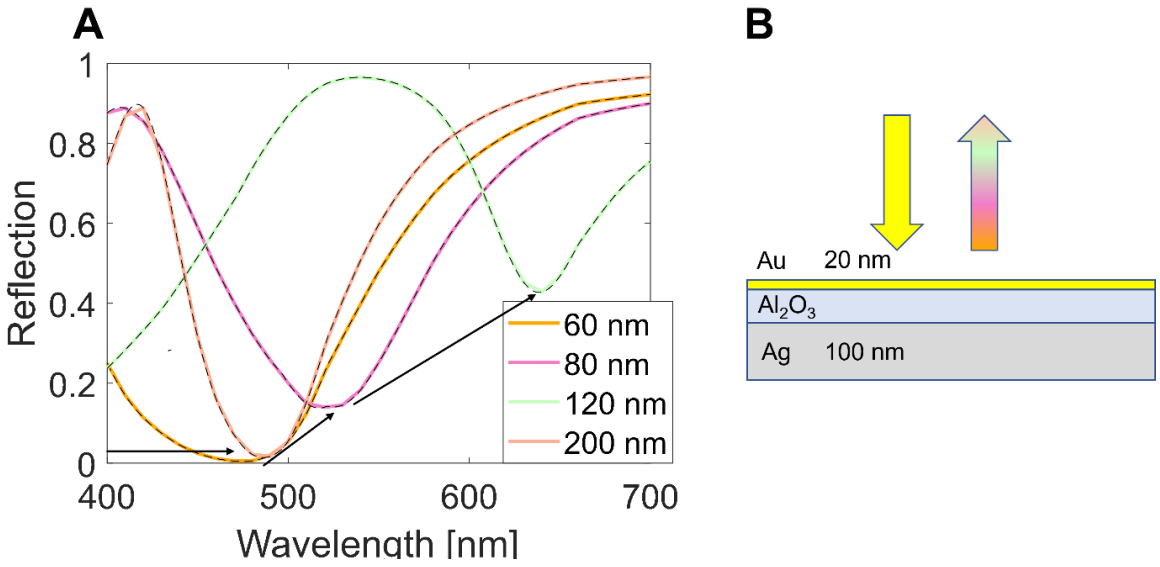

Figure 4 A) A simulated spectra of silver-alumina-gold structure with varying alumina layer thickness. The arrows indicate the reflection minima and follow an increasing thickness. The line color is the "pseudo color" which mimics what the color would be for the human eye. Note that 60 nm and 200 nm have similar color but 200 nm have a sharper reflection dip. B) schematic of the simulated structure.

In Figure 4A, simulations of aluminum oxide as a spacer layer can be viewed together with a schematic of the structure Figure 4B. The color of the plot lines is the color of the pseudo-color which is generated from the spectra (explained more in section 2.4). For the color-blind reader… You are in my thoughts. At 60 nm the spectra resemble the spectra of gold, reflecting yellow light, although a hint of increased reflection is present around 400 nm. In the case of 80 nm, the reflection dip can be observed at 530 nm and is red-shifted to 640 nm when increasing the thickness to 120 nm. A higher-order reflection dip is also observed at lower wavelengths. Further increasing the thickness to 200 nm the orange/yellow color has been obtained again by the second order reflection dip at 490 nm. But wait a bit. There are reflection peaks at 450 nm for two thicknesses (80 nm and 200 nm), and it was previously mentioned that gold absorbs blue light. When light is reflected, standing waves are created within the cavity, and an electric field with a specific wavelength (450 nm in the case) is absent inside the cavity. Blue light is not allowed to penetrate into the cavity [20].

The major parameters that determine the reflected color of the structure is the thickness and the refractive index (especially the real part) of the spacer layer. If the spacer layer thickness and refractive index can dynamically be tuned by some external stimuli - spoiler - the color of the pixel can be controlled. In order to further enhance the saturation of the reflected colors, a nanohole array can be introduced into the gold metal to obtain a plasmonic effect. This effect scatters red light and thus gives a more enhanced coloration for blue and green samples [14]. More about this at the end of the next section.

2.1.1 Plasmonic

If there would be an electron-gas where the electrons don't interact with each other, it would be interesting to derive what the permittivity of the gas would look like. Without using so much math, and as promised to omit most of the equation manipulation, I will just state one equation for the permittivity of this electron gas $\epsilon_m(\omega) = 1 - \frac{\omega_p^2}{\omega^2}$ [21]. Here ω_p is the plasmon frequency and it is the natural frequency of the electron gas – longitudinal waves of alternating electron concentration. Above this frequency the permittivity is positive, and the electron plasma oscillates in phase - light

propagates through the plasma, which behaves like a dielectric. Below this frequency, the permittivity is negative and the material behaves like metal, reflecting light. In my mind, it is kind of like a speed limit. When higher frequencies of EM-waves are impinging on the material the electrons don't have time to react. They don't have time to follow and move back and forth. This equation also approximates the permittivity of a metal (although only around the plasmon frequency) since its response is dominated by the free electrons. Additionally, some scattering processes can represented by a factor which produces an imaginary component that makes the material absorb some light; $\epsilon_m(\omega) = 1 - \frac{\omega_p^2}{\omega^2 + i\omega\gamma}$. The parameter γ is representing how strong the *damping* is. If we also add the contribution of the nuclei, the electrons are less free and the nuclei apply an restoring force. This can be represented with an additional parameter ω_0 which represents the resonance condition where the atoms absorbs most of the energy and converts it to kinetic motion of the atoms, heat (Equation 2.1.5) [22].

$$\epsilon_m(\omega) = 1 + \frac{\omega_p^2}{\omega_0^2 - \omega^2 - i\omega\gamma} \qquad 2.1.5$$

The waves with the natural frequency, the plasma frequency, can be excited by shooting electrons, or high energy light, like x-ray, on a metal [21]. These kinds of plasmons are *bulk plasmons*. Focus will be shifted to another kind: Surface plasmons – the quantized collective excitation of the *surface wave*.

A simple example of surface plasmons is what is called *localized surface plasmon resonance* (LSPR), which is a property of a small metallic nanoparticle (50-100 nm) with a surrounding dielectric. The free electrons in the metal particle can collectively be excited and act as the "charged particle" – polarized- but now the charged particle is a finite collection of atoms. The restoring force of the nuclei makes it, again, act as a harmonic oscillator with a restoring force and thus also possess a resonance. A well-known example is gold nanoparticles suspended in water, also known as colloidal gold. The solution appears red to the eye due to the plasmonic absorption and scattering of green light and the gold's inherent absorption of blue. The resonance is very sensitive to its surrounding refractive index. This technique have been utilized to create dynamic color by tuning the refractive index [23]

Another kind of plasmon is the *surface plasmon polariton* (SPP) which is not localized around, say a sphere, but is propagating. SPPs propagate on a surface of a metal, or strictly speaking at an interface where the real part of the permittivity of one medium is negative, e.g. metals, and the other medium has a positive real part, a dielectric material. This surface wave is a mixture between light and matter – a *polariton.* As complicated as this appears to be, it is a tiny bit more mundane than it sounds. A light wave impinges on a surface consisting of electrons. These electrons start to oscillate and with the right conditions the light and the electrons resonate. The name for these surface waves is abbreviated as SPP, for Surface Plasmon-Polariton, or SPR, Surface Plasmon Resonance. The combined surface wave is confined to the surface – however it only propagates a slight distance (~10 -100 μm) before it decays. This is because the metal is not flawless and absorbs light [24].

A "restriction" for the surface plasmon is the dispersion of the SPP (derived from more manipulation of equations and displayed in Equation 2.1.6). This gives us information of the allowed wavelengths of the plasmon (remember $k_{x,SPP} = \hat{\boldsymbol{x}}\, 2\pi/\lambda_{SPP}$) for different frequencies. ϵ_m is the permittivity of the metal defined by Equation 2.1.5 without any restoring force ($\omega_0 = 0$) and an arbitrary damping constant ($\gamma = 10^{14}\ s^{-1}$). ϵ_d is the permittivity of the dielectric which is set to a constant value of 1.5.

$$k_{x,SPP} = \frac{\omega}{c}\left(\frac{\epsilon_m \epsilon_d}{\epsilon_m + \epsilon_d}\right)^{1/2} \qquad 2.1.6$$

The surface plasmon dispersion is represented by the black dots in Figure 5A. In Figure 5B the interface of the metal and the dielectric shows plasmon propagation in the x-direction. The electric field magnitude is decaying in the z-direction – for both media. Bio-researchers utilize the decaying electric field on the dielectric side in their work since it is very sensitive to refractive index changes and thus makes it an excellent technique for sensing [25]. The SPP dispersion in Figure 5A is not linear, but falls off when the wave vector, or k-value, increases (SPPs wavelength gets smaller). The plasma frequency could be regarded as a frequency limit. Note that the bulk plasmon dispersion starting at the plasmon frequency and extending to higher frequencies. In between the convergence frequency and the bulk plasmon frequency there are some available states that come from the non-idealities of the metal. This is where the imaginary component of the metals permittivity becomes too high and absorbs the light. The states at these frequencies are not confined to the surface and thus not surface waves [26].

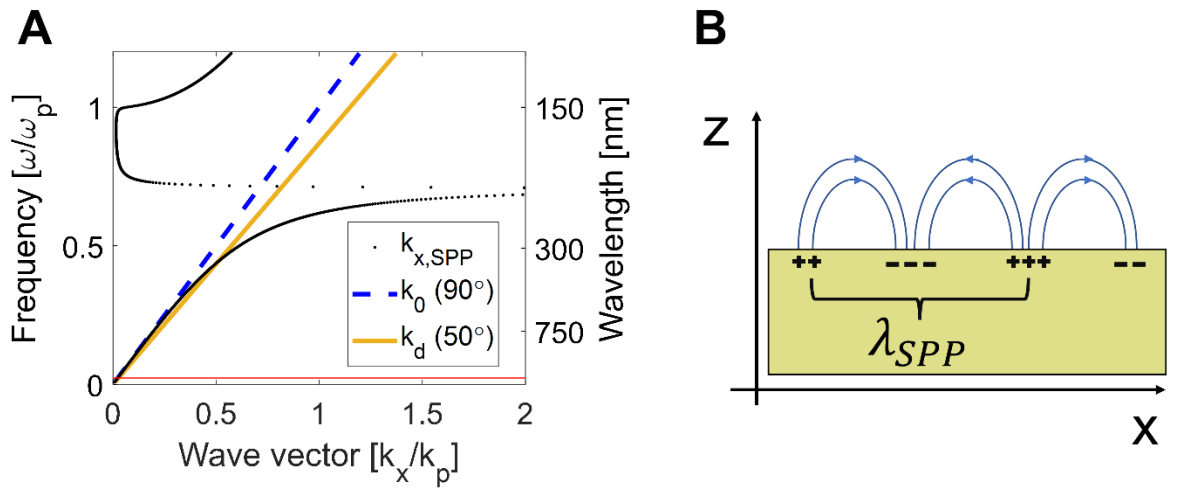

Figure 5 A) Dispersion for a metal-air surface with a bulk plasmon wavelength of 150 nm and a damping constant of 10^{14} s^{-1}. The dispersion of light in air (dashed) never crosses the plasmon dispersion (the 90° shows no crossing with $k_{x,SPP}$). The yellow line is light in glass (n = 1.5) with a 50° angle of incidence. The red line is the frequency of 670 nm light in air. The normalization constant k_p is the wave vector of the bulk plasmon: $\frac{2\pi}{\lambda_{SPP}}$. B) A schematic of how SPPs would look in a metal and dielectric. The plus and minus are the poles which generate the E-field in z-direction.

So how do you produce and use surface plasmons? We can try to excite plasmons by irradiating the surface with light at different angles. A higher angle gives a higher x-component $k_{light,x}\boldsymbol{x} = k_0 \sin(\theta)$. Light must couple into the surface-plasmon-polariton at the same wavelength and frequency. You have probably noticed that there are 2 lines drawn in Figure 5A with the SPP-dispersion. One is the *light line* – the dispersion of light in vacuum (or air since its refractive index is very close to vacuums). This line doesn't cross the SPP dispersion at any point - the light and plasmon cannot couple. You cannot shoot light in the air onto a surface and excite surface plasmons. What you do is shift the "light line" by letting the impinging light pass through a dielectric material. The frequency stays the same when light enters a medium with a higher refractive index but the wavelength changes and so does the k-value. But a zero angle of incidence has no x-component, so the k-value does not match. To match the k-value of the impinging light, an angle of 50° is more than

enough and matches conditions around half the plasmon frequency. But remember that the plasmon dispersion was derived for a surface with a lower refractive index (air =1). Reevaluating the dispersion with the refractive index for glass would again lead to no matching condition. To solve this, it seems that the surface needs to be in contact with both glass and air. The most common way to make such a configuration is to use a very thin metal film on top of glass. The light comes in on the dielectric side and passes through the metal to the air side. A schematic is seen in Figure 6B.

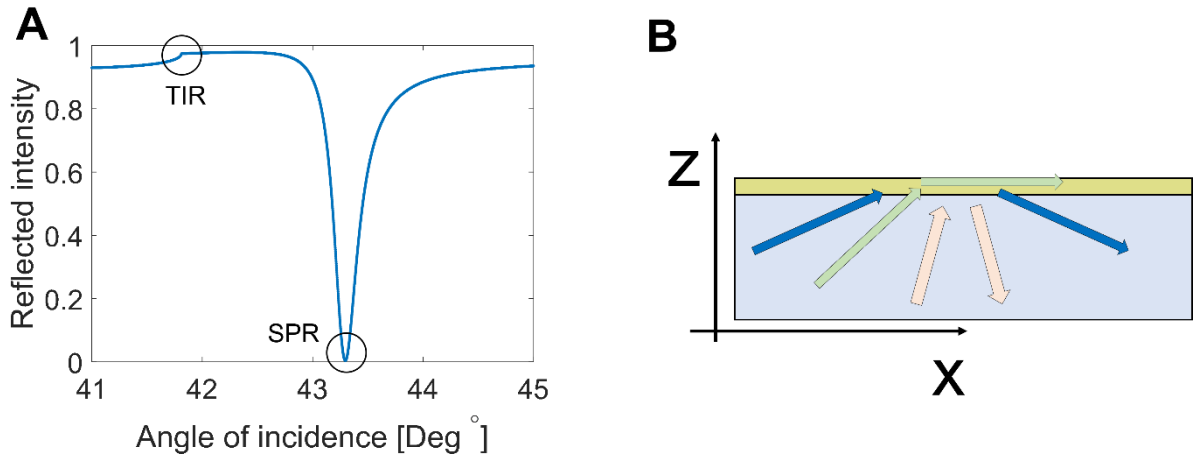

Figure 6 A) An angular spectrum which shows that at around 43°, light with 670 nm wavelength will exhibit a drastic drop due to coupling to SPPs B) A schematic of how a spectrum in B) could be generated by light from a dielectric on a thin gold film. At a certain angle there is no reflection.

in Figure 6A you can see an angular reflectivity spectrum of a thin film on a glass prism with metal described by Equation 2.1.5 without restoring force. The bulk plasmon wavelength is 150 nm and the damping is around one percent of the plasmon frequency ($\gamma = 10^{14}\ s^{-1}$). The incident angle is increased until a sharp dip in reflection occurs – the SPR-angle. At angles lower than the SPR-angle, the angle for total internal reflection (TIR) is first observed. TIR is a phenomenon that occurs when light travels at a high angle from a high refractive index medium to a low refractive index medium. All light is reflected. However, a small portion of the EM-field is present in the low refractive index medium and decays exponentially through it in an *evanescent wave.* This is the wave that is coupled to the plasmons to create a plasmon-polariton. The surface plasmon is also evanescent which makes it very sensitive to changes in the refractive index right above the metal surface. This sensitivity is utilized in surface characterization techniques and will at one point be used in this thesis to characterize a thickness change in an adsorbed layer. The resonance energy is dissipated as heat in the material. It should also be noted that the dispersion relation shown previously lacks validity since the metal film is not semi-infinite, it has two surfaces. More complicated behavior occurs where plasmons on the two surfaces can couple to each other and create two different modes with two different energies [27].

Another way of exciting SPPs is to use a periodic structure - a grating. When light impinges on a grating it scatters on the periodic structure and diffraction occurs. When the period is smaller than the impinging wavelength no far field diffraction occurs, however, some light is scattered in the perpendicular direction, or parallel to the grating. When the k-value for the grating is matched to the surface plasmon k-value, light can be coupled to electrons and excite SPPs. Note that the grating will, however, change the dispersion relation of the plasmons [27].

The value of the *in-plane* wave vector is described by Equation 2.1.7, where Λ is the periodicity of the grating and θ is the angle of incident light. Even with a zero angle of incidence the in-plane component is not zero. This can be explained by having scattering processes everywhere on the surface which constructively interfere in the in-plane direction.

$$k_x(\omega) = k_0 \sin(\theta) + \frac{2\pi}{\Lambda} \qquad 2.1.7$$

Similar to a grating there is another structure that can be used to excite plasmons - a nanohole array. This consists of a thin metal film that has holes in it. At first glance, it would be tempting to believe that it would act as a diffraction grating. The story becomes a bit more complex with this structure because it supports both the propagating SPPs and the localized (LSPR). The LSPR comes from holes that are the inverse structure of cylindrical nano disks on a surface. Interestingly, you don't require a metal particle to create LSPR but a void in a metal works as well [27, 28]. However, Equation 2.1.7 can still be used to predict the excitation wavelength by evaluating k_x and check the frequency in the dispersion relation [27].

Two examples of this can be viewed in Figure 7A-B where a light beam illuminates two thin gold films (20 nm on glass); one with holes and one without. It is clear where the light is impinging on the film with holes since it scatters red light at higher angles. On a surface without holes, light is only reflected, transmitted, and absorbed. A MIM-structure fabricated with and without holes in the top gold is shown in the same figure (Figure 7C-D). The structure without holes appears much more purple, which indicates that a large portion of the red light is reflected. However, when the nanohole array is introduced into the top gold film the structure appears much bluer [29, 30].

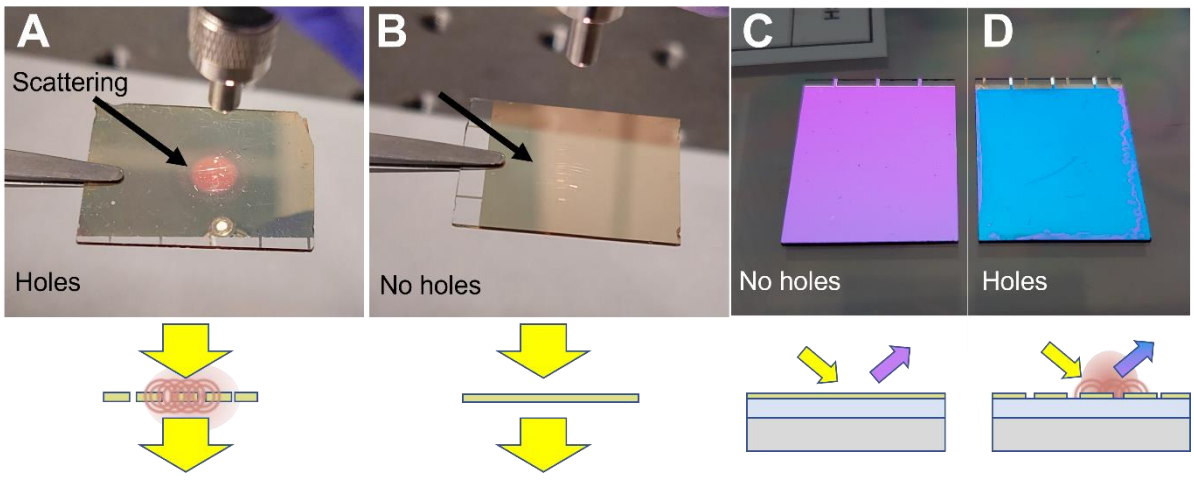

Figure 7 A) White light impinging on a gold surface with nanoholes exhibit red scattering. B) Planar gold does not exhibit this. C) In a structural color pixel this can enhance coloration by D) scatter away red light.

2.2 Electrochemistry

This section describes basic electrochemical concepts which are later used to explain some of the results. It is necessary to introduce some concepts because they play a significant role later in the thesis. Some concepts are explained because it has helped me get a more fundamental understanding of how to interpret the results. Most of the below discussion is information fetched from the electrochemical book – *Electrochemical Methods* by Bard and Faulkner [31]. Only the central and relevant concepts have been included.

Electrochemistry is sometimes introduced by describing a cell consisting of two metals (zinc and copper) each immersed in a bath of the metals' ions (Zn^{2+}, Cu^{3+}), connected together to form what is called a galvanic cell. Instead, by formulating the thermodynamics of the system of only one electrode immersed in an electrolyte, it is easier to derive the famous *Nernst equation.* Moreover, it is easier to understand why it is imperative to use a *reference electrode* when doing electrochemical experiments. After this derivation we will describe what happens in the bulk when you change the concentration of the boundary (the electrode). Cyclic voltammetry will be discussed after this where an example will be shown together with a simulation. Deviations between the collected voltammogram and the simulation will be discussed by adding complexity with initially adding a chemical step. After this electrode kinetics will be added and finally a short discussion of double layer and uncompensated resistance will be overviewed.

We will start with the *chemical potential*. The general equation for chemical potential is Equation 2.2.1 which describes what the change is in Gibbs free energy G when one particle, or a chemical species, is added to a system of N particles. A physical interpretation of the chemical potential is the 'tendency of a system to give particles'. A spatial difference in the chemical potential of a species is what gives rise to diffusion - a molar flux of the species e.g. from high concentration to low concentration. When there is no more spatial difference in the chemical potential the free energy cannot be lowered by changing the species place and the system is in steady state [32].

$$\mu = \frac{\partial G}{\partial N} \qquad 2.2.1$$

It is slightly easier to understand this in terms of analogies. The electrostatic energy of a charged particle can be expressed by the electrical potential multiplied by the charge of the particle - the potential is the energy divided by the charge. In the same way, the chemical potential of a species can be expressed as the chemical energy divided by one mole of the species. Pressure can be described as mechanical energy divided by a volume and temperature can be described as heat energy divided by entropy. In other words, pressure and temperature are potentials as well. Another way of phrasing the temperature case is that the temperature is the proportionality constant describing how much the energy changes when the "disorder" (entropy) changes. In the case of chemical potential, the chemical energy is described by Gibbs free energy, which is the *total* energy with mechanical and heat energy subtracted [33].

The chemical potential can be calculated for a species – j – from the concentration c_j. Strictly the concentrations should be activity coefficient –a_j - which is an effective concentration considering additional effects such as interactions between the species, but in many cases the concentration can be used (Equation 2.2.2). The concentration c_0 is a standard concentration, usually put to 1 molar and

μ_j^0 is the *standard chemical potential* which is obtained when the concentration is at its standard concentration $c_j = c_0$. Notice the logarithmic factor in the chemical potential. This logarithm will show to play a great role in how electrochemistry works, since it is the reason one of the most central equations in electrochemistry, is logarithmic. It is usually derived from the logarithmic quantity entropy. Further, statistical mechanics explains why entropy is logarithmic. This formalism is only valid for uncharged species i.e. not for ions. To make this useful for charged species an additional term is added $z_j F\Phi$ (Equation 2.2.3) where *F* is faradays constant; a measure of the amount of charge per one mole electrons i.e. $F = eN_A$. The amount of elementary charge is z_j, and Φ is the electric potential. This term considers the energy of the electrical potential, and when added to the chemical potential becomes the *electrochemical potential,* $\bar{\mu}_j$. The electrochemical potential is not only used in chemistry for chemical reactions but also used in (solid state) physics where the electrochemical potential of electrons in a solid is the *Fermi energy,* E_f, also known as the *Fermi level* (if T>0) (Equation 2.2.4). This parameter can be adjusted by altering the electrode potential by e.g. connecting it to a solar cell. The steady state - the equilibrium - has the condition that the electrochemical potential is spatially constant [32].

$$\mu_j = \mu_j^0 + RT \ln\left(\frac{c_j}{c_0}\right) \qquad 2.2.2$$

$$\bar{\mu}_j = \mu_j + z_j F \Phi_{\mathrm{j}} \qquad 2.2.3$$

$$E_f = \frac{-q}{F}\bar{\mu}_e \qquad 2.2.4$$

An electroactive species can be reduced, gain *n* electrons ($O + ne^- \rightarrow R$), or oxidize, lose *n* electrons ($R - ne^- \rightarrow O$) as represented by Equation 2.2.5 (remember that this is Equation 2.2.5 because it will be referenced throughout this section). In a solution of oxidized and reduced species, a metal electrode provides (and receives) electrons.[1]. The electron transfer between the solution and the electrode is said to be *heterogeneous* because the phases are different. How will the electrodes Fermi level depend on the concentration of oxidized and reduced species? (We are not necessarily interested in the Fermi level, rather the electrode potential, but let's start with it). Assuming that the electrode is just electrons in the solution and then applying the condition that the electrochemical potential is constant at equilibrium (Equation 2.2.6) we get an expression for the electrochemical potential of the 'free electrons' of the solvent (Equation 2.2.7). When we input the expressions for the electrochemical potentials (Equation 2.2.2) we get, after some manipulation (Equation 2.2.8 to 2.2.11), that the Fermi level depends on the standard chemical potentials and the concentrations with an additional term of the electrical potential of the solution ($\Phi_{\mathrm{sol}} = \Phi_O = \Phi_R$) (Equation 2.2.12). This potential term is referenced against something which we don't care about. It could be some state outside the beaker

[1] This reminds me of my girlfriend, who is a physicist in a stricter sense, telling me about her chemistry classes at university. The teacher was, allegedly, repeating as a mantra that *"Electrons don't come in a jar, and that's why we need to learn how to manipulate them in chemistry".* Every day he said this apparently. Well, in electrochemistry your metal electrode is basically your jar of electrons that can be provided into the solution by changing their (the electrons) energy. So Italian university teacher – zero, Oliver- one.

or in a galaxy far away. However, it is an electrical potential and the work involved in bringing an electron from this reference state into our solution is $e\Phi_{\mathrm{sol}}$ [32, 34].

$$R \rightleftarrows O^{+} + ne^{-} \tag{2.2.5}$$

$$\bar{\mu}_R = n\bar{\mu}_e + \bar{\mu}_O \tag{2.2.6}$$

$$\bar{\mu}_e = \frac{1}{n}(\bar{\mu}_R - \bar{\mu}_O) \tag{2.2.7}$$

$$\bar{\mu}_e = \frac{1}{n}(\mu_R^0 + RT\ln\left(\frac{c_R}{c_0}\right) + z_R F\Phi_R - \mu_O^0 - RT\ln\left(\frac{c_O}{c_0}\right) - z_O F\Phi_O) \tag{2.2.8}$$

$$\bar{\mu}_e = \frac{1}{n}(\mu_R^0 - \mu_O^0 + RT\log\left(\frac{c_R}{c_O}\right) + z_R F\Phi_R - z_O F\Phi_O) \tag{2.2.9}$$

$$\bar{\mu}_e = \frac{1}{n}\left(\mu_R^0 - \mu_O^0 + z_R F\Phi_R - z_O F\Phi_O\right) + \frac{1}{n}RT\ln\left(\frac{c_R}{c_O}\right) \tag{2.2.10}$$

$$\bar{\mu}_e = \frac{1}{n}(\mu_R^0 - \mu_O^0) + \frac{1}{n}(z_R - z_O)F\Phi_{sol} + \frac{1}{n}RT\ln\left(\frac{c_R}{c_O}\right) \tag{2.2.11}$$

$$E_f = \frac{-q}{nF}(\mu_R^0 - \mu_O^0) + \mathrm{q}\Phi_{sol} - q\frac{RT}{nF}\ln\left(\frac{c_R}{c_O}\right) \tag{2.2.12}$$

Now an expression for how the Fermi level is related to concentrations has been obtained. However, it is difficult to directly assess this quantity due to the unknown factors such as the electrical potential in the solution (Φ_{sol}) and the standard chemical potentials of the species ($\mu_R^0 - \mu_O^0$). What is easy to do is to measure the voltage over two metals which gives the electrochemical potential difference, or voltage. Subtracting another potential which consists of the H_2/H^+-redox couple (Equation 2.2.13) and assigning the chemical potentials of the half reaction to be zero. This is done by convention. The logarithm cancels if the concentration of protons is in it standard concentration and the pressure of hydrogen is in its standard pressure [35]. The electric field components are subtracted and what remains are displayed in Equation 2.2.14. An expression for the voltage of the redox-couple can be obtained in what is called the *Nernst equation* (Equation 2.2.15). The voltage measured is now referenced to what is called a *normal hydrogen electrode* (NHE) which consists of a platinum electrode in 1 M of H^+ with 1 bar hydrogen bubbled at the electrode [32, 34]. $U^{0\prime}$ is the voltage of the redox-pair when both species are in their standard state, 1 mol at 25 °C (Equation 2.2.16). The prime sign indicates that the concentrations are used without the activity factors and thus the corrections (difference between the activity and the concentration) are 'baked in' into $U^{0\prime}$ - *the formal potential* of the redox pair. When activity is used in the Nernst equation the *standard potential* is used (no prime). There are conversions to get the *absolute* potential (against vacuum) of the redox couple by adding a conversion factor of 4.44 V to the NHE [36].

$$E_f - E_{\text{ref}} = E_f + \frac{q}{F}(\frac{1}{2}\mu^0_{H_2} - \mu^0_{H+} - \mu^0_e) - \text{q}\Phi_{\text{sol}} + q\frac{RT}{F}\ln\left(\frac{a^{0.5}_{H_2}}{a_{H+}}\right) \quad 2.2.13$$

$$E_f - E_{ref} = \frac{-q}{nF}(\mu^0_R - \mu^0_O) - q\frac{RT}{nF}\ln\left(\frac{c_R}{c_O}\right) \quad 2.2.14$$

$$U_{\text{F vs.NHE}} = \frac{1}{q}(E_f - E_{NHE}) = U^{0'} - \frac{RT}{nF}\ln\left(\frac{c_R}{c_O}\right) \quad 2.2.15$$

$$U^{0'} = -\frac{1}{nF}(\mu^0_R - \mu^0_O) \quad 2.2.16$$

The normal hydrogen electrode (NHE) is cumbersome to use in experiments, so alternatives are mostly used. For aqueous experiments, a silver-silver chloride (Ag/AgCl) electrode is immersed in an electrolyte containing chloride ions. For non-aqueous experiments, a silver wire immersed in an organic solvent with silver nitrate is commonly used (Ag/Ag^+). Another common practice is to use the compound Ferrocene (more about this below). At equilibrium with the electrode the energy of the solution's 'free electrons' must be equal to the electrode's fermi level. The Nernst equation gives us the reversible thermodynamic equilibrium of the redox couple to the energy of the 'free electrons' in the solution. Reversible means the system can be adjusted instantly, and electrons can be transferred fast. To avoid confusion regarding the word reversible, the word *Nernstian* will instead be used to describe a reaction governed by the Nernst equation.

One way of understanding the Nernst equation is as a boundary condition for our system [37]. The *Nernst-Planck equation* (Equation 2.2.17) describes how the species moves in the solution. The molar flux for species *j* is $\boldsymbol{J_j}$ - the number of species transported per time and area. The molar flux consists of three terms. The first term is due to diffusion where D_j is the diffusion constant. The second term is due to *migration*, drift of charged species in the electric field, $\boldsymbol{\nabla}\Phi$. With a supportive electrolyte added, this term can be mitigated in the bulk because the excess ions redistribute themselves to make the electric field in the bulk zero. The third term is *convection* which describes any stirring or forced flow. In a non-stirred electrolyte, this term normally is zero. When only diffusion is accounted for the Nernst Planck equation diminishes to *Fick's first equation* (Equation 2.2.18). The *continuity equation* (Equation 2.2.19), states that the divergence - the flux in and out of a bound surface - must equal the accumulation. With Fick's first equation and the continuity equation, we can obtain Fick's second equation (Equation 2.2.20). The measured current on the boundary is proportional to the flux of the oxidized species into the electrode (Equation 2.2.21). The proportionality constant is the area of the electrode, *A*, Faraday's constant, *F*, and the number of transferred electrons for each redox reaction, *n*. A minus sign is also added to make the reductive current negative as IUPAC convention. The American version uses a positive sign which has the consequence of displaying a positive current with a negative potential[2] [31]. From this last equation we can see that the current can, in fact, be regarded

[2] *I was recently at a conference where one of the speakers showed one plot using the American version. She apologized but the room still got filled with murmurs.*

as a measure of the flux at the electrode. It is easy to be tricked into thinking that applying a potential over a metal conductor and obtaining a current is the same as applying a potential over an electrolyte (with electrodes dipped in them). The first is due to the electric conductivity of the metal. The voltage is a difference in the Fermi level which generates a flux of electrons – a current. However, the current you get from an electrochemical system isn't just due to the electrolyte's ability to conduct electricity. Something, some species, are required to give or take electrons at an electrode for this to happen steadily (in reality there is also capacitive currents and adsorbed species, these will be discussed later).

$$\boldsymbol{J_j} = D_j \boldsymbol{\nabla} c_j + D_j \frac{F z_j}{RT} c_j \, \boldsymbol{\nabla}\Phi \, - \boldsymbol{u} c_j \qquad 2.2.17$$

$$\boldsymbol{J_j} = D_j \boldsymbol{\nabla} c_j \qquad 2.2.18$$

$$-\boldsymbol{\nabla J_j} + \frac{\partial c_j}{\partial t} = 0 \qquad 2.2.19$$

$$\frac{\partial c_j}{\partial t} = D_j \boldsymbol{\nabla}^2 c_j \qquad 2.2.20$$

$$I = -n \, F \, A \, J_{Ox}(x = 0) \qquad 2.2.21$$

A few idealized examples of how electrochemistry is used to understand reactions will be discussed. If a system only consists of one species with a concentration, c_{Red}, with an electrode at a low enough potential, the boundary at the electrode will have the same concentration as the bulk. Once the potential increases to a very positive value, the concentration at the boundary becomes very low, approximately zero, because all species oxidize immediately when at the surface. Solving Fick's second law for this equation and applying that the current is directly obtained from the flux, the *Cottrell equation* can be derived (Equation 2.2.22). This shows that the measured current falls with $\frac{1}{\sqrt{t}}$.

$$I = \frac{nFAc_0\sqrt{D}}{\sqrt{\pi t}} \qquad 2.2.22$$

The experiment of measuring the current with an applied potential is called *chronoamperometry.* The discussion of this experiment was introduced in this thesis to give a foundation for what electrochemistry is. The Cottrell equation is not used in this work and chronoamperometry is used infrequently. Measuring current with a potential step is a simple experiment, however, the experiment only includes information about one potential.

A more common experiment is *cyclic voltammetry* (CV) which consists of an applied potential that is scanned within a potential window at a fixed rate while simultaneously measuring the current. The current is plotted against the potential to create a *voltammogram*. In Figure 8A two of these experiments have been performed with the compound Ferrocene which is known to have a Nernstian redox reaction (if you weep slow enough) as can be described by Equation 2.2.15. Ferrocene is also a common "reference" since it is said to have a very fixed formal potential invariant of the environment. (The shape of the CV looks a bit like a duck if you have some imagination.) A simulated voltammogram

can be created if only diffusion and a Nernstian boundary condition are considered, as shown in Figure 8B. This CV looks slightly different. The higher scan rate doesn't have the same shape, the potential of the reduction peak is closer to the oxidation peak. In the model the two peak potentials are the same for the two scan rates. Let's find out what these peaks describe and why my measurement on ferrocene diverges from the model.

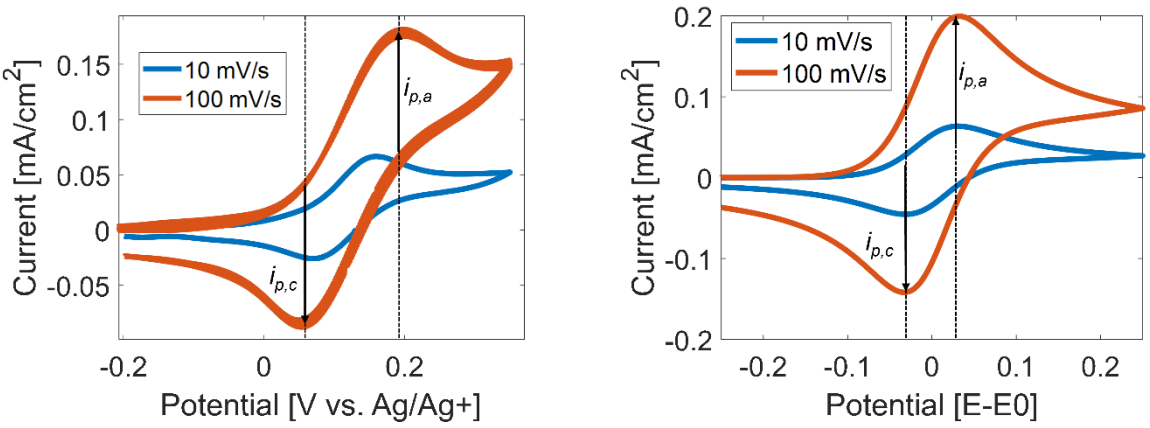

Figure 8 A) Collected CVs of 1 mM ferrocene in EtOH and 0.5 M TBAP. B) Simulated CVs with diffusion coefficient set at 1.5 cm^2/s and concentration set as 1 mM. The dashed lines indicate the location of the peak currents for the fast sweep. The arrows indicate the values of the peak currents measured from the onset of the wave.

Instead of simulating the CV we could try to solve it analytically. The problem of mathematically recreating the IV-curve can be formulated similarly as for the potential-dependent chronoamperometry above but with a time-dependent potential where v is the scan rate. Note that this is only valid for the first sweep in one direction. Solving this system of equations can be done analytically, although the final expression which relates the current to the potential contains is rather complex, tabulated values exists. Some highlights can be expressed rather easily. Finding the maximum current - the peak current - can be done by finding the maximum of the current expression which maximizes when the tabulated value equals 0.4463. The peak current is summarized in the Randle-Sevcik equation (Equation 2.2.23). As Nicholson and Shain were acquiring the solution to this problem, Randle and Sevcik first stated it.

$$I_p = 0.4463\, nFAc_0 \sqrt{\frac{nFDv}{RT}} \qquad 2.2.23$$

It could come as a surprise that the peak current increases with the scan rate. However, one point to keep in mind is that the current, once again, is a measure of flux. When a fast sweep is conducted the flux is required to be high to fulfill the Nernst equation. If the potential where the potential stops and reverse is enough below the formal potential (35/n mV) the height of the reverse cathodic peak current is equal to the anodic peak current. This we see for our example (Figure 8A). The difference in peak potentials (the distance between them) should be around 60 mV. This we don't see in our example (Figure 8A), the potential distance is larger than 60 mV which could mean that our system is not Nernstian. If it is known that the used electrochemical system behaves as this idealized example the formal potential could be obtained from the peak potentials. What you usually do is take the potential in the middle of the peaks - the half wave potential - as the formal potential. This is how you

use ferrocene as a reference. It is also common to use Randle-Sevcik equation to obtain the diffusion constant [31]. A simulation where the scan rate has been varied can be seen in Figure 9A and it can be seen that the potentials where the currents peak is independent of the scan rate but the peak current is proportional to the square root of the scan rate (Figure 9B). It should be noted that reactions are often much more complicated than what is stated in Equation 2.2.5 and the derived equations above are not strictly true for most physical systems. (Just because you have peaks in a CV doesn't matter that this equation can be used.) However, these simple examples give us a foundation to understanding what peaks represent when collecting voltammogram [31].

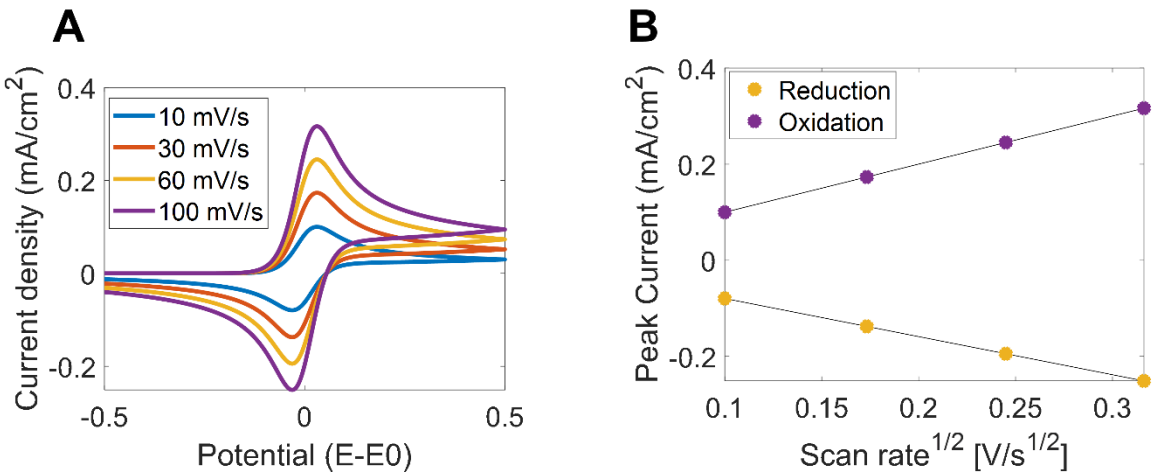

Figure 9 A) Simulations of CV diagrams for various scan rates. The concentration is 1 mM and the diffusion constant is 1.5E-5 cm2/s. B) The peak currents plotted against the square root of the scan rate displays a linear relationship.

Our last paragraph concluded that physical systems are usually far more complex than one electrochemical reaction, so we will now elaborate by adding a chemical step after the oxidation (Equation 2.2.24). This is not uncommon because there is a possibility that the oxidized species can chemically react with both the solvent and the salt, sometimes even the electrode. Impurities are also common culprits, and noteworthy are oxygen and water in organic solvents. A simple chemical step is a *first-order reaction* – the reaction rate depends on the concentration of the reactant (Equation 2.2.25). This reaction is called *EC*, where *E* is the electrochemical reaction and *C* is the chemical reaction and an endless combination exists of *E* and *C*. It is possible to derive formulas for how the current would trace with a potential step and for a cyclic voltammogram, however, it is enough to visually see how the voltammogram alters when this modification is added. In Figure 10 the reverse peak is diminished when the rate of the chemical step is increased because there is no product to re-oxidize. If the scan rate is increased the chemical reaction does not have enough time to convert the reductant and more of the reductant is available to be reoxidized, making the reverse peak current more like the initial sweep [31].

$$R \rightleftarrows O^+ + ne^-$$

$$O^+ \xrightarrow{k} N \qquad 2.2.24$$

$$\frac{\partial C_O}{\partial t} = -kC_O \qquad 2.2.25$$

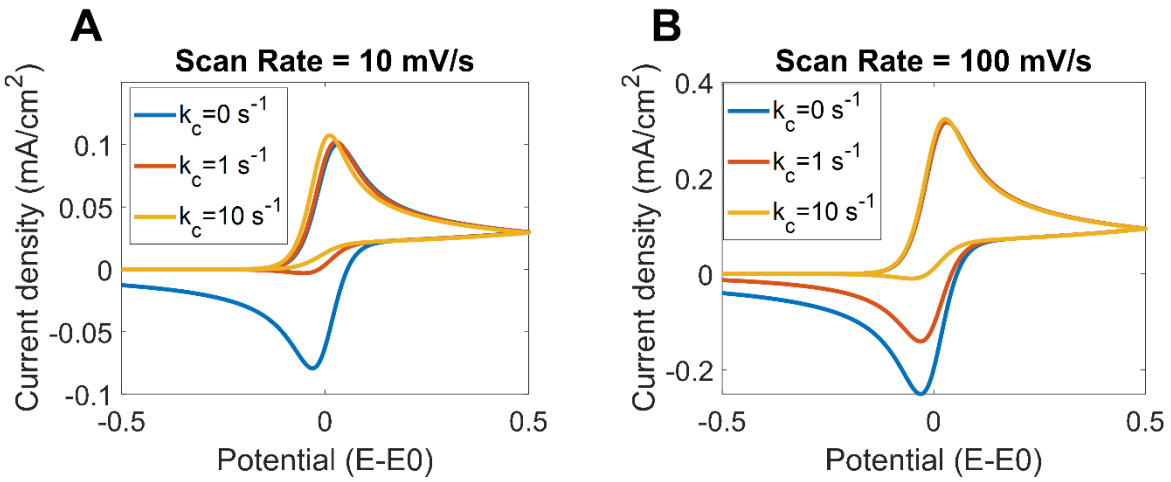

Figure 10 With a chemical step the reverse peaks diminish. For lower scan rates (A) no reverse peak can be seen but by increasing the scan rate B) the peak comes back for moderate reaction rates.

"When it comes to electrochemistry: All electrode-electrolyte interfaces are created equal" could be a quote from someone who has never experienced electrochemistry. Indeed, "nature" has a tendency to deviate from our models. Previously, the Nernst equation was derived from thermodynamics assigning the Fermi level in the electrode equal to the electrochemical potential for electrons in a metal. However, the Nernst equation does not include any information on how quickly electron transfer occurs. When a high-energy product, A, reacts and becomes B, with lower energy, *transition state theory* describes that for the reaction to take place there is a transitional state between A and B with higher energy. This energy barrier must be surpassed by A. The probability that this happens is proportional to the exponent of the 'energy hurdle' (divided by the thermal energy, *RT*) (Equation 2.2.26). The standard electrochemical reaction (Equation 2.2.5 $R \rightleftarrows O^{+} + ne^{-}$) can be described in this manner as well. In equilibrium – equal electrochemical potential – no **net** current flows and the rates are equal. The electrode potential is at the system's equilibrium potential. This potential is also the formal potential, $E^{0'}$. If a deviation from the equilibrium potential is applied, the free energy of the oxidized species (right-hand side) and the reductive species (left hand side) is shifted. The shift in energy is proportional to the voltage by Faraday's constant. Both new exponents have an additional factor; α – the symmetry factor or *transfer coefficient*. The net current is described in Equation 2.2.27 (reduction current minus the anodic current) where the currents are of first order kinetics (current is the rate of the concentration of oxidant which is proportional to the concentrations). The rate is proportional to the concentrations and two kinetic factors which are described in Equations 2.2.28 and 2.2.29. The standard rate constant, k_0, (also known as the heterogeneous rate constant) is a description of how 'fast' the reaction is. If the reaction rate (k_0) is high compared to the mass transport due to diffusion ($\sqrt{\frac{D}{\mathrm{RT/Fv}}}$) the system is once again Nernstian (thermodynamically reversible), and Equation 2.2.27 collapses to the Nernst equation. On the contrary, if the reaction rate is small compared to the mass transport due to diffusion, the reaction is thermodynamically irreversible, or sluggish [31]. There is a parameter which is used to decide if the reaction is sluggish or fast: $\Lambda = \frac{\mathrm{k_0}}{\sqrt{\frac{F}{RT}Dv}}$ (F is a Faradays constant, R is the gas constant, T is temperature, D is diffusion constant, and v is the scan rate). If Λ is above 10, the reaction is fast and if it below 0.01 it is sluggish. Between these values it is called quasi-reversible [31].

$$k = Ae^{-\frac{\Delta G}{RT}} \quad 2.2.26$$

$$I = nFA\,[C_{red}(x=0)\,k_b - C_{ox}(x=0)\,k_f] \quad 2.2.27$$

$$k_f = k_0 e^{-\alpha\frac{nF}{RT}(E-E_0)} \quad 2.2.28$$

$$k_b = k_0 e^{(1-\alpha)\frac{nF}{RT}(E-E_0)} \quad 2.2.29$$

Figure 11 illustrates how varying the heterogenous rate constant and transfer coefficient results in a peak separation with decreasing rate constant (k_0) and a slower reaction. (This could be the reason why the higher scan rates of ferrocene showed slightly higher peak separation in Figure 8A.) The symmetry factor, α, gives us information on which direction the reaction is 'favored'. When the value is 0.5 the reaction is symmetric which is translated into a symmetrical voltammogram. Deviations from 0.5 gives rise to a skewed voltammogram [31].

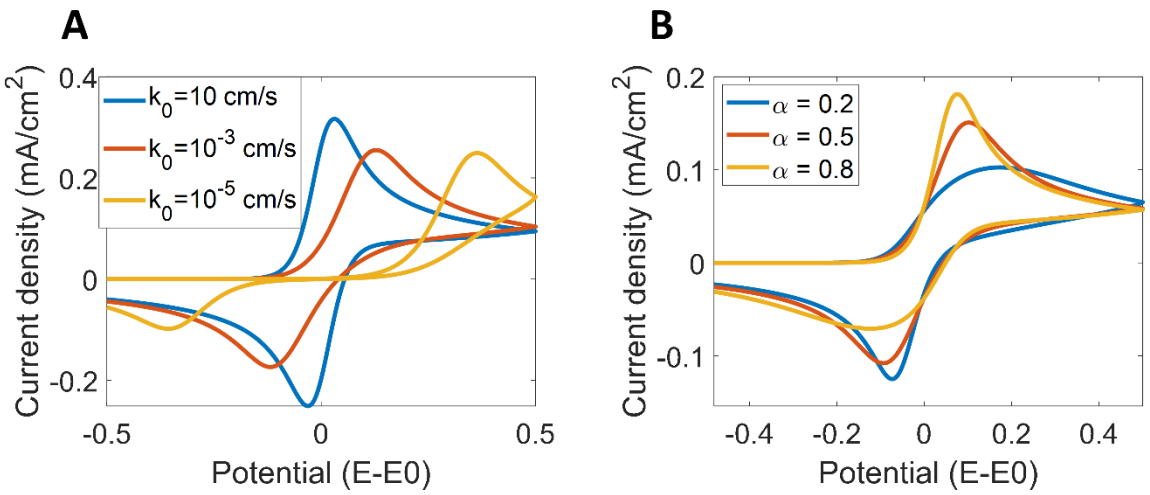

Figure 11 A) Peak separation can be seen when the standard rate constant decreases. B) How the symmetry factor alters the CV diagram.

The treatment of the heterogenous electron transfer described until now is named Butler-Volmer theory and shows the governing equations from macroscopical (thermodynamically) point of view with not as much insight into why the rate constant varies with different materials. Microscopical theories have been derived to further shed light on electron transfer where one of the most famous is Marcus-Hush theory which introduces an additional parameter – reorganizational energy - the energy required to reorganize the analyte and the solvent for electron transfer. In other theories, like Gerischer's, the density of states is used to determine how an electrode behaves based on the available states.

If the analyte is adsorbed on the electrode the equations gets reduced to only the boundary (Equation 2.2.30 and 2.2.31) [37, 38]. Here Γ_{ox} and Γ_{red} are the surface concentrations and k_f and k_b, are the previously introduced kinetic parameters (Equation 2.2.28 and 2.2.29). Solving the system of equations for a fast (not sluggish), symmetrical (α = 0.5) reaction with a maximum surface concentration of 10^{-9} mol/cm^2, different scan rates generate CV diagrams which can be seen in Figure

12A. the current is here defined as in Equation 2.2.32. There is no peak potential separation for a fast, symmetric reaction and the peak current is linear with the scan rate (Figure 12B) [31].

$$\frac{d\Gamma_{\mathrm{ox}}}{dt} = -k_f\Gamma_{\mathrm{ox}} + k_b\Gamma_{\mathrm{red}} \qquad 2.2.30$$

$$\frac{d\Gamma_{\mathrm{red}}}{dt} = +k_f\Gamma_{\mathrm{ox}} - k_b\Gamma_{\mathrm{red}} \qquad 2.2.31$$

$$I = -nFA\frac{d\Gamma_{\mathrm{ox}}}{dt} \qquad 2.2.32$$

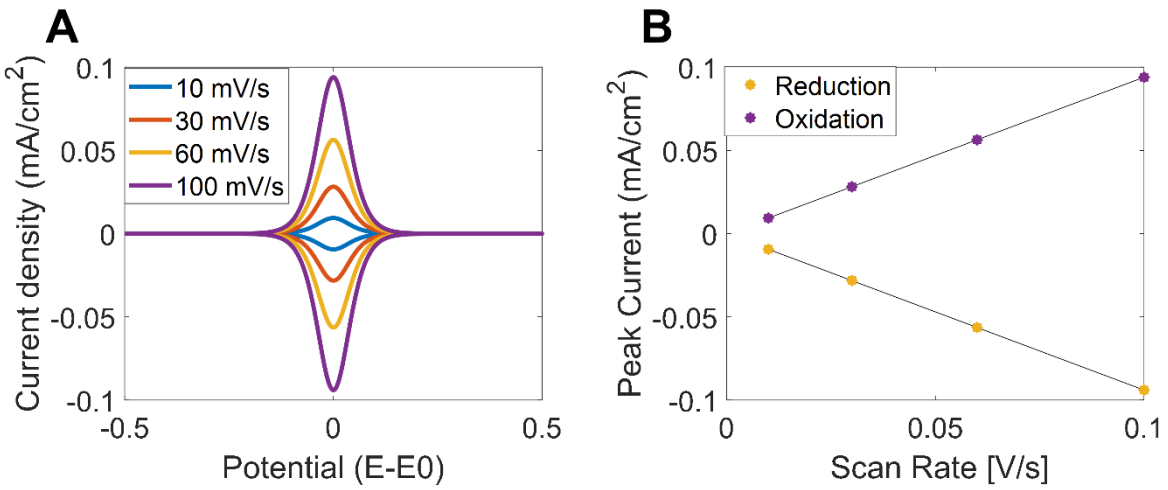

Figure 12 A) CVs of a surface adsorbed species with different scan rates. B) The peak current can be seen to vary linearly with the scan rate.

Three processes can prevent the poor electrochemist from obtaining values that fit into the ideal theories: Charging currents, uncompensated resistance, or the ideal derivations just don't fit the process. The last point is another example of how nature deviates from the models. Charging currents are due to a *double-layer* of ions charging up the electrode surface. This is a necessary step to polarize the electrode that makes the electric field localized at the double-layer. If no ions are present in the solvent, an electric field will stretch out throughout the solvent. The process of the double layer formation can be approximated with a capacitor and a resistor in series (RC-circuit). Figure 13A shows fast CVs on an Indium Tin Oxide (ITO) electrode in an electrolyte of propylene carbonate (PC) and 0.1 M lithium perchlorate ($LiClO_4$) together with a model of an RC-circuit (solid line) with a resistance of 200 Ω and 7.6 µF. The CV has a "box-like" appearance due to the capacitors ability to hold charge with the applied voltage and the plateau-current is linear with the scan rate, exactly as the peak current is linear for an adsorbed species. The capacitive contributions are also called *non-Faradic currents* [31].

Uncompensated resistance, R_u, is the resistance in the electrode and/or the electrolyte. When a current is running through the electrode due to a Faradic process on the electrode, the uncompensated resistance will have a current going through it as well. A voltage will be present over this resistance proportional to the current and the resistance, iR_u. Less of the applied potential will be applied to the electrode contra the reference. This results in a lower effective potential than desired. In Figure 13B the ramifications of this can be viewed where a similar CV as the simulation from Figure

8B can be viewed together with increasing uncompensated resistance. The peaks separate more and more and get a sluggish look. Increasing the current by e.g. increasing the scan rate will increase the iR_u even more and make the CV deviate even more from the ideal shape. This feature makes it complicates for us to draw conclusions regarding if the system is sluggish or fast.

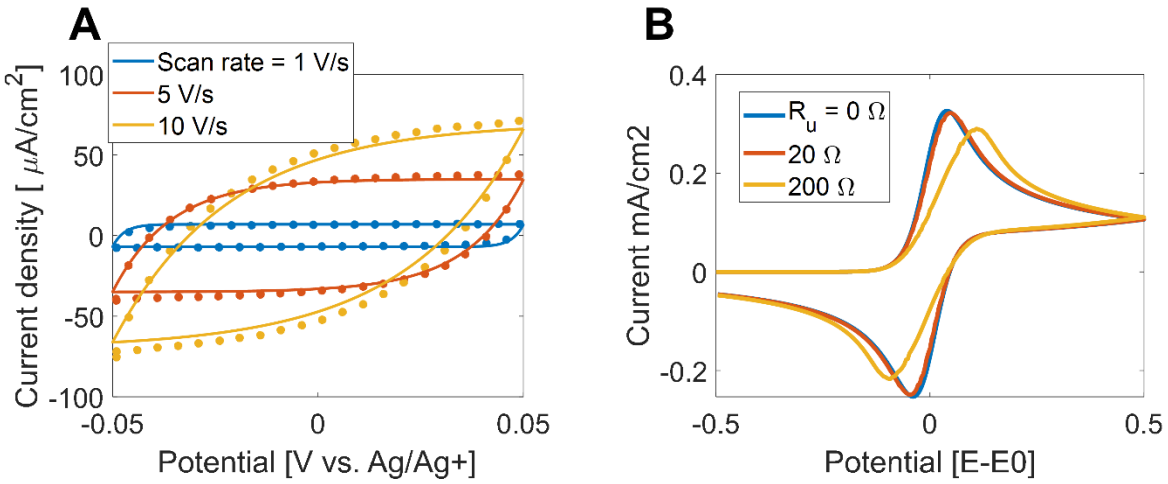

Figure 13 A) Fast CV sweeps on an ITO electrode exhibit a capacitive behavior (dotted) where a simulation of an RC-circuit (solid) fits perfectly with the parameters R = 200 Ω and C = 7 µF. B) How the uncompensated resistance affects the CV. Peak separation is visible with higher uncompensated resistance.

On the topic of approximating an electrochemical system with electronic components such as capacitors and resistors, there is a technique called *electrochemical impedance spectroscopy* (EIS). I briefly mentioned this technique because it is only briefly used. EIS can be used to approximate more than only the uncompensated resistance and the double layer charging of an electrochemical system. By applying a potential in the form of a sine wave with different frequencies, the response in the measured current can be used to further describe the system of electrical (-chemical) components.

There is a lot more to say, and write, about electrochemistry, and at the end of the next chapter we will go through how the electrochemistry of conjugated polymers behaves. They do not fall into the category of Faradic reactions, nor do they fall into the category of charging currents (unfortunately). Conjugated polymers exhibit more complex behaviors and use intercalation processes or pseudocapacitive behavior.

2.3 Conjugated polymer and electrochromism

Many authors begin similar sections as this by mentioning that in 2000 the Nobel Prize in Chemistry was awarded jointly to Alan J. Heeger, Alan G. MacDiarmid, and Hideki Shirakawa "for the discovery and development of conductive polymers" [39]. This section will discuss conjugated polymers, sometimes known solely as conductive polymers (even though polymers can be conductive without being conjugated). At the time of the Nobel Prize, conductive polymers had been researched for more than 30 years. Conjugated polymers have been found to be versatile material and can be used in many different applications ranging from synthetic metals to antistatic coatings. However, the focus here will be on their optical properties and how they can be tuned electrochemically to generate an effect called electrochromism.

This section has to include some quantum mechanics to explain organic chemistry and the phenomena that are observed. Briefly, electrons are described by *probability waves* – they are not in one definite position when they are moving but smeared out in space. There are fixed intervals for energy, so they cannot have whatever energy. As in previous sections, a short, idealized scenario will be used to lay the foundation for the material.

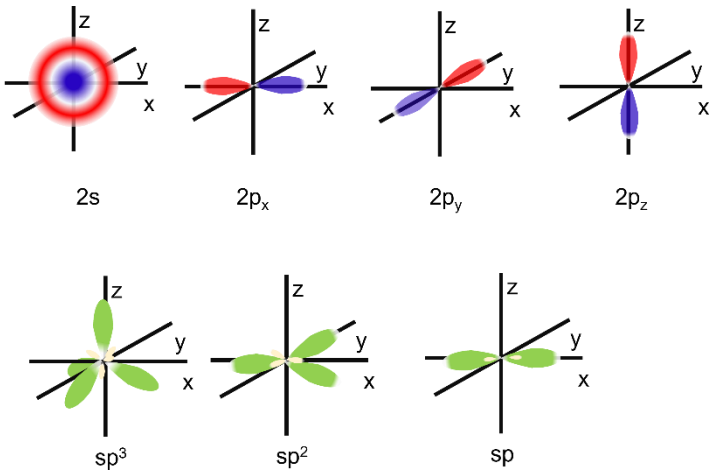

Figure 14 Top row: Orbitals of the valence electrons of carbon from the symmetric 2s to the three variations of the 2p-orbitals. The different shading of the 2p-orbitals represents the sign of the orbitals wavefunction. The bottom row: The three different hybridizations going from sp³ to sp² and finally sp.

Carbon is the backbone of a conjugated polymer, literally. Carbon has 6 electrons, each placed into an *atomic orbital* [40] – a tool to describe where electrons of a certain energy are allowed to exist. Electrons are not allowed to have the same state (with "state" being an abstract construction that contains all information such as energy, position etc.). Each atomic orbital can only possess 2 electrons each, one for each value of the intrinsic property *spin*. The lowest energy orbital is the 1s-orbital where 2 electrons are arranged. The second lowest energy orbital is the 2s orbital in which 2 electrons are situated. The 2 remaining electrons are placed into the 3 *degenerate* – equal energy-orbitals: $2p_x$, $2p_y$, or $2p_z$. However, the 2p orbitals can be mixed with the 2s orbital to create hybrid orbitals sp, sp^2, and sp^3, where the superscript indicates how many of the p-orbitals are included in the hybridized state. In Figure 14 the orbitals can be viewed.

Conjugate polymers have two 2p orbitals mixed with two 2s orbitals - sp^2 hybridization. One of the remaining electrons is placed in this sp^2 orbital, and the last is placed in the 2p orbital. When two atoms are in proximity they can be described by *molecular orbitals*. In the case of two carbon atoms bonded together where both are hybridized in sp^2-orbitals, two bonds will form. One bond is made by overlapping sp^2-orbitals, a σ-bond. The remaining p-orbitals will bond together and form a π-bond. Due to constructive or destructive interference, the molecular orbitals are split into *bonding,* σ and π, and *anti-bonding*, σ* and π*. Electrons are in the *bonding* orbitals with lower energy. The highest energy level which is occupied with electrons is called HOMO, the *highest occupied molecular orbital*. The lowest energy which is unoccupied is called LUMO, the *lowest unoccupied molecular orbital.* Note that LUMO is higher than HOMO [40-42]. This process can be viewed in Figure 15A. These two-valued

states are the results of two interacting waves could be regarded as constructive and destructive interference.

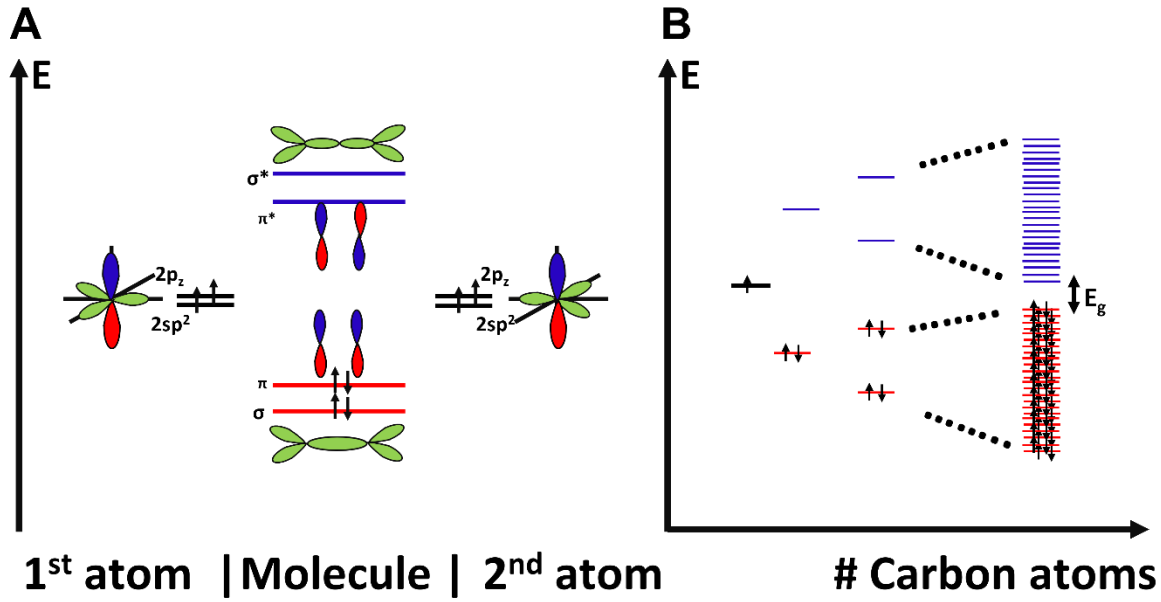

Figure 15 A) A molecular orbital forms from two atomic orbitals. The two atomic orbitals have one sp2 hybridization each which forms the bonding σ-bond with lower energy and the antibonding σ-bond with higher energy. The π-bond is formed by the $2p_z$-orbitals are, as the σ-bond, split into bonding and antibonding. B) Formation of the electronic-bands with increasing amount of carbon atoms each contributing with one electron in the $2p_z$-orbital.

When carbon atoms are added to a chain the energy levels will further split. In the case of very large molecules, or continuous materials, the states eventually merge into bands with an energy gap. The higher energy band is called the conduction *band* and is vacant for conjugated polymers, thus making its band edge the LUMO. In the lower energy band, electrons occupy the states, and HOMO is the edge of the *valence band*. The evolution of the energy states when carbon atoms are added can be viewed in Figure 15B, only the electrons in the 2p-orbital are shown [43].

This system is similar to the famous school problem of a *particle-in-a-box* which is used to introduce quantum mechanical concepts. One electron (our 2p-electron) is trapped in a potential well where it requires infinite energy to get out of it. The well have a certain width (our polymer length) and with the allowed energy levels are derived by solving *Shrödinger's equation*. The energy gap for such a system will be proportional to the number of electrons and to the inverse of the length squared. Thus, it disappears in the case of infinite length [40, 44].This does not happen in real life and there are severeal sources that cause a band gap. One source of the band gap is the bond length alternation [44] which sometimes are referred to as *Peierl's distortion*, or instability, which says that the spacing between the atoms in a one-dimensional crystal is not uniform but has two different values [40, 42, 45, 46]. Other sources of the finite band gap include the finite conjugation length, which can be explained by distortions in the chain such as twists which cause the polymer to not be planar - a requirement for orbital overlap and bonding. Another reason is a substitution of other atoms or molecular groups on the chain [44].

Figure 16A shows this alternation of the single and double bonds in the simplest conjugated polymer which is called "polyacetylene". The alternation of single and double bonds is what gives rise to a *conjugated* system. Polyacetylene is what is called the first generation of conjugated polymers. The second generation has more complex monomers with usually *heteroaromatic cycle compounds* (rings

that contain more than carbon). An example of this is polythiophene which can be seen in Figure 16B with the single and double bond alternations highlighted. Conjugation includes not only bond alternation, for example, but also the lone electron pair on the sulfur [47]. The monomers relevant to the thesis are also included (Figure 16C). There is a third generation which utilizes different monomers on the same chain to change the properties, such as the band gap, by what is called a "Donor-Acceptor" method [48].

The above discussion indicates that there is something significant about the band gap, which is true. It describes a lot of the properties of your material, or molecule, where it is usually referred to as the energy gap. If there is no band gap such that the valence and conduction bands are overlapping, the electrons that are at the edges are allowed to slightly increase or decrease their energy. An example of this is electric fields which can change the kinetic energy of the electrons. If the conduction band becomes occupied, the material conducts electricity and is a *conductor*. An example of this is metals. If there is a large band gap the applied electric field will not change the electrons' energy levels since there are no nearby available states to move into. This is why the material is an insulator. Dielectrics such as glass are common insulators, as are plastics, which are non-conjugated polymers. If the band gap is small the material is called a *semiconductor* and this is the class that some of the conjugated polymers belong to [45].

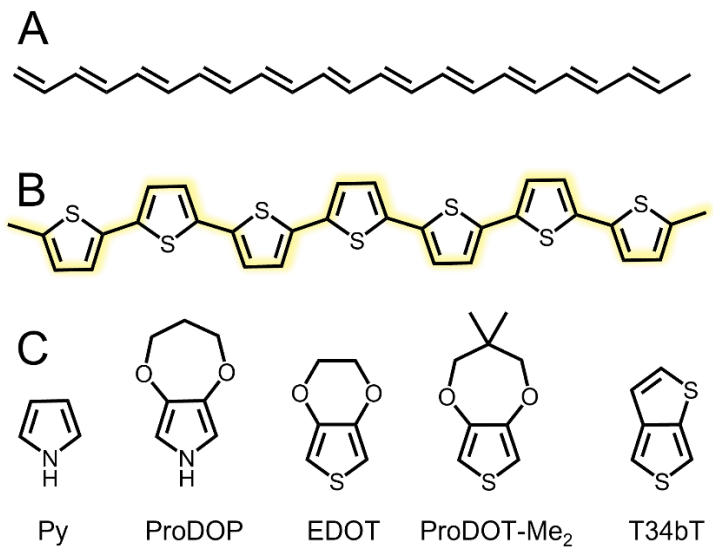

Figure 16 A) trans-polyacetylene B) Polythiophene C) remaining monomers relevant to this thesis.

Another feature of the band gap is that it absorbs light, or light of a certain energy is allowed to be absorbed if it has the same energy as the band gap [40] (even though the electronic and optical band gap isn't exactly identical [49]). The energy of the light is not determined by the intensity but the frequency. Now the photon comes in. A constant - Planck's constant - determines the relation between energy and frequency - $E = h\nu$. The electron in the valence band gets "promoted" to the conduction band when it absorbs light. When irradiated with equal energy light, the probability of electrons being in the conduction band increases. In the reversed case of this, electrons from the conduction band can drop down to the valence band and photons are emitted.

The charge distribution of electrons gives rise to a *dipole moment.* This is the charge difference times the distance between the positive and the negative poles. This determines which *transitions* are available. Electronic transitions are usually found in the visible spectra, where electrons are excited (promoted) into higher energy electron configurations. Other transitions such as *vibrational* – the molecule start to vibrate in a special fashion - are excited by lower energy infrared photons [50].

It is not only the *intramolecular* properties – the properties of one isolated polymer chain - that determine the properties of the material. In a solvent in which the polymer is not soluble to a high degree - a bad solvent - aggregates are formed. The polymer stacks together with other polymers in a crystalline, or semi-crystalline form, which also alters their properties. As a result of various stackings

of the polymer chains, the material has anisotropic (directional dependence) optical properties. Vibrations of the polymer change the electronic structure and thus also alter the dipole moment. Chain vibrations give rise to more possible optical transitions. This is why some polymers exhibit more than one absorption peak. This phenomenon is commonly known as Frank-Condon excitation [48, 51].

A lot of effort has been devoted to engineering the polymer's band gap. This has involved e.g. changing the rigidity of the polymer to render it more planar, changing the HOMO and LUMO of the monomer by introducing additional functional groups, etc. One application is to decrease the band gap to make synthetic metals and another purpose is to use it in optoelectronic devices such as photovoltaic solar cells or electroluminescence [44]. Polymers that absorbs light throughout the entire visible spectrum have also been developed [52, 53].

The band gap can be altered by oxidizing the polymer chain. By removing an electron from the polymer, a *radical cation* is generated in the polymer chain. This is similar to what happens in an inorganic semiconductor when it is p-doped, electrons are removed and what are called polarons are created. Thus, the word polaron is frequently used to describe the polymer cation. P-doping is usually also used to describe the oxidation process. If a radical anion can be formed by reduction, n-doping is used to describe this. Polarons are charged collective excitations trapped because of their own charge distorting the lattice. If an electron is added to the chain, it will change its surroundings. If a potential well is created and the electron is stuck there it is a negative polaron. As opposed to adding an electron, removing on electron leaves a positively charged hole. If this gets trapped in its well it is called a positive polaron [45, 54].

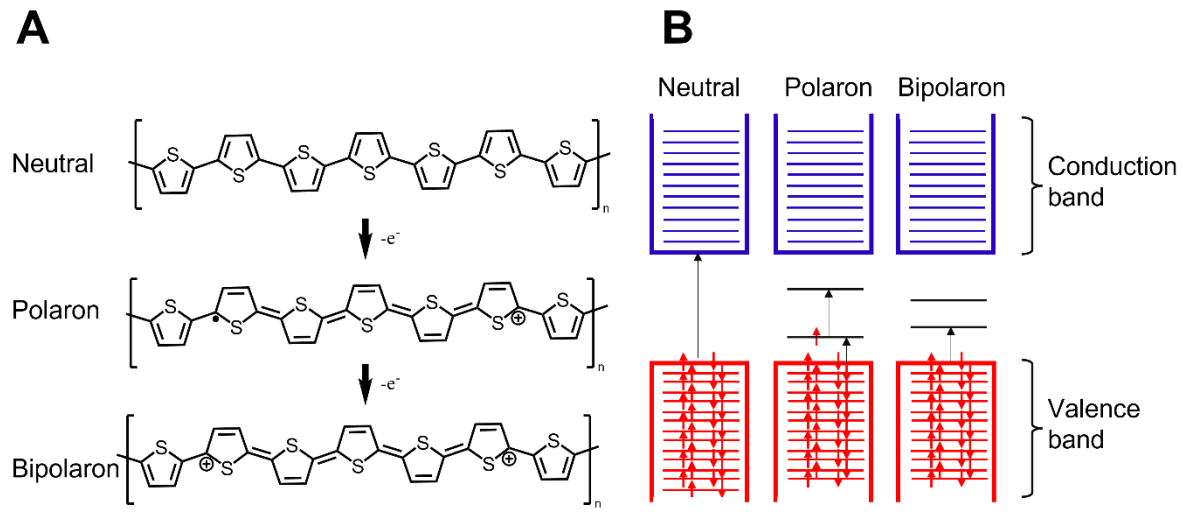

Figure 17 A) Polaron and bipolaron formation on a polythiophene chain. B) how the bandgap alters a polymer with oxidation and polaron / bipolaron formation.

In Figure 17A polythiophene can be viewed in its neutral state and together with the structure when it has lost one electron due to oxidation. A polaron is formed and is localized over ~4 monomer units. The chain of the alternated single and double bonds alters as well. Single bonds are now double bonds and vice versa (what was once a single bond is now a double bond). The first, neutral structure is called the *aromatic structure*. The oxidized structure is called the *quinoidal structure* because it resembles a compound known as quinine [45].

With the formation of a polarons, two additional energy states have shown up in the band gap. These levels have their lower value occupied by one electron. Early theoretical work showed that if further oxidation occurred and more polarons were produced, another quasi-particle called a bipolaron would

be energetically favorable. In the rederived band structure for this configuration, the two additional states in the band gap have moved further from the band edges but none of them are occupied. This process is displayed in Figure 17B where a neutral band structure is transformed into a polaronic and later into a bipolaronic. The black arrows show the transitions that are allowed by the traditional picture. Other transitions are *forbidden*. The bipolaronic structure of polythiophene can be seen at the bottom of Figure 17A [45, 47, 54]. In some cases at high doping levels, the polarons (or bipolarons) can create their own bands which can make the polymer a conductor if the fermi level is inside the band [45, 55].

Spectra of neutral PProDOT-Me_2 and PProDOP are shown in Figure 18A. When PProDOP is oxidized it can change from its pristine colored state to its transparent doped state (oxidation of PProDOT-Me_2 is not shown). The absorption does not disappear, but rather is shifted, or changed, into lower energy absorptions. At moderate levels of doping, the absorption peaks are traditionally associated with polarons, while the lower energy peaks are associated with bipolarons (not shown). This view has recently been challenged by Zozoulenko et al. [56] that show a more nuanced picture in which polarons and bipolarons do not exclusively absorb in different spectral regions for PEDOT [56].

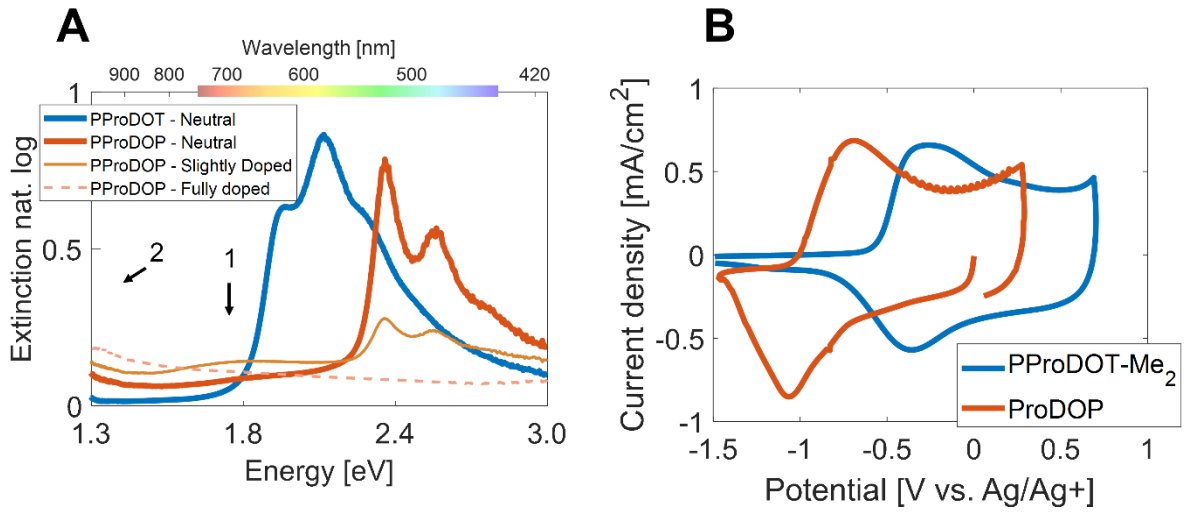

Figure 18 A) Optical spectra of the polymers PProDOT-Me_2 and PProDOP. The neutral polymer exhibit absorption in the visible spectra while the doped (shown for PProDOP) displays an additional peak at moderate levels (1) and with higher doping levels only a second peak (2) which is outside of the figure, sorry. B) Cyclic voltammetry for both polymers.

The positively charged polymer chain gets balanced out on the charged sites by negatively charged anions to create a polymer-ion complex [45]. Oxidation and reduction can be done by adding oxidizing or reducing agents to the polymer, but they can also be electrochemically oxidized or reduced. This process is reversible and gives rise to the electrochromic effect: applying a potential and changing the color. The polymer is usually coated onto an electrically conductive electrode such as the transparent conductor indium tin oxide (ITO) or gold. Figure 18B shows CV scans for PProDOT-Me2 and PProDOP. From this we could also get the oxidation potential as ~-0.5 V for PProDOT-Me_2 and ~-1 V for PProDOP.

The CV can be modeled by a pure *faradic reaction* of the adsorbed polymer. This would generate a symmetric CV and the peak current would be proportional to the scan rate. This can occur in some cases, such as when the film is thin. For thicker films the film cannot be regarded as being on the surface anymore and the ion movement in the film is a limiting factor. There is also a plateau after the peak (to the right), which indicates capacitive behavior. If adding a capacitive element to the adsorbed faradic species model can be further improved [57] but cannot explain why the CV possesses what

seems to be many different overlapping peaks. This would suggest that a model that uses many redox couples should be applied [58].

Another model of the doping process is that if a neutral polymer coated on an electrode that is positively polarized, a double layer is formed on the electrolyte-polymer interface. Polarons are formed on the polymer chain and creates a polaron-ion pair. These pairs later diffuse through the polymer film [59]. By using the *Nernst-Planck equation* together with an equation that relates the charge density to the electric field – the Poisson *equation* - a model for PEDOT:PSS has been shown to simulate the CV pretty well [60]. Other methods introduce *conformational relaxation* – which takes into account the energy required for the ions to open up the polymer film to pass through it. This method has been shown to simulate a chronoamperogram (constant potential) pretty well [61]. The ESCR-model (electrochemically stimulated conformational relaxation) [62] has been further improved by including ion movement due to migration [63].

As if it isn't complicated enough yet, the polymer can also undergo two processes if it gets reduced in its oxidized state with anions intercalated. 1) The polymer gets neutrally charged by expelling the anions out of the film or 2) the polymer gets neutral by admitting cations which create ion-pairs. If the anion in the film is big and bulky it can get stuck and it is easier to admit the cations instead of expelling the anions [58]. A feature of cation doping is that it can cause a volume change in the polymer film. This is because the cation is 'dragging' the solvent into the film. This makes these systems candidates for microactuators [64] and artificial muscles [65]. An example of this is polypyrrole in water with either dodecylbenzenesulfonate (DBS^-) or tosylate (Tos^-) as bulky anions. Smaller anions, as previously mentioned, will undergo anion doping and examples of these are perchlorate (ClO_4^-) and hexafluorophosphate (PF_6^-) [62].

Electrochromism of conjugated polymers can be divided into two categories: cathodically coloring – absorbing light when reduced, and anodically coloring – absorbing light while oxidized. PProDOP, PEDOT, and PProDOT-Me_2 are cathodically colored, whereas PPy is anodically colored. Once again, the band gap is what determines this property. Anodically colored polymers occur when the band gap is large, while cathodically colored polymers occur when the band gap is small [66]. There are also polymers that exhibits low or very mild electrochromism and are transparent in both states [67], one of which is PT34bT [68]. Different polymers differ not only in color, but also in how much they can absorb. This is particularly relevant for electrochromism since you want your material to be able to switch from a very dark, or saturated, state to a very transparent state. The difference between the two states is what is referred to as optical contrast. This value is not invariant of the thickness of the film. If a very thick layer would be used it would probably be non-transparent in both its oxidized and reduced state. In the same way, a very thin layer would be transparent in both states. There is a sweet spot for the thickness to achieve the highest contrast. PProDOT-Me_2 has higher optical contrast than both PEDOT and PPy and the absorption is located in the middle of the visible spectrum [69-71]. PProDOP exhibits a high contrast, however, its spectra are shifted, so the neutral state appears orange [72].

Enough talk about the properties. How do you prepare them? Both spin coating and spray coating [52] can be used to deposit materials on a surface. Screen printing has also been used to manufacture large areas on flexible plastic [73]. In these cases the polymers are already synthesized from monomers and dispersed in solvents. Another way of synthesizing a polymer film is directly from the monomer. One such technique is vapor phase polymerization [74] where an oxidant is coated on a substrate and exposed to monomer vapor. A popular method, and the method used for the rest of the thesis, is

electropolymerization [75, 76]. This method involves electrochemistry. The monomer is dissolved in an electrolyte and an anodic potential is applied to an electrode. Once you have performed the correct procedures, they begin to grow on the surface. (The correct procedure typically involves "failing to electropolymerize" multiple times before.) The mechanism of how the polymer is synthesized from the monomer is shown in Figure 19. There are various suggestions of different mechanisms but the one that has been generally accepted is called the Diaz *mechanism* [77]. The mechanism is derived for polypyrrole but is similar for other polymers.

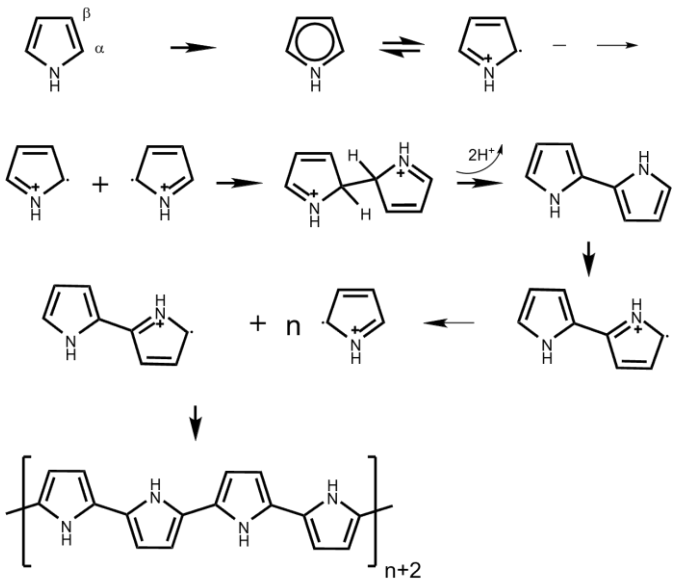

Figure 19 the Diaz's mechanism for electropolymerization. Explanation is in the main text.

First the monomer becomes oxidized and forms a cation radical. The radical can be on all positions but the most stable is the α position

Two of these radicals dimerize and stabilize by losing 2 protons

The dimer gets oxidized to create a cation radical which, again, can form a bond with another radical monomer.

The steps repeats and a polymer, or shorter chains called oligomers, are formed.

In some cases the polymerization can propagate at the β position and create a branched polymer chain [64]. In other cases, non-conjugated polymers can be formed if the proton content is too high [78].

Why the polymer sticks to the surface is still a mystery, at least for me. It is not bonded since it can be easily removed by a paper wipe, so it is most likely a *physisorption* – not chemically bonded but adhered due to other, physical mechanisms.

This concludes the section regarding polymers. They can be built by electrochemical oxidation on an electrode. They absorb light because of their electron structure. The electron structure can be changed by oxidizing the polymer, thereby making it change color.

2.4 Other electrochromic materials and graphical display

Electrochromism is the property of a material to change its color with an applied voltage, so it is not surprising that there are other categories than conjugated polymers. The material is coated on an electrode that is immersed in an electrolyte, or the material is directly dissolved in the electrolyte. The material changes its color during oxidation and reduction. Some other examples are metal oxides, viologens, and Prussian Blue [11, 12].

Apart from polymers, tungsten trioxide (WO_3) has been used in this work. Most importantly, contrary to conjugated polymers, any kind of work regarding WO_3 has yet to win a Nobel Prize. WO_3 is one of the most common electrochromic materials available today and even though it has been around for a very long time the cause of the coloration is still not fully understood. However, there are some theories. Originally the material is transparent but while reduced in an electrolyte containing protons or lithium ions the ions intercalate and color the material blue. The color is thought to emerge from polarons that alter the band gap. WO_3 is commonly deposited by reactive *sputtering*. However, it can also be electrodeposited or spin coated from a ready solution [79].

All electrochromic materials have a drawback which is their lifetime. As a result of coloration-decoloration cycles, the material degrades and the contrast weakens. For conjugated polymers it is thought that overoxidation is a contributor to degradation [80, 81]. Another cause is delamination of the film from the electrode subsequent to the stresses building up with the accompanying volume change of the redox cycles [82]. Utilizing special electrolytes, *ionic liquids* – a pure salt that is liquid at room temperature - one million switches have been achieved [83]. Recently that number was increased one order of magnitude by changing the configuration of the electrodes [84]

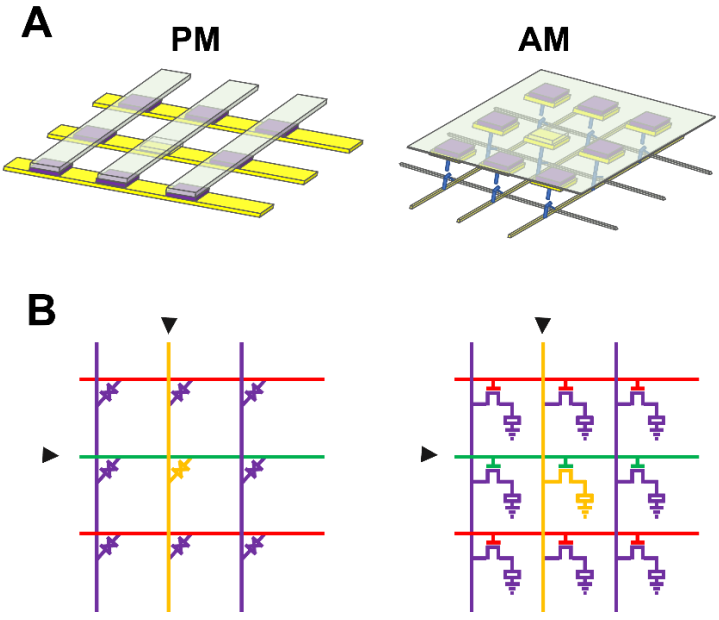

Figure 20 A) Visualization of a 3x3 passive and active -matrix with the middle pixel turned ON. B) Schematic of the passive and active matrices. The pixels in the PM is shown as diodes.

Let's assume we know how to make a material switch colors in an electrochemical cell. How do we make a display out of this? The term display usually refers to a device that can show any image at any time. There are more rudimentary displays such as the *7-segment display* which only has 7 pixels and is used to display numbers. (You might remember them from some old calculators.) A true graphical display is made by a grid of pixels that can have their optical properties adjusted individually. In the case of the 7-segment display, each electrode can be contacted individually but for a graphical display the number of pixels is hundreds of thousands and it becomes cumbersome to make a contact for each pixel. What is commonly done is to use a *matrix scheme* such as an *active matrix* (AM) or *passive matrix* (PM). In your smartphone specifications, you might have seen an "AMOLED", which is an active-matrix organic light-emitting diode. The active matrix technology utilizes *thin film transistors* (TFT) to block signals to a line of pixels. In Figure 20A a schematic can be seen where each pixel has its own transistor. Each row is connected

to the *gate* of the transistor – the connection that controls whether the transistor is open or closed. Each column is connected to the *source* – the contact that receives the signal. A channel connects this contact to the drain where the pixel is located. The gate controls the resistance of this channel. To update an image all the transistors in every row except one are closed. Signals are sent through source lines to only reach the pixels on open rows. The transistors on this row are now closed, and another row is opened. For a video display, each row must be updated at least 24 times a second. If there are 240 rows each line receives an allocated pulse time of around 0.2 ms. This is not enough time for many materials to respond. To solve this an additional storage-capacitor is incorporated in parallel with the material. The storage capacitor can then continue to switch the material after the row has received its allocated pulse time. The schematic in Figure 20B only shows the basic features, various configurations of AM exists: LCD, for example, are driven by an electric field while OLED is driven by a current. The difference require different architecture for optimal driving [18]. Bao et al. recently built their own TFT-array and displayed how conjugated polymers exhibit both electrochromism and actuation on individual pixels [85].

In the passive matrix configuration, no transistors are used. The electrodes are stripes (schematic in Figure 20B), and two stripes (counter and working electrode) are perpendicular to each other with separated electro-optical materials or stacking e.g. conjugated polymers and electrolyte in between the crossing points. If one pixel should be addressed a voltage is applied to that specific row and column and the rest of the rows and columns are set to another value, we will use zero in an example for simplicity. A disadvantage of this technique is that other pixels also get an unwanted voltage which can cause *crosstalk* – the neighboring pixels also change color when a certain pixel is addressed. It is tempting to leave the unaddressed rows and columns at "open circuit", or "floating". This means that they are disconnected. This configuration have another kind of crosstalk associated with it. Even though it appears that only one pixel is addressed, current can pass trough the remaining pixels as well. This can give rise to crosstalk [86]. In thesis both rows and columns are always biased with a voltage.

Designing passive matrix configuration without crosstalk puts some demands on the materials. Liquid crystal display (LCD) was a common display technology that used PM configurations (AM technology is nearly exclusively used today). Liquid crystals work by twisting the light inside two perpendicular polarizers. The light is twisted with an applied electric field and to be employed in a PM-configuration the electro-optical (EO) curve (how the transmission changes with applied voltage) needs to be non-linear and have a *threshold*. For an electrochromic passive matrix, it is similar but not exactly equivalent. An example will be provided now to introduce this hypothesis.

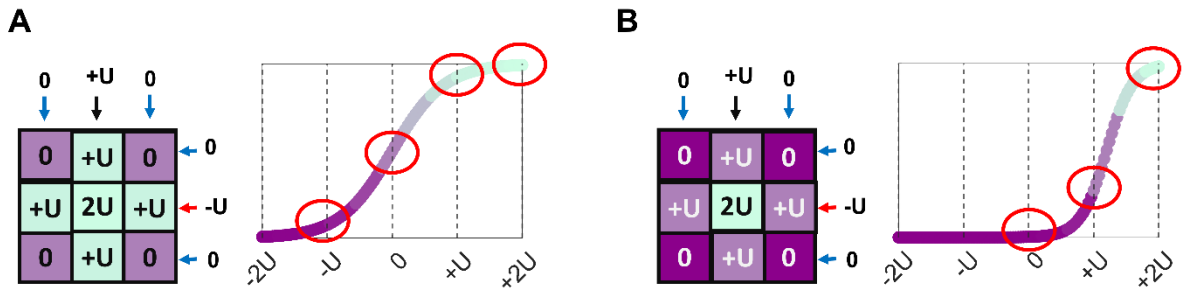

Figure 21 The middle pixel is being addressed. A) If the EO curve does not have enough threshold, crosstalk will be present. B) If the EO curve is steep (have a threshold) the crosstalk can be mitigated. The red circles indicates the location on the EO curve for the applied voltages.

In Figure 21A we assume that the middle pixel is supposed to be addressed. This is done by applying -U to the middle column and +U to the middle row which results in a +2U voltage over the middle pixel. The EO-curves +2U occur in a bright state as shown in the figure. However, there is a lot of crosstalk since the remaining pixels get a potential of +U or 0 which also results in a color change. By steepening the EO-curve, this can to some extent be mitigated. If the same potentials are applied Figure 21B shows the results with the steepened curve. The crosstalk voltages are still present but do not change the color as much as before.

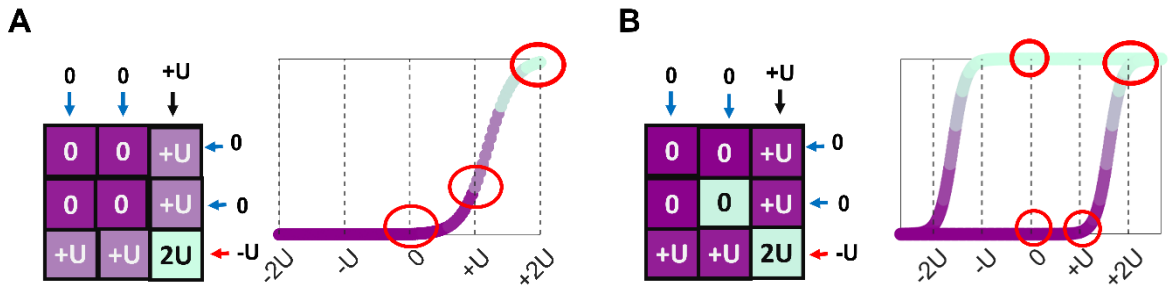

Figure 22 Bottom right pixel is being addressed. A) Addressing subsequent pixels could erase the previously addressed pixels due to the crosstalk voltages. B) By having a box-like shape of the EO curve the crosstalk voltages does not have a fixed state but can either be dark or bright. The previous state is retained when the crosstalk voltages are applied.

In Figure 22A we move on to try to address the bottom right corner. -U is applied to the rightmost column and +U is applied to the bottom row resulting in a +2U in the right bottom corner. The pixel switches as desired but what we also can see is that the middle pixel has turned dark again. Because of crosstalk, the previous bright state has been erased. In Figure 22B we alter the EO-curve to solve this problem by having a box-like shape. If the voltage changes from -2U to 0 the pixel remains in its dark state. If the voltage changes from +2U to 0 the pixel will remain in its bright state. If the voltage is swept between -2U and +2U, it will generate a counter-clockwise direction in the EO-curve, resulting in pixels with "memory ". One way of getting this box-like shape is to introduce hysteresis. The crosstalk voltages are half of the applied voltage and thus this configuration are named the V/2-system. However, some EO-curves can look more sinister than the curve in Figure 22B.

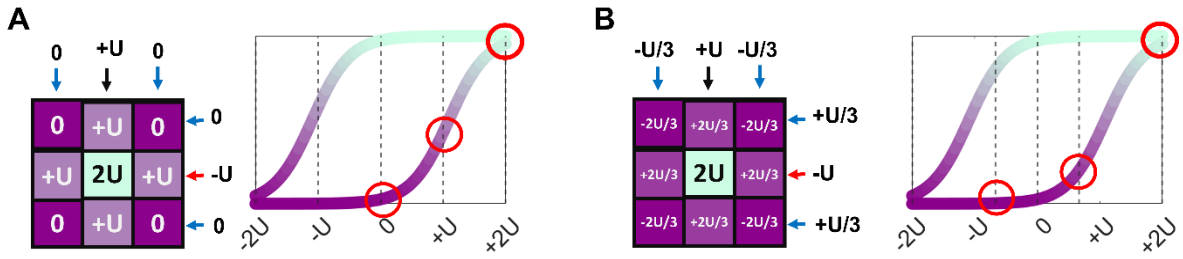

Figure 23 The middle pixel is being addressed. A) A box-like shape with not steep enough curves still can possess crosstalk. B) Crosstalk can be mitigated by reducing the value of the crosstalk voltages. This is done by using the V/3 system. Reversing the polarization of all the potentials will address the middle pixel to obtain a dark state (-2U).

In Figure 23A we can, again, see the ramifications of not having a steep enough curve. The crosstalk voltages (±U) are laying in between bright and dark. Instead of applying a constant zero (0 U) on the non-selected columns and rows, crosstalk voltages can be "pushed" in toward the zero. Figure 23B shows the crosstalk voltages being ±0.66 U by using ±0.33 U on the unselected rows and columns. This is called the V/3 system since the crosstalk is one third of the applied voltage (2U/3 = 0.66 U). One issue with the V/3 system is that dark (-2U) and bright (+2U) cannot be addressed at the same time

since the unselected rows and columns do not have the same applied potential. When addressing a pixel to its dark state (-2U) the unselected rows need to change its polarity as well (from -1/3U to +1/3U).

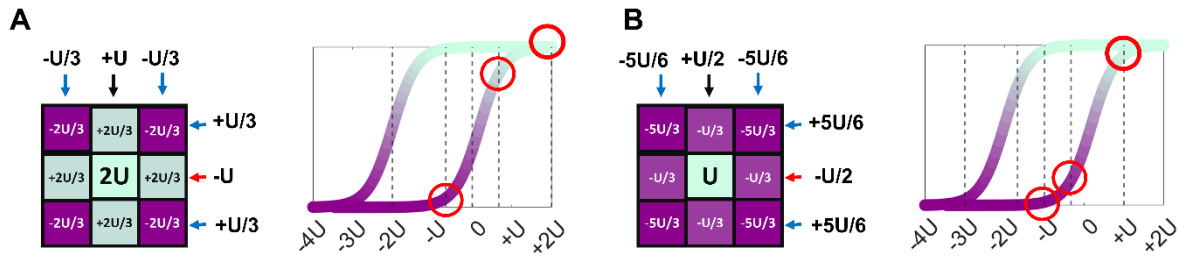

Figure 24 The middle pixel is being addressed. A) If the EO curve is not centered around the zero (0) but shifted crosstalk will still be present. B) By adjusting the potentials the crosstalk voltages can be shifted as well.

Figure 24A shows the same EO-curve that is not centered around 0 V but shifted 1 U to the left. Clearly, the same potentials cannot be used. Instead of using addressing voltages -2U to +2U, we shift them by -1 U to -3U and + 1U, respectively. In Figure 24B the bright addressing voltage is now +U by applying +U/2 on the column and -U/2 on the row. A potential of ±0.83 U are applied to the remaining columns and rows. The crosstalk voltages are now -U/3 and -5U/3 (-0.33U and -1.66U).

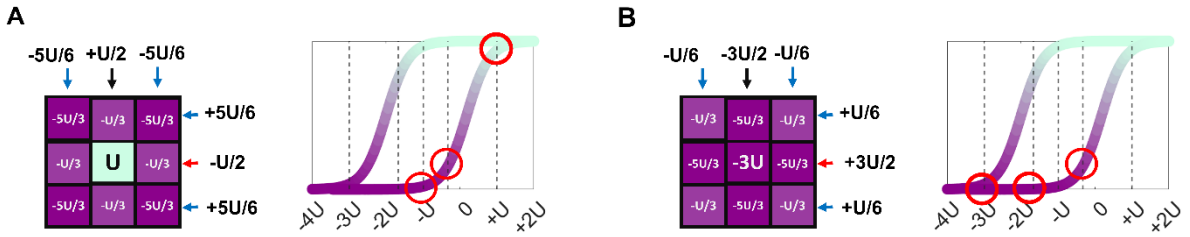

Figure 25 The middle pixel is being addressed. Having a shifted EO curve relative to the zero requires the values of the potentials for the dark state and bright state to be different. Only reversing the polarity is not feasible.

It is not possible to only reverse the polarity of all applied potentials in Figure 24B to address the middle pixel to its dark state. To receive a voltage of -3U on the middle pixel ±1.5 U should be applied to the row and column (Figure 25B). The unselected columns and rows are biased with ±0.166 U to make the remaining, unaddressed pixels receive the crosstalk voltages of -U/3 and -5U/3 (-0.33U and -1.66U).

The transmission of electrochromic materials is sigmoidal against the applied potential (see Results). This is also how the charge (integrated current) depends on the potential for a surface-adsorbed species. However, there is no hysteresis if the reaction is Nernstian (reversible, fast, non-sluggish). If, however, the reaction is sluggish the current peaks will separate with fast enough sweeps, and hysteresis is introduced.

The previous discussion regarding electrochemistry and electrochemistry of conjugated polymers only discussed one electrode. However, to get a current the circuit has to be closed and another electrode is required. For measuring, or applying, a potential the Ag/Ag+ was used as a reference but usually electrochromic devices use a 2-electrode setup with the counter electrode acting as reference. An electrochromic device consists of 5 layers: the working electrode (WE), the electrochromic material, an electrolyte, an *ion-storage-layer* and, and the counter electrode (CE). The ion-storage layer is

usually present to balance the charge. In order for the electrochromic material to be reduced, something must be oxidized. When the electrochromic material is reducing, a current pass through both the WE and the CE. If there is no ion-storage layer, and the CE and the WE have the same area, the only current that can come from the counter electrode is due to double-layer formation which is usually much less than the current (and charge) that the electrochromic material requires. If the working electrode is cathodically colored, coating the counter electrode with an anodically coloring material is an elegant solution. Then they will switch together to colored or bleached. Another way is to use a material that is transparent in both states such as the colorless polymers briefly mentioned in the previous chapter [87].

To a first approximation, the electrochromic effect is determined by the amount of colored material (reduced in most instances) and bleached material (oxidized). This also suggests that the absorbance change is dependent on the amount of charge that has been used in reduction or oxidation. And sure enough, one parameter to characterize an electrochromic material is the *coloration efficiency* – the difference in optical density (which is the logarithm of intensity ratio) over the charge consumption [88]. (How much bang you get for your buck.) In theory, it should be independent on the amount of material (though different for each wavelength) and also a constant. However, the change in absorbance is usually not constant with the amount of injected charge but decreases for high values of injected charge. Thus, the coloration efficiency decreases as well.

The current flowing through the counter electrode has to be the same as the current flowing through the working electrode. If the counter electrode has something that resembles a sluggish reaction, hysteresis would be introduced. A previous example of this involved using PEDOT:PSS as the working electrode and electrochromic material with a counter electrode made of carbon paste. In combination with a polyelectrolyte, this generated the desired box-shape EO-curve, which could be converted into passive matrices [89, 90].

Beni. G. at Bells Laboratory laid out the theoretical framework for a similar configuration where a “short circuit memory” is speculated to be required for an electrochromic passive matrix. This is argued to be achieved by having a “*free energy barrier”.* As an example, an ion intercalating into a metal oxide is presented. A careful selection of electrolytes is believed to increase reorganizational energy and thus the energy barrier [91]. One year later another paper with an example was published but with the “hysterectic” material coated on the counter electrode, however, a passive matrix which proves the function was not realized [92].

The electrochromic material viologen has previously been used to produce a 3x3 passive matrix [86]. This is, however, used in "open-circuit" mode. Non-addressed rows and columns are disconnected - also known as floating rows and columns. This still requires the electrochromic device to have some non-linearities. If the middle pixel in a 3x3 matrix is addressed within the "open-circuit" mode, the remaining pixels will eventually be addressed with 1/3 the of the applied voltage. Hysteresis is not present in this electrochromic device. Aliev et al. used WO_3 with TiO_2 as a counter electrode and a 0.2 Li_2O–0.2 CeO_2–0.6 SiO_2 layer coated on top of WO_3 to increase the non-linear electrochromic effect. A 7x7 matrix is only simulated and it is described how it would function in “open circuit” mode [93]. Edwards uses a hybrid viologen-TiO_2 material with a ferrocene couple at the counter electrode as ion storage. All pixels are addressed with a potential and pixels in a 3x3 matrix can be independently controlled [94].

2.5 Characterization parameters

This section summarizes some parameters which are being used throughout this thesis. **Contrast** is the difference in either transmission or reflection between the bleached and the colored state: $\Delta T = T_{bright} - T_{dark}$. This is specified at a certain wavelength, usually where the contrast is the greatest. An example can be seen in Figure 26A. **Switching time** is the time to reach 95% of the full contrast of a switch (Figure 26B). Sometimes "switching speed" is mentioned but not measured. **Bistability** is the time an applied state will retain with no applied potential (Figure 26C). In the same way as for switching time, a percentage can be assigned to quantify the bistability e.g. 11 seconds for the colored state until the intensity have increased to 10% of the full contrast. Out of these three parameters contrast have the most significance since it is a direct measure on how good an electrochromic material is at being electrochromic.

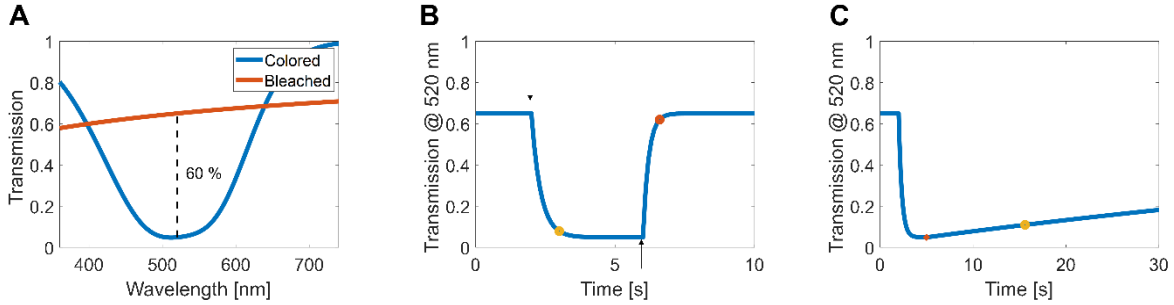

Figure 26 A) An example of two spectra of the same electrochromic material. One spectrum is on colored state and one is in bleached state. The contrast is defined as the difference in either transmission or reflection at a specific wavelength. B) An example of switching of an electrochromic material. One wavelength is tracked. The arrows indicate when a different potential is applied. The rings indicates where 95% of the full contrast have been reached. C) An example of how bistability can be measured. A potential is applied to until max contrast has been reached. The potential is then removed (orange ring) and transmission or reflection is measured. The yellow ring indicates where the increase in transmission is above 10% of the full contrast.

To quantify the "color" of a spectrum it is converted to the CIE 1931 color space. This is done by Multiplying the spectrum with one of the three color-matching functions, $\bar{x}, \bar{y}$ and $\bar{z}$. These represent the eyes' sensitivity to different wavelengths. Three *tristimulus values*, Z,Y, and Z are obtained by integrating the visible spectra. How to obtain X is shown in Equation 2.5.1.

$$X = \frac{\int_{\lambda=360nm}^{740nm} R(\lambda)\,\bar{x}(\lambda)\,d\lambda}{\int_{\lambda=360nm}^{740nm} \bar{y}(\lambda)\,d\lambda} \qquad 2.5.1$$

The remaining two, Y and Z, are calculated analogously. A *standard illuminant spectrum* is sometimes included by multiplying it with the spectrum. This function contains information about the lighting conditions. The tristimulus values can be transformed to lowercase x, and y by normalizing the capital ones (X, Y) with the sum of all three values: $x = \frac{X}{X+Y+Z}, y = \frac{Y}{X+Y+Z}$.

Two example spectra can be viewed in Figure 27A, both spectra are converted to the xy values. These values can be plotted in the 2D CIE diagram, where a saturated color is ending up at the edge, far away from the *white point* (Figure 27B). However, highly saturated color gives low overall reflection. The tristimulus value, Y, is used to quantify how bright the reflection is. The XYZ can also be transformed into other color spaces such as CIELab and RGB. The latter can be used to create the pseudo color which is displayed in plots [95, 96].

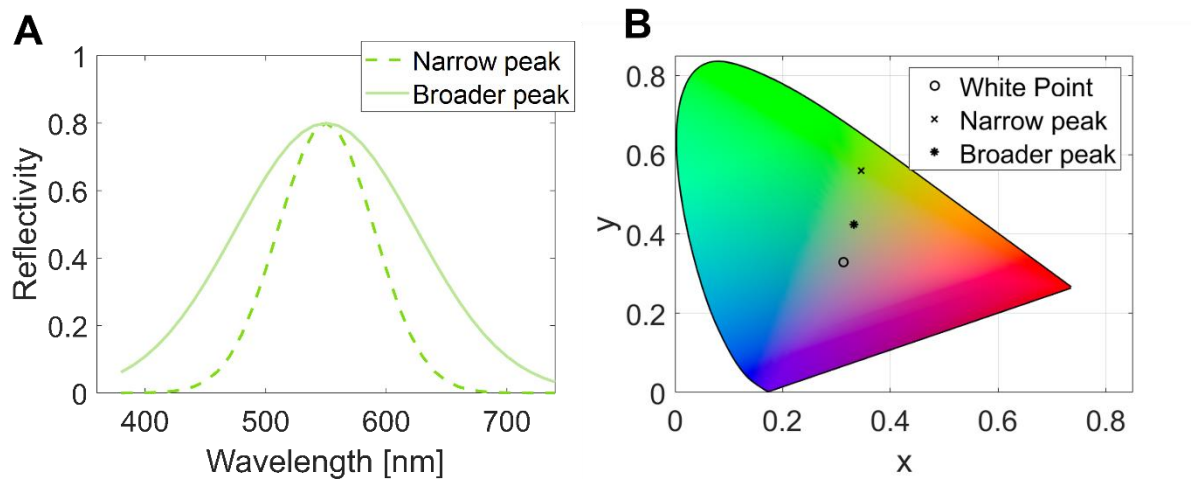

Figure 27 A) Two example spectra centered around 550 nm. A narrower peak (--) reflects less light while a broader peak (-) reflects more light. The color of the spectra lines is the corresponding 'pseudo-colors' for the spectra generated by converting the XYZ values to sRGB. B) Corresponding xy-graph for the spectra to the left with the white point (o). Note the narrow peaks point (X) is further from the white point than the broader peak (*) and thus has a higher chromaticity. The example spectra are generated by a computer.

3 Methods

3.1 Fabrication of plasmonic metasurfaces and thin film substrates

All plasmonic metasurfaces and bare gold substrates (20 or 100 nm) were done in "the clean room" MC2 at Chalmers. I (the author) did not have access to the clean room, so I did not perform nanofabrication by evaporation or sputtering. [3]

The plasmonic structural colors are made by first depositing an aluminum mirror on glass. Around 100 nm are deposited by physical vapor deposition. The spacer layer, aluminum oxide, is evaporated directly on the mirror. The plasmonic effect from nanoholes is not desired on the red pixel as it reduces color quality, so 20 nm gold is directly evaporated on top. 1 nm of chromium is evaporated before the gold as an adhesion layer. For the green and blue pixels, colloidal lithography is performed prior to chromium and gold deposition. Nanohole arrays are formed when the particles are removed. Photolithography are used to create patterns such as pixels in different colors next to each other.

3.2 Spectroscopy measurements

The spectroscopic setup for transmission measurements is as follows:

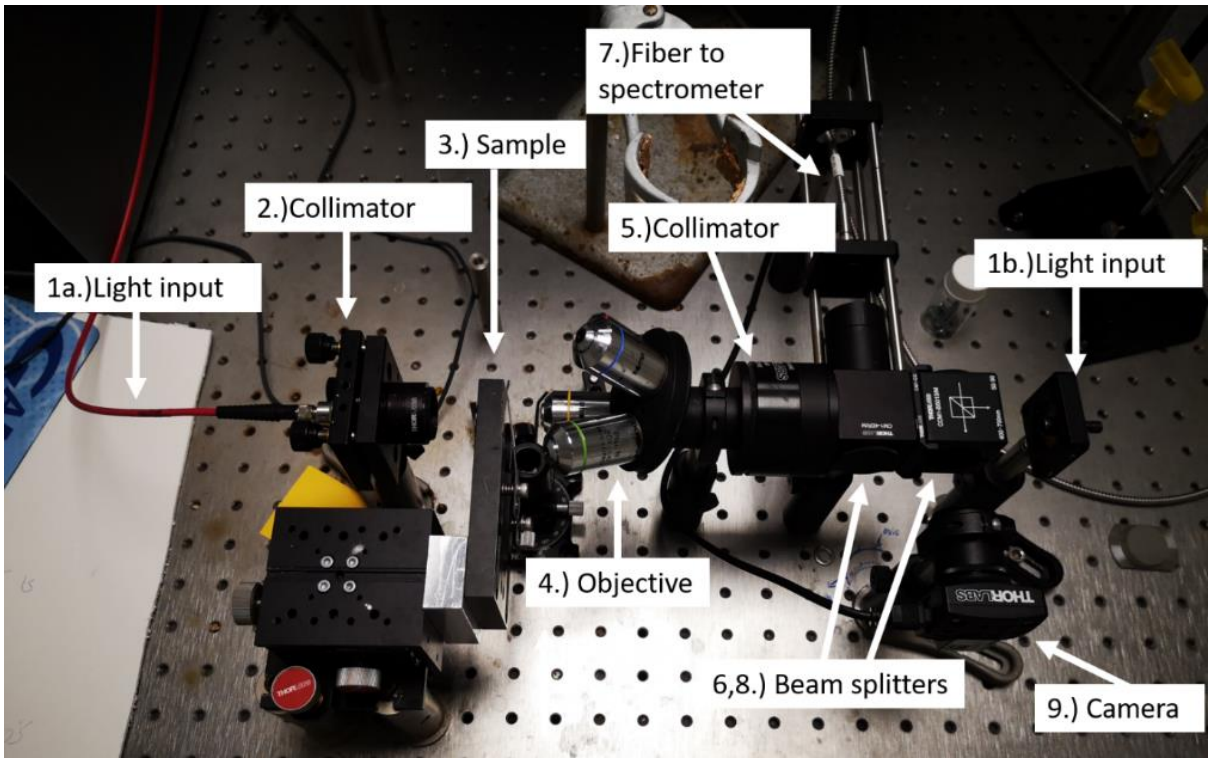

Figure 28 A photo of the spectroscopic setup for transmission mode

[3] I visited the clean room once to see how the metasurfaces were really made. I performed colloidal lithography on a sample, but I dropped it in the sink. The finished sample could still scatter red light; however, it was very apparent which of the samples I had handled.

(1a) A fiber optical cable guides the light from a light source (Azpect Photonics). (2) The light is collimated and (3) illuminates the sample. (4) An objective (4x / NA 0.1) collects the transmitted light which is (5) passed through a collimator. (6) A beam splitter divides the light and one part is directed to the (7) spectrometer (B&WTek) and the other part is routed to (8) another beam splitter. (9) A camera takes one part. The other part is for illumination in reflection mode.

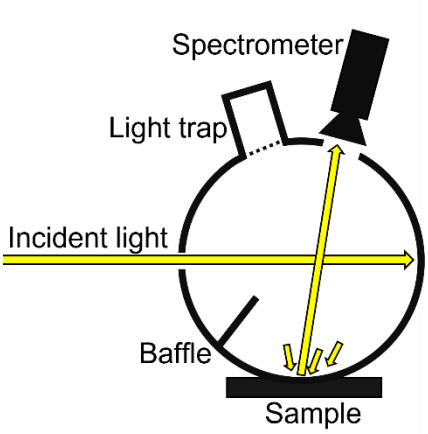

Figure 29 Light is illuminating the integrated sphere which produces diffuse light. The sample is illuminated with diffuse light and the reflection is measured.

Before the measurement, a dark spectrum and a reference spectrum are obtained. In transmission measurements, the reference spectrum is the light intensity in the air (no sample) or through a surface without the polymer. For reflection measurements, the reference is a dielectric mirror (BB005-E02, ThorLabs). Dark spectra represent intensity without any light exposure, the lamp is off. The dark is subtracted from both reference and sample intensity as $T=\frac{I_{sample}-I_{dark}}{I_{reference}-I_{dark}}$ for transmission. For reflection measurements, the fiber optical cable is attached to the rightmost input (1b in Figure 28 and the sample is illuminated through the objective. When using an electrochemical cell, it is attached to the stage which makes it possible to maneuver it by translating it in the x and y direction and rotating it Figure 28). In reflection measurements of only the polymer (**Paper I** and **II**), a homemade silver mirror was measured in the flow cell filled with electrolyte and this mirror was later compared to the dielectric mirror. This was done to only get the contribution of the metasurface and the electrochromic material ontop. Effectively subtracting the contribution from the rest of the flow cell (glass window and electrolyte).

The reflection spectrum was also measured with an integrated sphere configuration Figure 29. A handheld instrument (Konica Minolta CM-700d) was used to measure the pristine metasurfaces [97]. This configuration gives diffuse reflection, with or without the specular component. The integrated sphere is illuminated by light. As the light scatters from the sphere, it then scatters from the sample. This is diffuse light. The reflected light is later collected by a built-in spectrometer 8° normal to the sample. This configuration is known as (di/8). There is also a light trap that can be opened to remove the specular component. This configuration is called (de/8).

When infrared spectroscopy of thin films was measured, a commercial instrument (Perkin Elmer) was used. The surfaces were measured in *attenuated total reflectance* (ATR) mode with an additional accessory (GladiATR).

3.3 Preparation of chemicals

ProDOT-Me_2 was bought by Sycon Polymers (100 g). The monomer was yellow/brown as received and was purified by the unconventional method of making a milky dispersion of around 1 g in a water solution. The "dirt" seemed to separate from the milky solution. The milky solution was collected and mixed with hexane. The hexane was later evaporated to yield white crystals. T34bT was received as a black tar-like liquid. A small amount was transferred to hexane and sonicated. The tar-like liquid seemed to separate and the monomer was dissolved in hexane and collected. The hexane was evaporated and the monomer, a brown tar-like liquid, was dissolved in EtOH. The EtOH was diluted and measured in a spectrometer (Hewlett Packard 8453) in a quartz cuvette. The absorption spectra of the monomer were identical to the literature [98] and were used to determine the concentration. The EtOH was evaporated under nitrogen until only the monomer was left. The monomer was mixed with $NaDBS_{(aq)}$ 0.1 M and sonicated to produce a dispersion. Other chemicals were used as received and purchased from Sigma (or wherever we had a procurement agreement). All electrolytes were degassed with nitrogen prior to use. When non-aqueous electrolytes were used "standard" O-rings were replaced by Kalrez (FFKM) or FPM rings.

3.4 Electrochemistry

The potentiostats used were Gamry Reference 600+, Gamry Interface 1000, or Gamry Interface 1010E. The purpose of a potentiostat is to keep a fixed potential between two points, the working electrode and the reference electrode, without current flowing in the reference electrode (Figure 30A). Instead, current flows through a third electrode, the counter electrode. A schematic of this can be viewed in Figure 30. The Gamry reference 600+ Had the option to connect an external auxiliary cable which could measure the voltage over two points. Experiments were done in either a beaker (Figure 30B and C) or in a flow cell Figure 31. Figure 30B displays a beaker that is open to ambient air. Figure 30C displays a beaker that is sealed, either nitrogen (99.95%) or oxygen (99.5%) was bubbled trough the electrolyte in the cell to make it completely oxygen free or saturated. A grip holder is used to clamp the sample. The sealed beaker were only used in **Paper V**. The beaker consists of a glass jar and a lid with holes. A platinum net was used as a counter electrode. A silver wire immersed in acetonitrile TBAP 0.1 M with 10 mM $AgNO_3$ is used as a reference electrode in non-aqueous electrolytes. For water-based electrolytes, Ag-coated with AgCl in 3 M $KCl_{(aq)}$ was used (Redoxme AB).

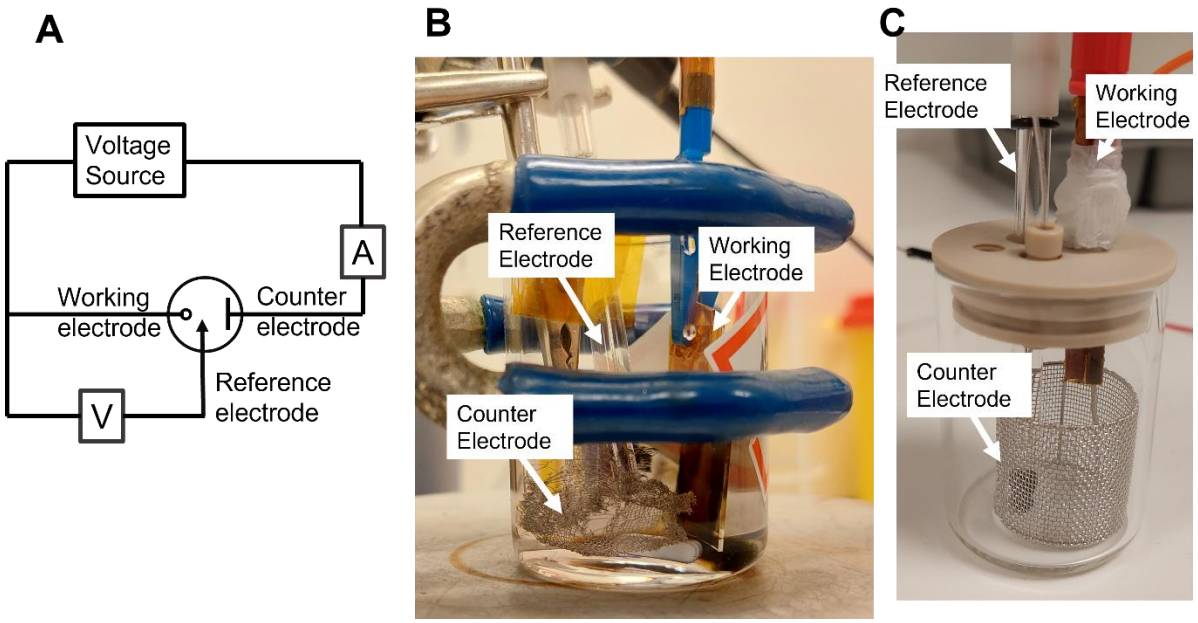

Figure 30 A) schematic of a three-electrode setup. B) A 3-electrode setup in a beaker. The counter electrode a Pt-net. The working electrode is a gold film on the glass. In the image, the polymer PProDOP has been produced on the surface. No lid is on, so the electrolyte is exposed to air. C) Another setup that has a Pt-cage and a lid to protect the electrolyte from the air.

Most experiments, such as electropolymerizations, were done in a spectroelectrochemical cell (Figure 31, Redoxme AB). The cell is made out of PEEK and have two slots for two different samples (working electrodes). The size of the area exposed to liquid is 1 cm^2. The reference electrode is the same as for the beaker. The counter electrode is a platinum coil with 4 cm^2 surface area. There is one inlet and one outlet for liquids. A tripod or a stand compatible with the optical setup can be used for mounting the cell. Electropolymerization of PPy, PEDOT and ProDOT-Me_2, were made in PC-$LiClO_4$ 0.1 M with 10 mM of the monomer. Polymerization of ProDOP uses TBAP instead of $LiClO_4$. All solutions were degassed with nitrogen before usage.

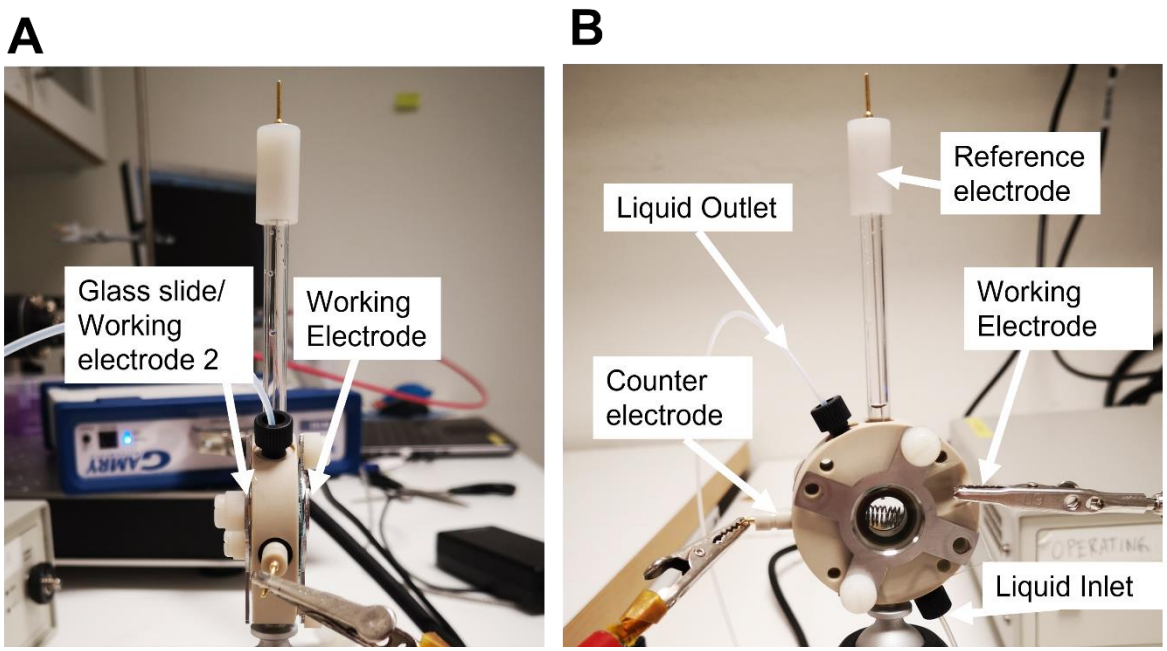

Figure 31 A) Side view of electrochemical flow cell for spectroscopic measurements. Note that it is possible to have two working electrodes. B) Front view of the cell.

3.5 Electrochemical Impedance Spectroscopy (EIS)

EIS was used one time in **Paper IV** to investigate the difference between sputtered and electrodeposited WO_3. The DC -potential was -1 V vs. Ag/AgCl and the excitation amplitude was 25 mV (rms). The experiment was conducted in the flow cell with 1 M $LiClO_4$-PC. The surface was conditioned with -1 V vs Ag/AgCl for 10 min before the start of the EIS. The flow cell was placed in a faraday cage during measurements.

3.6 SPR

To quantify the thickness change of the polymer PT34bT an attempt to use electrochemical surface plasmon resonance (ESPR) was used. The SPR machine was a BioNavis Navi 220A and had a separate electrochemistry cell with an integrated counter and reference electrode (Figure 32A). The reference electrode was measured against the commercial water-based reference electrode in the same electrolyte. The working electrode is a gold sensor that is bought directly from BioNavis. These consist of a glass substrate with 2 nm Cr and 50 nm Au. Four different channels with four different lasers are used to illuminate the sample. Two channels use 670 nm wavelength laser, one channel use 750 nm wavelength laser, and one channel use 980 nm wavelength laser.

PT34bT was polymerized in NaDBS on the sensor in the flow cell (schematic of cell in Figure 32C). The sensor with polymer was measured in air in the machine and then NaDBS was injected with a pump. Potentials were applied to the working electrode while measuring the angular spectra. After the measurements, the sensor was taken out of the machine and cleaned with TL1 (basic piranha, NH_3(~30%):H_2O_2:H_2O 1:1:5) at 70°C. The same, now clean sensors were inserted into the machine and the procedure was repeated to obtain a reference (unmodified surface). The reference spectra was measured after the sample for two reasons. To easier mimic the experiments that was conducted on the sample surface e.g. applying the correct potentials. Secondly, if the potentials used for the polymerizations to occur would change the properties of the gold film by e.g. etching the reference would be taken on the etched surface.

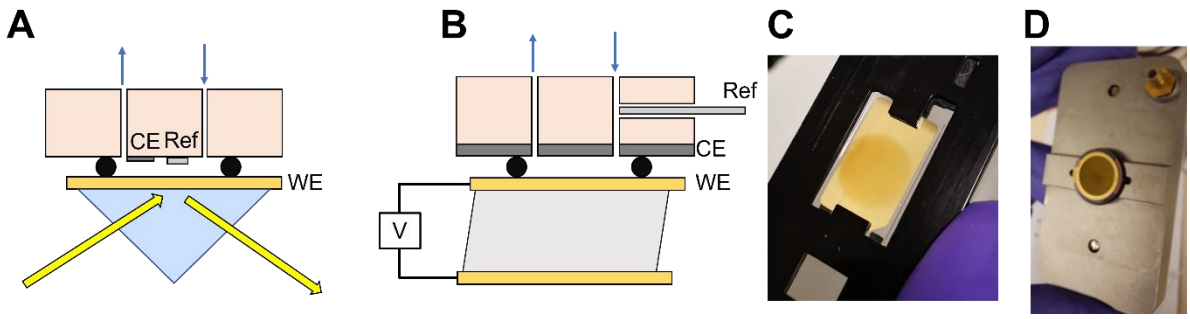

Figure 32 Simplified schematic of ESPR configuration. B) Simplified schematic of EQCMD configuration. C) An SPR sensor with a thin polymer film. D) A QCMD sensor with polymer on top placed in the cell.

The procedure to find the refractive index and thickness of the film is as follows: 1) Fit the spectrum of only the gold sensor. A model using the transfer matrix method is used to model the sensor and parameters are varied until the model fits data. The parameters are the thickness and refractive indexes of gold and chromium. 2) Fix the parameters for the gold and the chromium. 3) Assign a refractive index (n-value) to your adsorbed layer and vary the thickness until the model fits. 4) Save the obtained thickness for the assigned n-value. 5.) Assign another n-value and repeat step 3. Eventually, a curve of possible n-value and thickness pairs is obtained. By varying the refractive index in the bulk solvent and setting up another curve the correct refractive index and thickness can be determined where the two curves intersect. This is called the "non-interacting probe method" [99] because you inject something (probe) in the bulk to increase the refractive index. A condition is that the probe does not interact with your adsorbed layer.

3.7 EQCMD

A Q-Sense D4 with an electrochemical module was used to measure the mass change of the polymer PT34bT:DBS or oxygen reduction on ITO in PC (schematic of cell in Figure 32B). The cell required special sensors which had a quartz crystal sandwiched in between two gold films. One gold film was exposed to the liquid. Polymerization of PT34bT:DBS was done on gold (Figure 32D). ITO was sputtered on the gold for the non-aqueous experiment. Water-based solutions (NaDBS) are compatible with standard o-rings and reference electrodes (Ag/AgCl, WPI). Chemically resistant o-rings had to be custom ordered when using non-aqueous solvents. The reference electrode was a pseudo-Ag wire that was held in place with another o-ring. The QCMD sensing technique is based on acoustic waves. A quartz crystal is sandwiched between two conductive films, usually gold. Quartz is piezoelectric so it can expand and contract with an applied voltage. In the case of the QCM sensor, the applied voltage will shear the two metal films. Sending in a sinus wave the response to the shearing will be different depending on the frequency. Stresses will be built up that wants to relax the deformation. At a specific frequency (around 5 MHz depending on the thickness) the sensor will resonate. The resonance frequency is highly dependent on the mass of the metal. If the mass increases in an adsorbed layer the resonance frequency will decrease. A common technique for measuring "soft layers" is to stop the applied sinusoidal voltage and measure how the oscillation decays with time. With this information, energy dissipation rate is obtained, which is the "D" in QCMD. In this thesis work, we were blessed with not having to model soft layers. All adsorbed layers were solid, and not viscoelastic. This simplifies the method tremendously and the mass coverage is directly proportional to the frequency shift by the Sauerbrey equation [100].

3.8 Device fabrication and passive matrix

In **Paper V**, electrochromic devices are made by using a glass slide with 100 nm gold with electropolymerized PProDOT-Me_2 on. A double-sided tape (~ 100 µm) is placed on two sides and an ITO slide (Naranjo Substrates) is attached to it. With a thin needle, the cavity between the ITO and the gold electrode was filled with a UV-curable electrolyte. The curing is done in a UV-oven (the oven is originally manufactured for curing nails polish). The wavelength was 365 nm. To "collimate" the light it is led through a 50 cm long tube down to the sample (Figure 33A and B). A mask specifies the curing pattern on the sample. By using a laser printer, the mask is printed on transparent plastic paper (overhead-plastic). The print was made several times on the same plastic to really block the light. The cross-linker used was polyethylene glycol-diacrylate (M_n = 700 kDa) (PEG-DA). Figure 33C and shows patterned PEG-DA and Figure 33D shows a square of electrolyte photopatterned on a circle of electropolymerized PProDOT-Me_2 on gold.

An PC-based electrolyte was used as a plasticizer in the UV-curable electrolyte. Polyethylene glycol-diacrylate (M_n = 700 kDa) was used as crosslinker. 2,2-Dimethoxy-2-phenylacetophenone (DMPAP) was used as photoinitiator. Different compositions were used e.g. 5 g of electrolyte, 5 g of crosslinker, and 20 mg of DMPAP. This was sonicated in a vial for mixing. 10 min was sufficient for curing with the UV-oven setup. The remaining uncured electrolyte was flushed away with isopropanol and the devices were carefully dried with nitrogen.

Screen printing is another common technique for patterning thin layers. A co-polymer, Poly(vinylidene fluoride-co-trifluoroethylene) (PVDF-TRFE) was mixed with a propylene carbonate electrolyte-based electrolyte and screen printed (120-34 mesh) by hand. One print was made on the ITO and another on the polymer. Both substrates had to be heated to reduce the viscosity of the electrolyte and to evaporate away some of the solvents. When the electrolyte was still slightly wet and not as viscous because of the heat, the two substrates were pressed together, electrolyte to electrolyte. When the device cooled down the viscosity increased, and the two substrates were stuck to each other whilst also being slightly wet for ionic conductivity.

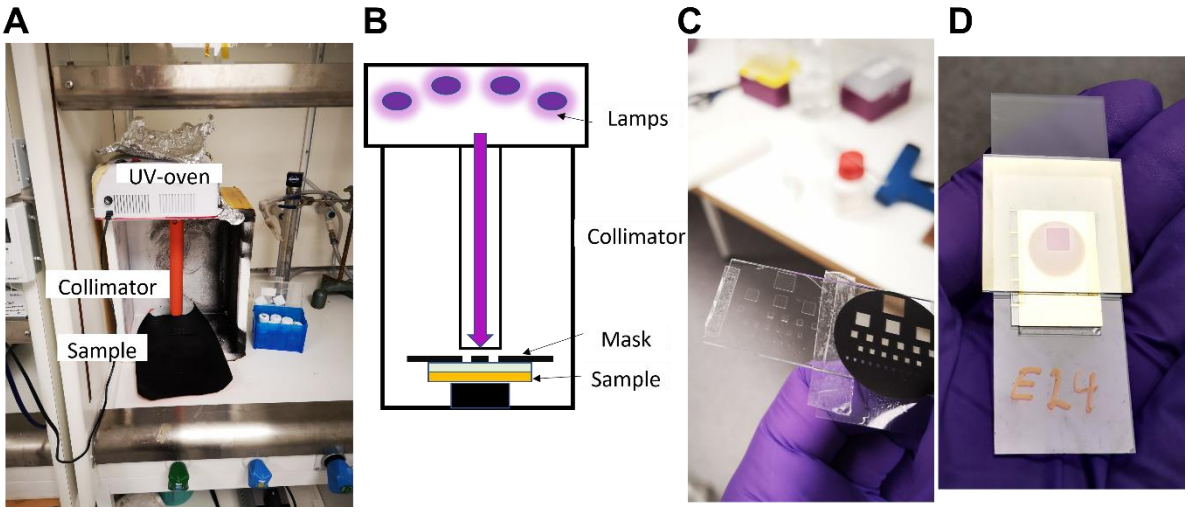

Figure 33 A) Photo of the UV-curing setup. B) Schematic of the UV-curing setup. C) Photo of photocured PEG-DA with its mask. D) Photo of an electrochromic device with a photopatterned electrolyte square. The circle is the conjugated polymer on top of the gold.

When fabricating a 3x3 passive matrix gold was evaporated in 0.5 cm stripes on a 3x3 cm^2 glass slide. The stripes were made by masking with Kapton tape. ITO slides were pattered by masking 3x3 cm^2 ITO

slides with Kapton and etching the exposed area with Piranha (H_2O_2:H_2SO_4, 1:4). The driving was controlled by interfacing an Arduino to LabVIEW. The Arduino analog pins (pulse width modulation) were fed into a low pass filter (integrator circuit, 1.47 kOhm and 1.5 µF) which later was buffered with op-amps TL082 with 100 nF filter capacitors. The Arduino can give 5V max, so a virtual ground was set to 2.5 V. Most of the code was implemented as firmware in the Arduino and the LabVIEW interface was used to send commands and receive data. The whole system was poorly executed, and the internal clock of the Arduino was not entirely correct. This resulted in that when executing a script where a potential should be applied for a certain time e.g. 100 ms the applied time was not really 100 ms.

3.9 Active matrix setup

The active matrix TFT backplanes were purchased from Plastic Logic. The information regarding the backplane is limited. A gds-file was provided to see the layout. The top pixels were 200x200 µm arranged in a grid of 240x400 lines. The fan out to contact each row or column was 20 µm with 20 µm in between. The fan-out was also coated with a protective plastic film with some perforation to the gold. Bundles of fan-out lines were connected with silver glue. In the case of individual contacting, the backplanes were sent to an external company that wire-bonded the individual lines to a custom-made printed circuit board (PCB) for easier contacting. The plastic was scratched away with a piece of wood before the wire bonding were performed. A glass vessel was fabricated by buying glass slides from a glass-cutting company and gluing them together with epoxy. The backplanes were fixed onto a separate glass slide that could be inserted into the glass vessel (Figure 34A). The potentiostat working electrode was connected to the source lines of the fan-out. The reference electrode was a commercial Ag/Ag+ electrode. The counter was either an old platinum net or a big piece of ITO plastic. To open the gate a separate power supply was used (RSPro, DF1760SL3A). The positive terminal was connected to the working electrode of the potentiostat and the negative terminal was connected to a desired gate line of the fan out. When optical measurements were conducted, one corner of the backplane was inserted into the electrochemical flow cell. When an automatic driver was tried a homemade potentiostat on a breadboard was constructed [101] where the working electrode was grounded (Figure 34B). The potentiostat was interfaced with LabVIEW by an Arduino. The working electrode was distributed (opened) to multiple source lines by a multiplexer. The counter electrodes altered the potential to accommodate the fixed potential between the working and reference electrode. The gates were opened by distributing the power supply's negative terminal to the gate lines by low-side MOSFETs (transistors).

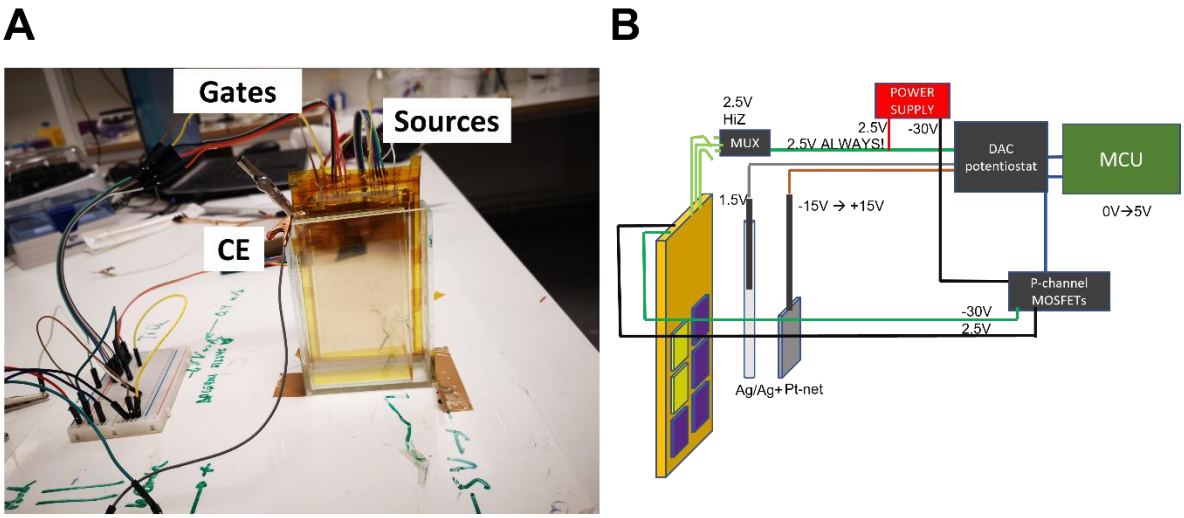

Figure 34 A) A backplane in a glass vessel with attached cables to bundles of sources and gates. B) the schematic of an automatic driving configuration.

4 Results and discussion

4.1 Electrochromic materials on top of plasmonic metasurfaces

Sputtered WO_3 and conjugated polymers were deposited on top of the plasmonic metasurfaces to act as shutters, with the purpose of turning the pixels ON or OFF. The two materials performance were later compared. The discussion will cover results from both **Paper I** and **Paper II**.

4.1.1 Electropolymerization

In terms of uniformity of the films, propylene carbonate worked better than acetonitrile. Literature seems to agree [58]. For PProDOT-Me_2 cyclic voltammetry was the method which gave the most reproducible films. Cyclic voltammetry could also be performed while the cell was in an optical setup. After every reduction cycle, a spectrum could be taken to track growth (via the optical extinction) against the number of polymerization cycles. By integrating the current, the consumed charge for monomer oxidation can be obtained, which is linear with the number of cycles. In **Paper I**, Figure 2C is meant to show how extinction increases with the amount of charge consumed but there is an error. The abscissa is incorrect, which can be deduced from that it does not start from zero. The abscissa in the figure displays the absolute value of the current, for that particular cycle. This is more linear with extinction since it is the doping process of one cycle that is measured. It is not just the monomer contribution that counts for each cycle. The charge transfer is calculated by following: $Charge\ transfer = \sum_{n=1}^{N} \int_0^t I_n\ dt$. The integration ($\int_0^t I_n\ dt$) of one polymerization cycle, *n,* is giving the charge for 1) the doping process 2) building the polymer (oxidation of monomers) 3) dedoping the polymer. The doping process is a positive current and thus give a positive contribution. The dedoping process gives a negative current and thus subtracts the charge contribution of the doping process. What is left is the charge contribution of the polymerization for that polymerization cycle. For a polymer that is grown with *N* cycles all the charge contribution of the previous polymerization cycles are summed and give the total amount of charge used to polymerize the film. It is shown in Figure 35A how the extinction corresponds to the charge transfer. This is not perfectly linear which could be attributed to some of the formed polymers do not adhere to the surface.

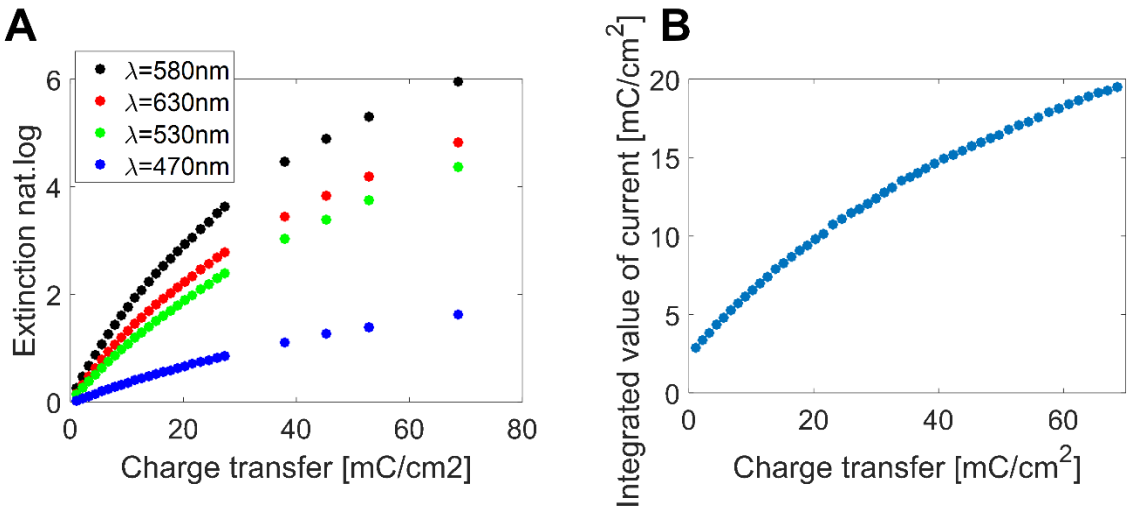

Figure 35 A) Extinction against charge transfer for polymerization. B) How the integrated absolute value of the current varies with the charge transfer.

The polymerization occurred above ~1.1 V and the potentials to fully reduce and oxidize the polymer were -1 V and +0.5 V. This made it possible to measure the transmission of the reduced and oxidized sample without further polymerization taking place, after a certain amount of polymerization cycles were performed. From this measurement, the contrast could be obtained. I call the samples made in this fashion “the lazy samples” since it was much quicker than fabricating separate thicknesses on separate gold films. It also gives more precise values since the background (gold sample and electrolyte) is identical. A sample set with separate surfaces was made anyways to measure the thickness. The contrast was similar for these samples. For PEDOT and PPy the lazy method was not used, and separate thicknesses were polymerized on separate surfaces and measured.

In **Paper II**, propylene carbonate was initially tried with PProDOP to polymerize on ITO. Constant potential was used, and a uniform film was obtained which gave similar transmission values for the dark and bright state as the literature. However, when switching from ITO to a gold film, polymerization occurred, but the film did not adhere to the surface. Something dark appeared to form at the surface but it stayed in the solution. We tried various methods to circumvent this: constant current and cyclic voltammetry, different potentials and different scan rates. Nothing helped. What helped was to polymerize in a beaker and polymerize multiple times with the same solution. After the first polymerization trial, the electrolyte turns darker because of the unadhered polymer. The polymerization was carried out for 10 minutes with a constant potential of +0.6 V vs. Ag/Ag+. After around 5 polymerization rounds in the same solution, the polymer started to stick. However, we also saw that the optical performance of the samples varied a lot. By eye, all samples looked the same, and had the same thickness. However, they were unable to be properly reduced to their neutral state and we speculated that some films might be permanently oxidized.

We tried substituting the electrolyte in which the testing occurred (monomer free) with a cleaner one. A new electrolyte was prepared and stored in a glove box. When using this electrolyte, some samples responded better but did not give the good contrast that had been achieved on the ITO. It turned out that what made the polymer stick in the beaker was not that there were more polymers swimming around in the electrolyte after some polymerization rounds, but the exposure to air. When propylene carbonate with lithium perchlorate is in the air, it sucks up water like a sponge. We tried different concentrations of water in a more controlled environment, our flow cell. Higher water concentration gave higher deposition current and thickness, while too little water gave a badly adhering film and bad optical performance. Too much water gave only bad optical performance. One good sample set was made with 1500 ppm water added to the deposition solution.

To investigate various thicknesses, they had to be deposited on different gold surfaces. The lazy method would not have worked since, still, there were some unadhered polymers which would have complicated the background intensity measurements. However, one good data set was completed. Unfortunately, when some additional samples were created later, the optical performance was not as good and the optical performance was not well reproducible. A lot of datasets with varying different parameters were tried after this to reproduce the best performing samples. Not using sonicate to mix the solution did not help. Switching the solvent from the glovebox to the one from the solvent cabinet helped, but not every time. Recrystallizing the monomer did not help.

Although a sufficient number of successful samples had been obtained, it still bothers me that the method was not robust. In retrospect, I do believe that oxygen contamination could be the culprit. It worked splendidly on ITO, which seems to have a larger window for not having side reactions than gold (see later sections). The flow cell is not good enough to keep oxygen out and degassing the

electrolyte and transferring it with a syringe exposes it to more than enough air to give a clear electrochemical activity from oxygen. The literature describes that with too low pH, a non-conjugated polymer can be formed. Adding NaOH in water could maybe also solve this issue.

4.1.2 Contrast

In **Paper I** it was found that the thin film interference of the polymer on top of a gold film in electrolyte was negligible. We believe that this occurs because the refractive index of the electrolyte is similar to that of the polymer. When there is no mismatch in the refractive indices on an interface no reflection occurs. This makes the absorption of the polymer depend on its thickness according to Lambert-Beer's law Equation 4.1.1. The t is here the thickness and c is the concentration of absorbing species, T is transmission, a is the optical cross section, and α is the attenuation constant. Absorption is here taken as the extinction assuming that the scattering is low. From Lambert-Beer's law, an expression for what the maximum optical contrast of a polymer is can be obtained (Equation 4.1.2). The parameter required to determine the optical contrast is the ratio of the attenuation constants in the dark state and bright state. This ratio is equal to the ratio of the measured extinctions (**Paper I**) for any arbitrary sample since the thickness cancel out, assuming the thickness is the same in both states. This ratio was found to be constant for the different samples of the same polymer, even though some variations were present. This makes the optical extinction ratio an excellent figure of merit in the analysis of conjugated polymers. The extinction ratios of the polymers can be found in Figure 36. Clearly the PProDOP has a higher contrast in the blue region than PProDOT-Me$_2$.

$$E_{\mathrm{d/b}} = a_{\mathrm{d/b}} c\, t = \alpha_{\mathrm{d/b}} t = \ln(1/T_{\mathrm{d/b}}). \tag{4.1.1}$$

$$\Delta T_{\max}(\lambda) = \left(\frac{\alpha_{\mathrm{col}}}{\alpha_{\mathrm{ble}}}\right)^{\frac{1}{(1-\frac{\alpha_{\mathrm{col}}}{\alpha_{\mathrm{ble}}})}} - \left(\frac{\alpha_{\mathrm{col}}}{\alpha_{\mathrm{ble}}}\right)^{\frac{\frac{\alpha_{\mathrm{col}}}{\alpha_{\mathrm{ble}}}}{(1-\frac{\alpha_{\mathrm{col}}}{\alpha_{\mathrm{ble}}})}} \tag{4.1.2}$$

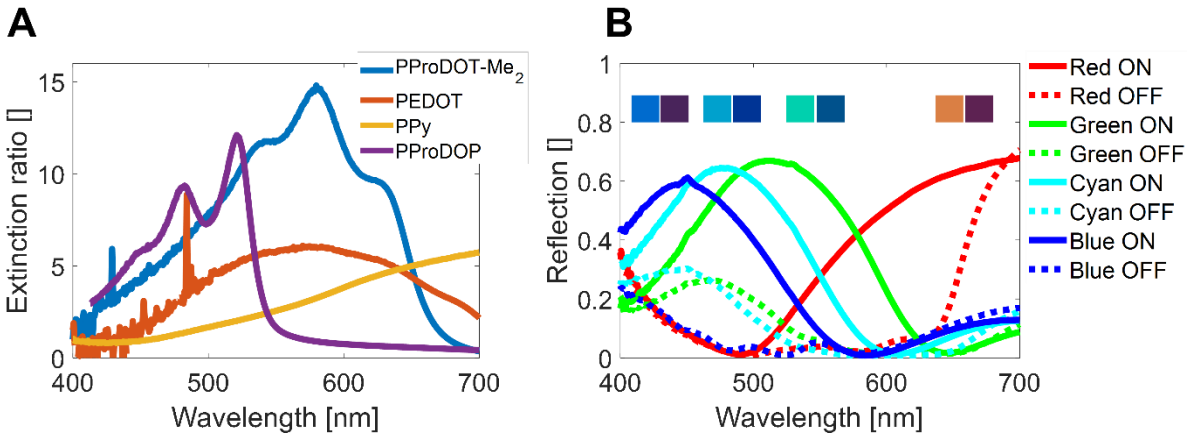

Figure 36 A) Extinction ratio of the tested polymers B) Reflection in bright and dark state of PProDOT-Me$_2$ on red, green, and cyan metasurface. PProDOP is on the blue metasurface. The rectangles are the bright and dark pseudo-colors.

Polymerizing on top of the metasurfaces was straightforward after developing the methodology on bare gold. Since the metasurface samples are used in reflection mode the optimal thickness of the polymer had to be halved. This is because light travels twice through the film. Optical contrast on top of the metasurfaces could be approximated by multiplying the polymer's contrast with the reflectivity

of the metasurface. This is shown in **Paper II** Figure 4. The optimal thickness to give the highest contrast for each RGB surface was polymerized on top of the pixels. These are summarized in Figure 36 where the data from **Paper I** and **II** have been merged into one plot. Around 50% of contrast for every color can be achieved by using PProDOP for blue color and PProDOT-Me_2 for green and red color. There is one more caveat regarding the difference between PProDOP and PProDOT-Me_2 on blue samples. Even though the blue samples were made in the same way, the reflection peak differed between the two papers. In **Paper I**, the metasurfaces had a more cyan color with a peak centering around 490 nm, whilst in **Paper II** they had a deeper blue color centering around 450 nm. This issue stems from the margin of error in the evaporation of Al_2O_3. As a result, it is difficult to precisely compare PProDOP samples with PProDOT-Me_2. The thickness of the highest contrast in blue was 200 nm for PProDOT-Me_2 and 100 nm for PProDOP.

Sputtered WO_3 had a maximum contrast of around 50-60% for each color. Thin film interference occurs with WO_3 on top of another metal because WO_3 has a high refractive index, both in its dark and bright states. This generates Fresnel reflections on both the metal- WO_3 interface and the WO_3-electrolyte interface. The Lambert-Beer's law does not work due to thin film interference. To find the maximum contrast for e.g. a red sample, both the aluminum oxide and the WO_3 thickness have to be tuned. The transfer matrix method was used to determine the optimal thicknesses to generate high-contrast samples.

4.1.3 Switching time

When it comes to switching time, polymers were around one order of magnitude faster than WO_3. Around 0.5-1 second for PProDOT-Me_2 and around 2 seconds for PProDOP. Sputtered WO_3 required 1 to 10 seconds to fully switch in $LiClO_4$-PC. In the next section other deposition methods are shown to have a lower switching time (this is not tested on top of metasurfaces though). It should be noted that the switching time can be lowered by increasing the value of the applied potential. The potentials used are the ones that are sufficient to achieve the maximum contrast.

4.1.4 Bistability

Bistability is measured with the dark state at open circuit since WO_3 has its equilibrium in the bright state. The polymer's equilibrium state is also shifted towards its bright state. WO_3 has a very long bistability and it can retain its dark state for hours. It is more difficult for polymers to retain their dark state. PProDOT-Me_2 moves to equilibrium within minutes and ProDOP within seconds. This is most likely because PProDOP has a lower oxidation potential and then easier gets oxidized (doped). The CVs shown in Figure 18B (Chapter 2.3) confirm that the onset of oxidation for PProDOP is lower than for PProDOT-Me_2.

4.1.5 Life time and power consumption

Lifetime was not tested in **Paper I**, only in **Paper II** for ProDOP was two measurements done. This showed that the contrast degraded very rapidly, within 100 cycles much of the contrast had been extinguished. This is much more rapid than the literature values. This could be because the samples were old. Newly fabricated samples did not have good contrast. Since it seems that PProDOP is more sensitive to oxidation, traces of oxygen could destroy the polymer. On gold, oxygen reduction in LiClO4-PC occurs between -0.9 to -1.2 V (see results section 3) which is what is required to fully reduce PProDOP. As a side note: our group has successfully switched PProDOT-Me_2 more than 10 million times with a special configuration [84] and we have been able to switch WO_3 ~2000 times in our lab [102].

The polymers have around 10 times less charge consumption than WO_3. For a thickness which gives maximum contrast, PProDOT-Me_2 requires around 2.5 mC for a full switch while WO_3 requires 25 mC.

4.1.6 Comparison to previous articles and final remarks

Prior to our work, two articles were made that used either electropolymerized polypyrrole in an aqueous electrolyte (PPy:DBS) [29], or screen-printed PEDOT:PSS on top of metasurfaces [30]. The contrast using PPY:DBS was between 30-50% where the highest was for red pixels and the lowest for blue. For the PEDOT:PSS-based devices the contrast was between 20% and 40%. However, these are the values for an entire device with ITO plastic as counter electrode. Based on **Paper I** and **II**, the scope of increasing the contrast of the pixels has been achieved by utilizing other polymers and an inorganic option. The metasurfaces have also been made compatible with non-aqueous electrolytes.

The structures used in **Paper I and II** are intended for use in a subpixel configuration which will lower absolute reflection. If the color red is to be displayed in an image the blue and green pixels have to be in their dark state. The whitest white would have a reflection of around 40% which is better than the commercial color EPD of 20%. However it is less than the newspapers reflection of 60%. The next section will discuss how dynamic pixels might be the solution to this.

4.2 Dynamic plasmonic pixels

This section discusses **Paper III** and **Paper IV**, two papers in which I was the second author and acted as a support to the main authors. In this section I will highlight my work but, of course, also summarize and discuss the main results.

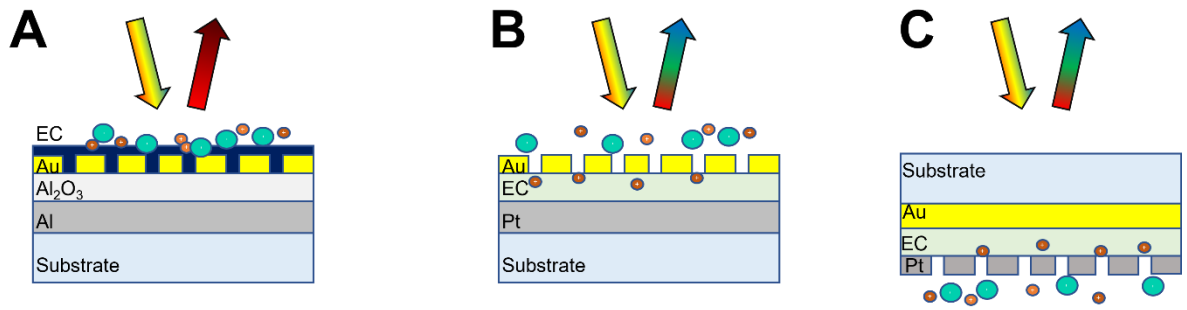

Figure 37 A) Metasurface with electrochromics (EC) on top. B) Electrochromic material as spacer layer in the metasurface. C) reversed structure where the viewer sees the color trough the substrate.

Paper I and **Paper II** discussed metasurfaces with an electrochromic material on top, acting as a shutter (Figure 37A). One problem is that the inorganic metasurfaces are static. Once they have been manufactured, they cannot be changed to another color. Blue will remain blue and green will remain green. If a structure could be "dynamic", it would be able to alter its color. The color stems mainly from the MIM-cavity where the optical path length of the spacer layers determines the color. By dynamically changing the optical path length the color would change (Figure 37B and C). This can be done by either changing the thickness, or the refractive index. Conjugated polymers can alter their thickness with doping and this will be investigated in **Paper III**. WO_3 alters its refractive index upon intercalation and this will be investigated in **Paper IV**.

4.2.1 Polymer in cavity

The polymer used for the purpose was one that was transparent in both the reductive and oxidative states. This is to reduce absorption with the desired thickness change and have a high reflection throughout the whole visible. For this purpose, the polymer PT34bT was chosen. This polymer is not frequently used but there are some papers discussing how it is transparent in both states. However, the bar for what is considered transparent seems to be very low. With a dry thickness of 100 nm on ITO the reported absorbance value are 0.3-0.7 [103]. This is 20 to 50% in transmission which is rather dark, even for being on an ITO slide which has around 85-95% in transmission.

The polymerization was carried out in NaDBS since this has been shown to facilitate a high actuation process with PPy [104]. The polymer was polymerized with constant potential on a thin gold film on glass. A 50 nm mirror layer of aluminum was later deposited. Different thicknesses of the polymer gave rise to different colors. The whole visible regime could be spanned with thicknesses between 114 nm and 271 nm. Increasing the thickness redshifted the resonance peak (**Paper III**, Figure 1). Dynamically switching the cavities with electrochemical doping was possible. However, the samples were very non-uniform, and it was challenging to get ions to traverse through the aluminum mirror which was exposed to the electrolyte. To measure the reflection change, a microscope was used to zoom in on a small area. The aluminum was also patterned with slits to expose the polymer to the electrolyte on the sides. Decreasing the size to 5 x 5 mm^2 pixels was also an option to make the colors more uniform. The cavity could change its peak reflection value from 450 nm to 670 nm, which is

basically the whole visible spectrum. Around 50% to 60% of the light was reflected regardless of color. The red shift of the cavity with reduction indicates that the thickness increased. This is in total agreement with how cation doping works, which is known to happen in PPy:DBS. During the reduction of the polymer the anions don't get expelled, but cations ingress, thus increasing the volume [62]. Simulations showed that spanning the whole visible regime would require the polymer to double its thickness during doping. Alternatively, change its refractive index with more than 1 units.

Besides developing the protocol for preparation of PT34BT films, my other task was to figure out if the thickness change could be measured in situ with SPR and EQCMD.

EQCMD had the option to polymerize within the setup. A frequency shift of -1300 Hz was observed during polymerization. Assuming the density to be 1.1 g/cm^3, the thickness of the polymer is 210 nm from the Sauerbrey constant. Electrochemical switching only showed a frequency change of 50 Hz, with mass deposition with a reductive potential. This corresponds directly to a less than 5% thickness change if the density is constant. The density is, however, not necessary constant since the films gets filled with ions.

For the SPR measurement, the polymer was deposited on a SPR sensor (glass, 2 nm chromium, 50 nm gold). (This was not done in situ to avoid the extremely smelly monomer leaking down into the electronics of the instrument.) The plan was to obtain a definite thickness together with a refractive index at least for the wavelengths used in the SPR instrument. Could we use the “non-interacting-probe method” to find both a definite thickness and refractive index of PT34bT: DBS? The technique was tested with another layer but gave different values for the complex refractive index: n, k and t by just changing small parameters. The parameters include: how big the span is to fit around the SPR angle, or how the reference gold is fitted. Instead of finding a definite thickness and refractive index we found the possible states. This generated a “function” that maps the n-value to the thickness and k-value. The reduced and the oxidized state of the polymer was then compared.

The SPR has four channels: two channels with 670 nm wavelength, one channel with 750 nm, and one channel with 980 nm. Figure 38 displays the four different channels with the reference spectra (only the gold sensor without the polymer, dashed curve) with both a positive (red) and negative (blue) potential applied. The sample (the sensor with the polymer) spectra for the channels are shown in the same plot (solid lines) with a positive potential (red, +) and a negative potential (blue, -). The dips of the sample are not so sharp with a well-defined SPR-angle (compare to the dips for the reference). For the sample, the channels using the 670 nm wavelength displays a large shift in reflection (shift in the direction of the y-axis) when changing polarization. For the same wavelength there is miniscule shift in SPR-angle. The data from both 670 nm channels were not used. The channel for 980 nm wavelength exhibited no definite peaks and were neglected. The channel with 750 nm wavelength exhibited a good shift in the SPR-angle between the samples reduced and oxidized form. This high distinction between the two states was used for finding individual fits of the two states.

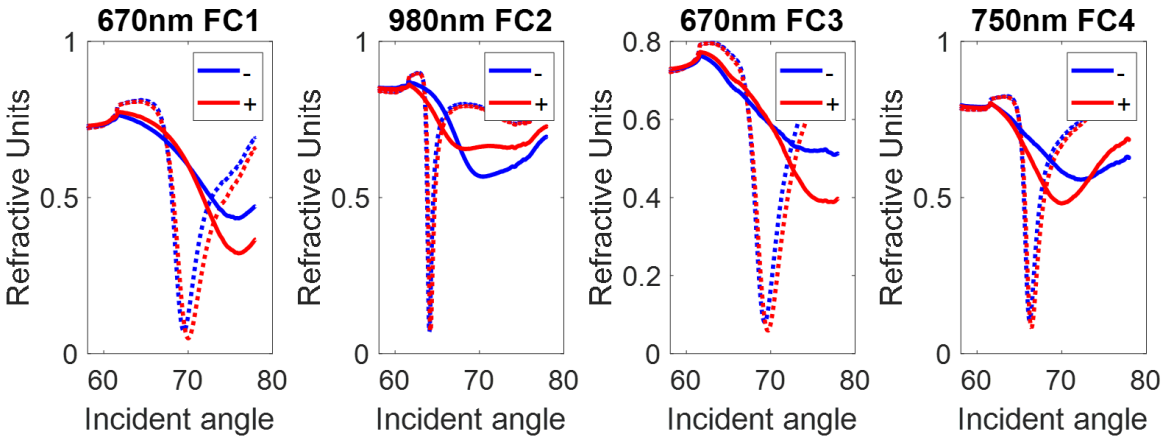

Figure 38 All the wavelength channels for the electrochemical switching of PT34bT:DBS. Gold reference is dashed lines (--) with a negative potential in blue and a positive potential in red. Sample spectra are solid lines (-) with a negative potential in blue and a positive potential in red.

I got a lot of help from my colleagues who use this method on a daily basis but for transparent polymers. As described in methods section, the method consists of assigning a n-value as one fitting parameter, then the thickness and k-value are altered in the fit until the fitted spectra fits the sample spectra. A perfect fit for the whole spectrum was not achieved. The problem was reduced to only fitting a very small span of angles around the dip, not the full spectrum. The focus was to fit so that the SPR-angle of the sample would be the same as the SPR-angle of the fit. This generated a new problem: when assigning a thickness and fit the spectra to find a refractive index, many solutions were found. In Figure 39A this problem is illustrated. A simulation with 50 nm gold and 20 nm of an adhered layer with water as bulk can be viewed. By altering both the thickness and the k-value, all the n-values 1.35, 1.4, and 1.45 can be made to have the same SPR-angle. Clearly, the curves are not the same and what differs is the width of the dip, and the reflection (0.7 to 0.8). The imaginary part of the refractive index, the k-value, mostly affects the width of the dip but also slightly the position. Note that the y-axis is very zoomed in.

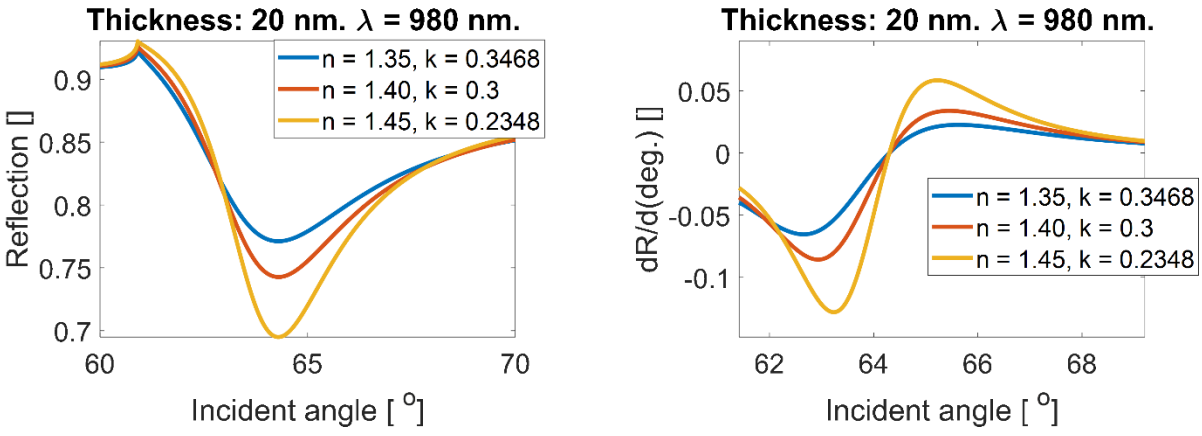

Figure 39 The minimum in the angular spectra depends on both the n-value and the k-value. The width of the dip is determined by the k-value. I the differentiated spectra the slope around the minimum is then determined by the k-value.

Instead of only focusing on varying the parameters so the SPR-angle of the fitted spectrum is the same as the collected spectrum, the width or the absolute reflection of the dip also have to be considered. My colleagues had a similar problem with the absolute values of the dip when fitting data for their more transparent polymers. Since the SPR-angle is what matters in their systems, a constant value

could be added to either the data or the fitted model the absolute reflection was not considered. I used the same method, but instead of adding an offset I used the derivative of the spectra with respect to the angle span to effectively remove the "offset". A former dip can now be found at the zero intersect and the imaginary part affects the differentiated spectra by reducing the slope around the SPR-angle Figure 39B displays the differentiated spectra of the example simulation. For fitting the sample of PT34bT:DBS I found that it was easier to find a good fit when using the differentiated spectra. It was easier to implement constrictions to force the computational solver to focus fitting the correct things: that the SPR-angle of the fit was the same as for the collected spectra, and the slope around the SPR-angle. Another way of simplifying the fitting was to, as aforementioned, reducing the span of angles to around ±0.7 ° around the SPR-angle and also approximate the dip with a second-order polynomial. The rest of the spectrum was neglected during the fitting. After a good fit have been found the full spectrum is plotted. In Figure 40B the fits for various assigned n, and k -values can be viewed with the measurements. Both the SPR-angle and the width have been fitted good. One differentiated spectra and the fitted differential can be seen in Figure 40A, smoothed data is the small angle span that is used to fit. Using differentiated angular spectra is not a novelty and has been utilized before [105].

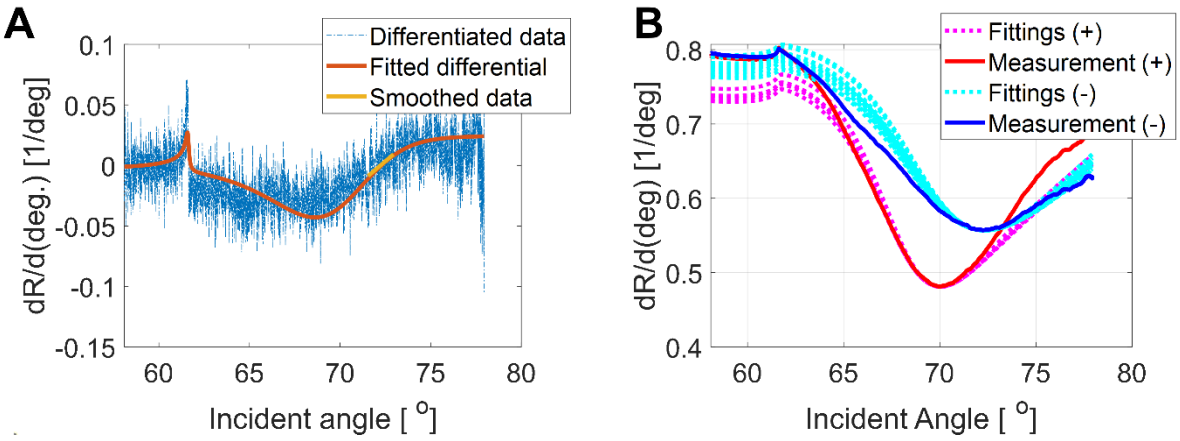

Figure 40 A) Differentiated SPR spectra with the fitted differential and the polynomial (smoothed) B) Various fits for different assigned n-values. An offset have here been added to superimpose the dip.

Figure 41A and B the fitted heights and k-values (imaginary part of refractive index) are plotted against the assigned n-values (real part of refractive index). If we assume that the n-value of the PT34bT:DBS is constant during reduction, the reduced state is thicker than the oxidized state. The solid arrow displays a doubled thickness upon reduction if the n-value remains constant. However, if we look at the right side of the figure the imaginary part, the k-value, is lowered in this case. Literature [103] and experiments (**Paper** III, Figure SI 2) describes that the absorbance of PT34bT is decreasing upon oxidation at the wavelength 785 nm. However, the k-value is not what is measured in spectroscopic experiment, the absorbance is. If converting the fitted values to absorbance ($A = t\alpha = t\frac{4\pi k}{\lambda}$) the reduced state was higher than for the oxidized for all fits. This makes it possible for both the case of constant n-value to both exhibit an increase in absorbance but also a decrease in k-value. Another case (dashed arrow) use the assumption that there is no thickness change for reduction. The dashed arrow indicates an increase in the n-value. In this case, the k-value is also increasing. It is hard to get

a definite answer of what is really going on but it seems that if the k-value have to increase upon reduction, the n-value have to increase as well.

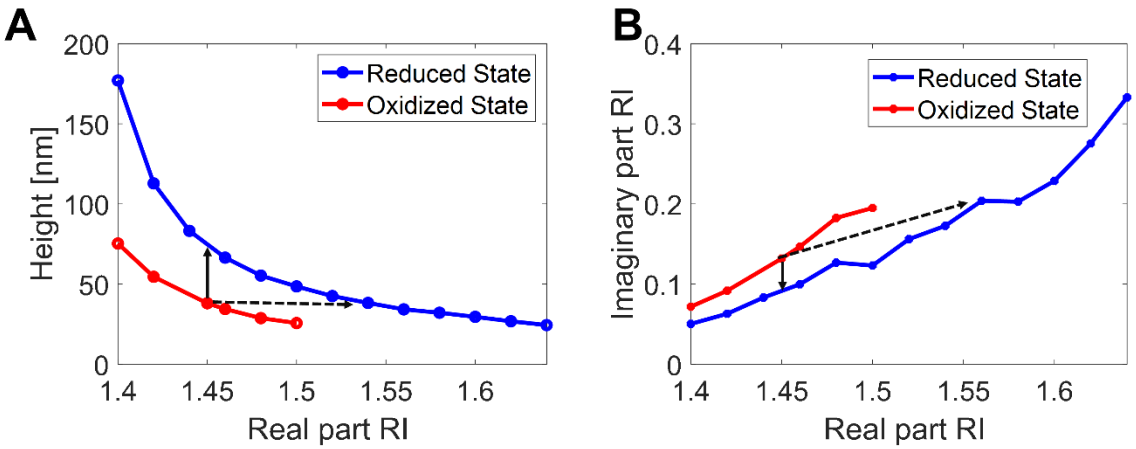

Figure 41 The fitted height against the n-value for both oxidized and reduced. B) The fitted k-value for each n-value for both reduced and oxidized. The arrows indicate two different scenarios upon reduction. The wavelength is 785 nm.

It should be mentioned that previous publications have determined the thickness change and the refractive index when electrochemically switching PEDOT, but the swelling was then determined from EQCMD by assuming a fixed density [106]. Other methods aimed to uniquely determine the thickness and refractive index by using data from multiple wavelengths. For instance, the different wavelengths can be connected to each other by e.g. assuming the dispersion is small and linear between the used wavelengths [107].

4.2.2 WO_3 in cavity

Instead of incorporating conjugated polymers as a spacer layer, WO_3 can be used. Contrary to conjugated polymers, the real part of the refractive index of WO_3 is known to decrease by ~ 0.2 upon doping [108]. This also alters the optical path length and the structure's reflection changes by blue shifting when a negative potential is applied. However, there is an increase in the imaginary component as well which makes it tough to predict the exact outcome without full Fresnel modeling. Sputtered WO_3 had been successfully incorporated into dynamic cavities by our group [3]. The scope was shifted from sputtered WO_3 to electrodeposited because a previous article by Cai et al. showed increased contrast and switching speed [109]. By applying the potential in pulses during deposition, the morphology should become more porous, which facilitates faster intercalation. The pulsed electrodeposited WO_3 also exhibited and increase in the contrast. By dissolving a tungstate salt, Na_2WO_4, in water and letting it react with hydrogen peroxide, $W_2O_{11}^{2-}$ is formed. Together with protons and electrons (negative potential on an electrode), H_xWO_3 is formed. The X factor depends on the number of protons and electrons. The deposition proceeded smoothly by following the recipes in prior publications. However, one key ingredient that is not included in prior articles' recipes is time. After mixing the electrodeposition solution it has to stand idle for several days. This gives the hydrogen peroxide and tungstate salt time to react.

The sputtered films were compared to the electrodeposited films in **Paper IV**. The substrate used was ITO. The integrated contrast weighted with the luminosity function, i.e. the color matching function y, was used to compare the films. We found that, in propylene carbonate, the contrast was higher for the sputtered films. The weighted transmission difference for the sputtered film was 90% for a thickness of 250 nm and around 50% for a similar thickness of the electrodeposited film. When sulfuric

acid was used the contrast was similar for both films. However, the electrodeposited film required a thicker layer to reach full contrast. This is attributed to a more open morphology.

The switching time was lower (faster) for the electrodeposited films in sulfuric acid but similar when using propylene carbonate. The CVs showed similar shapes (area) when using sulfuric acid and 50 mV/s. Increasing the scan rate lowered the current of the sputtered film because there was no time for the ions to intercalate. For a very slow CV in PC, the electrodeposited had less current than the sulfuric acid which stems from less material for the same thickness. Similar observations occurred when increasing the scan rate in the same electrolyte. From these results, it seems that the porous morphology is more open to proton intercalation. When using lithium in PC the two films exhibit similar characteristics. Electrochemical impedance spectroscopy (EIS) showed indications that the electrodeposited film was more porous.

The most important effect is when electrodeposited WO_3 is used as a spacer layer in a MIM-cavity. Prior results by our group showed a switching time of up to 30 seconds for the sputtered WO_3 cavity. The electrodeposited cavity reduced this to seconds, even in PC. A small disadvantage with electrodeposited cavities is a small reduction in the saturation of the colors. They look slightly duller than the sputtered samples. Also, the electrodeposited films are not as uniform as the sputtered ones, and this can lead to more scattering that reduces chromaticity.

Additionally, another deposition method was tried on ITO. This is the sol-gel method, which is based on spin-coating. It was challenging to achieve thick layers using this method. The weighted contrast was not able to reach higher than around 40%.

4.2.3 WO_3 in cavity with polymer on top (unpublished)

This section will conclude with some unpublished data regarding a solution to the grayscale problem. There is a choice of color with a monopixel, but another shutter layer must be incorporated in order to modulate the reflection intensity. A trial was made to deposit the polymer PProDOT-Me_2 upon a sputtered WO_3 cavity. Since WO_3 and PProDOT-Me_2 switch on different time scales it would be possible to alter their states individually. We demonstrated that four states can be reached with this configuration:

1. Cavity reduced (purple) and polymer reduced (colored)
2. Cavity reduced (purple) and polymer oxidized (bleached)
3. Cavity oxidized (blue/green) and polymer reduced (colored)
4. Cavity oxidized (blue/green) and polymer oxidized (bleached).

State 1 and State 2 could be reached by applying a negative potential (-1.5 V vs. Ag/Ag+) for 10 seconds with a 1 second positive pulse of (+0.4 V vs. Ag/Ag+). Four times (44 seconds) was required to get the cavity to reach its purple state. When the one second positive pulse was applied, the polymer changed from colored state to bleached state. The cavity did not have time to change to its blue/green state making this State 2. To reach state 3 and 4 an anodic potential of +1.5 V and a cathodic potential of -0.8 V vs Ag/Ag+, each had a pulse time of 0.2 seconds. State 3 could be reached within 20 seconds. State 4 could be reached by using -0.8 V and +0.4 V vs Ag/Ag+ (which is the switching potentials for PProDOT-Me_2). In Figure 42A the reflection for three wavelengths can be seen together with all the potential waveform Figure 42B. A representation of the cavity structure can be seen in Figure 42C and the structure with PProDOT-Me_2 on the gold can be seen in Figure 42D.

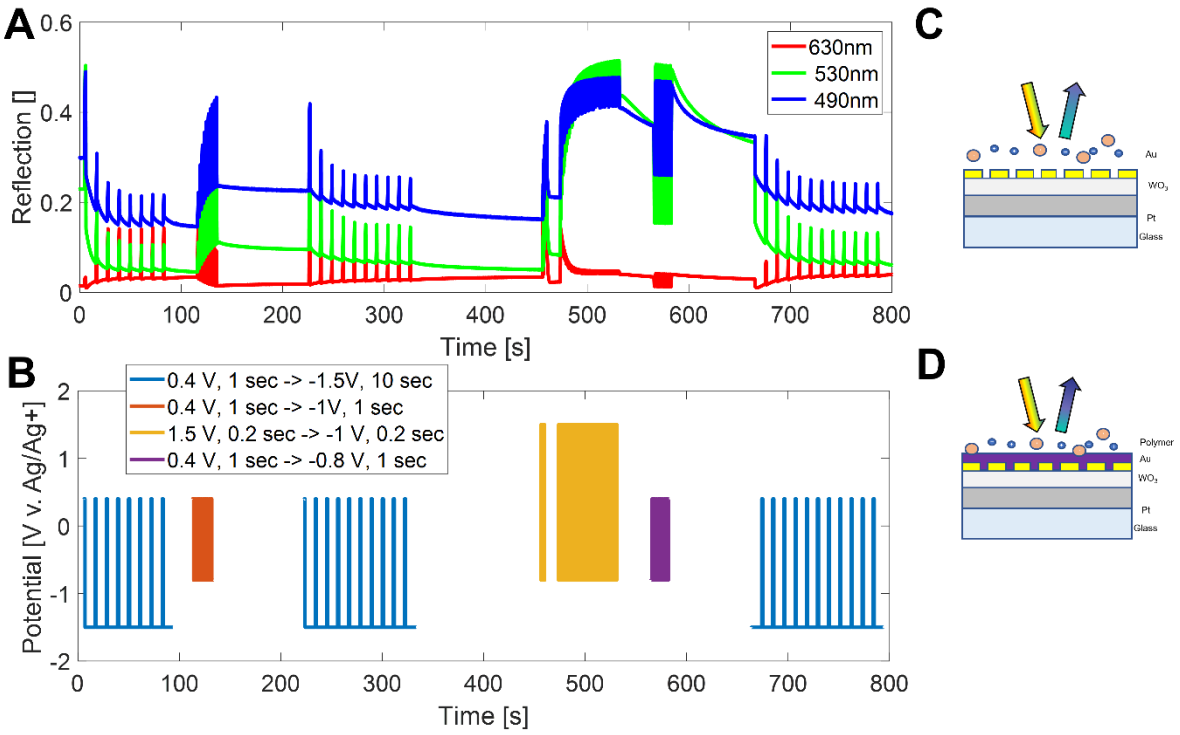

Figure 42 A) Reflection trace of three wavelengths representing red (630 nm), green (530 nm) and blue (490 nm) colors. B) The applied potentials waveform. C) A schematic of the cavity with WO_3 as a spacer layer. D) A schematic of the cavity with the polymer PProDOT-Me_2 on top of the gold.

In Figure 43A spectra can be seen for the WO_3 cavity in purple state. The pristine cavity, without polymer on top is represented by the dashed line. With the PProDOT-Me_2 on top, State 1 and State 2 can be achieved. Figure 43B and Figure 43C shows photographs of State 1 and State 2 respectively. In Figure 43D spectra can be seen for the WO_3 cavity in blue/green state. The pristine cavity, without polymer on top is again represented by the dashed line. With the polymer on top, State 1 and State 2 can be achieved. Figure 43E and Figure 43F shows photographs of State 1 and State 2 respectively.

4.2.4 Final remarks regarding dynamic cavities

Both the inorganic and the organic system worked as expected. The pixel could alter color while keeping a high reflection. To further improve the dynamic cavity other materials could be tested. An example is titanium dioxide, which have been shown to exhibit a change in refractive index upon lithium intercalation in a similar configuration [110]. Other polymers that are transparent in both reductive and oxidative state could also be tested [67] and also various electrolytes.

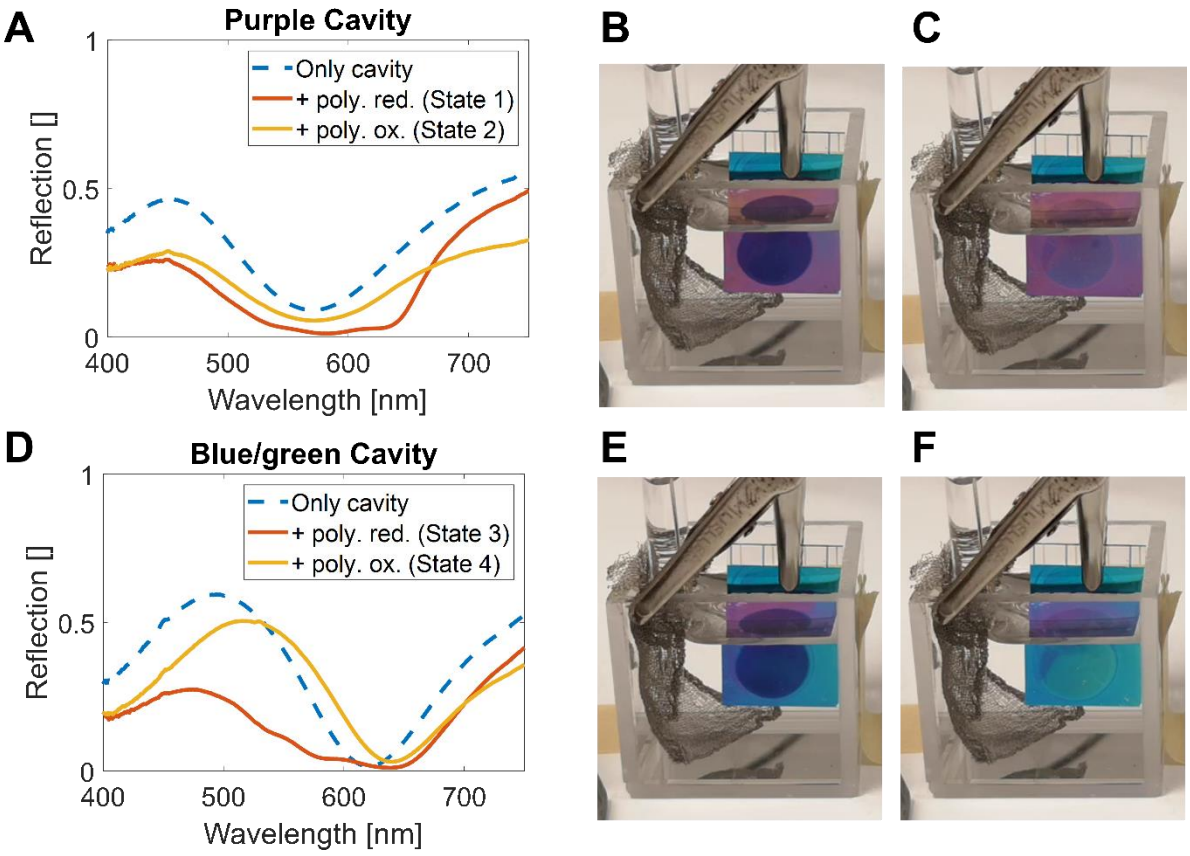

Figure 43 A) Spectra of only the cavity in purple state (--) and the cavity in purple state with PProDOT-Me_2 on top in either its colored or bleached state (-). B) A photo of State 1 and C) State 2. D) Spectra of only the cavity in blue/green state (--) and the cavity in blue/green state with PProDOT-Me_2 on top in either its colored or bleached state (-). E) A photo of State 3 and F) State 4.

4.3 Electrochromic matrix configurations

This section contains two subsections: active matrix (AM), and passive matrix (PM). All results regarding AM are summarized in a manuscript (**Paper VI**) and only a shorter a summary will be given. The second section regarding PM is more extensive.

The front page of this thesis shows my crude plan to achieve a graphical display from electrochromics. The far left represents the work with characterizing both the electrochromic material and the counter electrode separately. In the second panel the two materials are characterized together to see how they optically look and how one materials charge can balance the other. This is still done in a flow cell. The third panel represents the step from the flow cell to and electrochromic device. Now there might be a patterned, gel-electrolyte. The final step is to create either a passive or active display and test how the material works in a configuration with multiple pixels.

4.3.1 Active matrix

Active matrixes, or TFT-backplanes, are not easy to procure. After searching far and wide, we were able to buy some from the company Plastic Logic. My experiments with utilizing this backplane as electrochemical substrates are summarized in **Paper VI** (manuscript in preparation). However, a summary will follow. The TFT arrays came on a plastic PET substrate and the top pixels were 200 x 200 μm^2 gold electrodes. There are 240 gates and 400 sources. Each source and gate line could be contacted with 20 µm wide gold lines which had a spacing of 20 µm. The gold lines were also coated with a protective top layer which had to be removed by scratching it away. To make individual contacts to the lines, wire bonding was performed by an external company. The bonds were made from the lines to a printed circuit board (PCB). In Figure 44A the polymerization of many different areas can be viewed. Figure 44D and Figure 44E show the zoomed-in area with one of the pixels in a bright state and switched to a dark state. No crosstalk can be seen. In Figure 44B and Figure 44C the individual wire bonds can be seen.

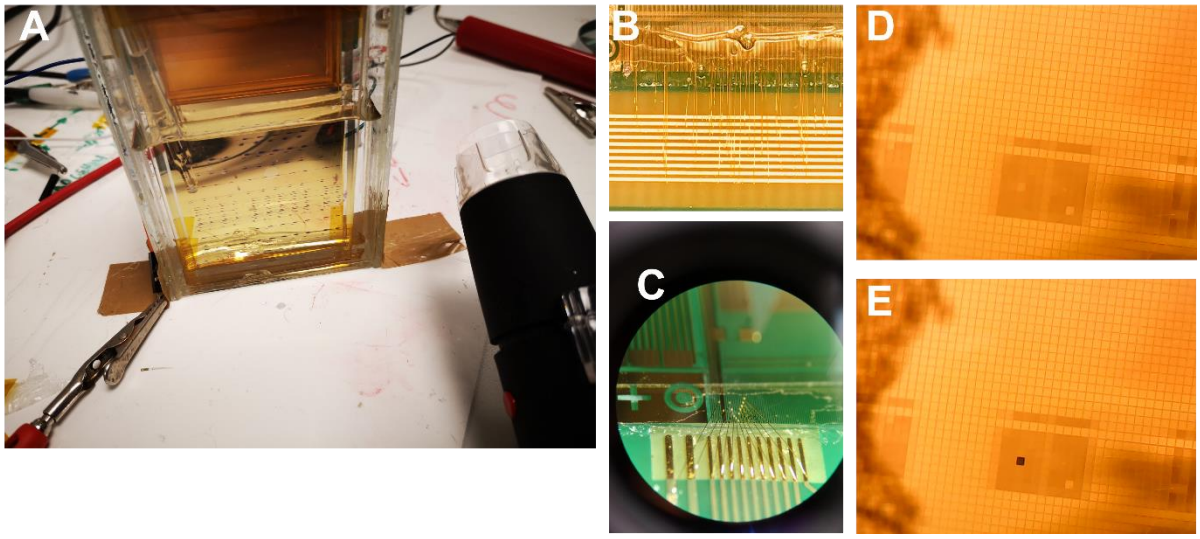

Figure 44 A) The many small dots are the areas where polymerization have occurred. B) and C) shows the wire bonds in two different microscopes. D) shows one pixel addressed to be in bright state and E) shows the same pixel switched to dark state.

My colleagues successfully deposited the RGB metasurfaces on a piece of the TFT array (Figure 45A-B) and the reflection of the RGB subpixels were ~40% (**Paper VI,** Figure 2). The polymerization was tested on a backplane with every third line having a red metasurface Figure 45C-D). An automatic

driving circuit was built to switch the pixels. The circuit was tested only with many pixels bundled together in a 6x2 grid. In Figure 45E and Figure 45F two images of the backplane in two different states can be seen. The switching time was increased when using the TFT-array as a substrate, comparing to a bare gold surface. The switch time could, however, be lowered by increasing the applied voltage. It was sufficient to switch the material with a 100 ms pulse of -10 V. Incorporating the pixel storage capacitor did unfortunately not decrease the switching time.

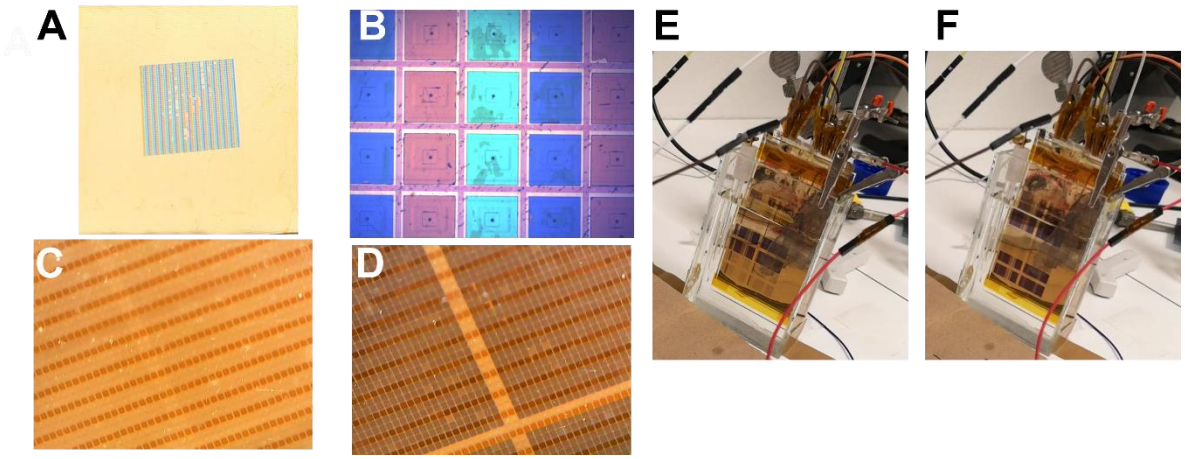

Figure 45 A) The metasurfaces deposited on a backplane. Red, green and blue metasurfaces deposited on ever third pixel. B) Picture from microscope C) polymer in bright state deposited on the array with 1/3 red metasurface and D) the dark state. E) Driving a 2x3 bundled grid with a microcontroller displays 2 different states.

4.3.2 Passive matrix

The theory section introduces electrochromic passive matrix displays and the importance of hysteresis. Using ITO as a counter electrode, we found an electrochemical reaction that when used as a counter electrode results in a hysteresis effect. In Figure 46A CV scans for PProDOT-Me_2 on gold can be viewed together with a CV scan of ITO in an electrolyte consisting of propylene carbonate (PC) and lithium perchlorate ($LiClO_4$). There is clearly a diode-like shape of the CV for the ITO. Within a certain potential span no current is passing, when sufficiently high potentials are applied, current pass. This is not the case for PProDOT-Me_2. As a result of the capacitive behavior, current passes easily in either direction depending on polarity. Combining the reaction on ITO with the polymer (ITO as counter and PProDOT-Me_2 on gold), restricts the current until sufficiently high potentials on ITO have been achieved. This translates into the high voltages of the device being required to let the potential of the ITO be sufficiently large to inject charge. Figure 46B shows that the combination of the two electrodes exhibits the characteristics of the voltammogram of the ITO electrode. By depositing PProDOT-Me_2 on ITO and use bare ITO as a counter electrode hysteresis was still obtained.

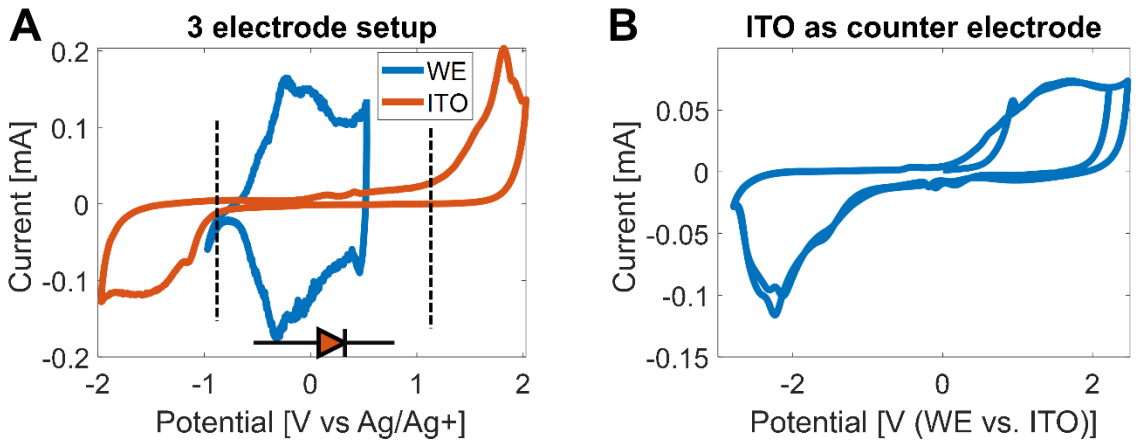

Figure 46 A) CV of PProDOT-Me_2 on gold (WE) and CV of ITO. Both are in 0.1 M $LiClO_4$-PC and scan rate is 100 mV/s. B) CV of PProDOT-Me_2 on gold as working electrode and ITO as counter electrode. 100 mV/s in 2 electrode setup.

The reflection of PProDOT-Me_2 on gold as a function of voltage does not have any significant hysteresis on its own. Each applied potential corresponds to an optical state as seen in Figure 47A (though this is not valid for all polymers, PProDOP exhibits small hysteresis for faster sweep rates). Unsurprisingly, the reflection exhibits hysteresis when combined with the ITO electrode as seen in Figure 47B. The electrochromic effect is proportional to the injected charge which only passes at higher voltages. How broad the hysteresis is depends on the scan rate, lower scan rate diminished the hysteresis.

For the active-matrix configuration, a global electrolyte is possible to use. This is not the case for the passive matrix. Each pixel created in the intersection of the stripes should be its own electrochromic device. This is done by patterning the electrolyte by either UV-patterning or screen printing.

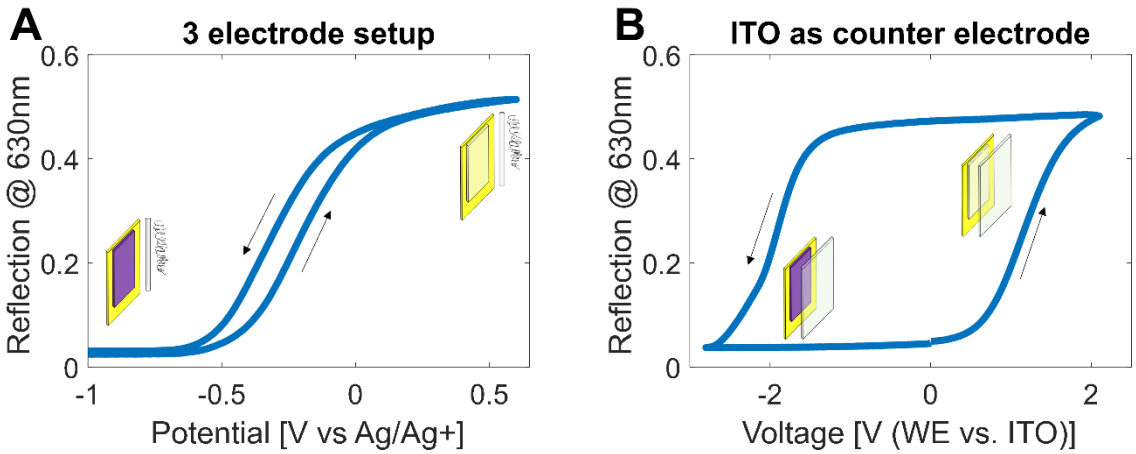

Figure 47 A) the reflection of PproDOT-Me2 on gold against the applied potential. B) with ITO as a counter electrode hysteresis are introduced.

A passive matrix was made by using stripes of bare ITO electrodes. The electrolyte was isolated using UV-patterning Figure 48 shows a the 3x3 matrix as a proof of concept. An image was shown which could later be inverted. Each pixel was addressed with a 150 ms pulse (swept through the pixel several times) and the full image required around 1 second to fully update.

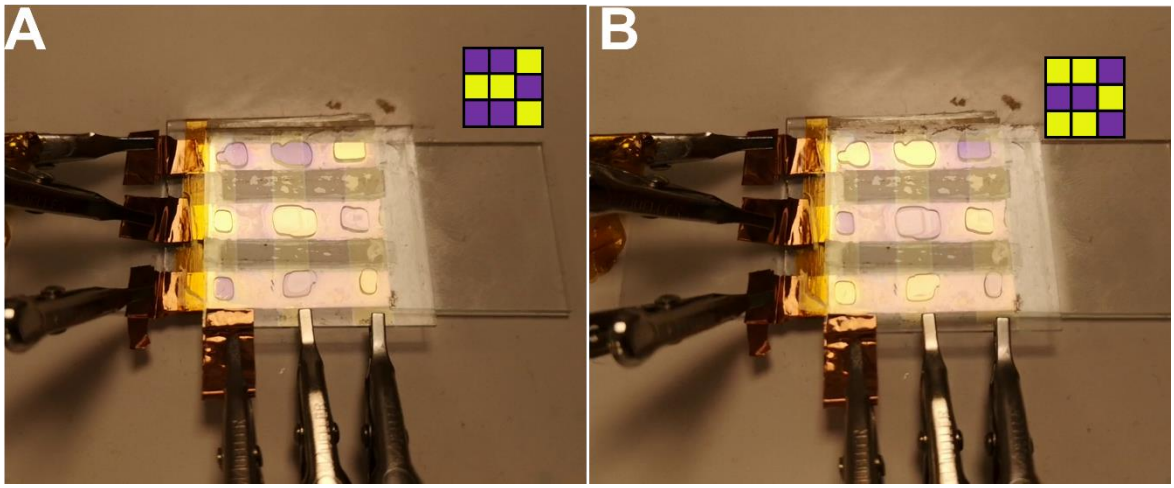

Figure 48 A 3x3 passive matrix with one frame in (A) which is inverted in in (B).

But what is the reaction on ITO? Is it the ITO that is participating itself or is it maybe the electrolyte? ITO has an electrochemical activity that has been utilized for electrochromic devices before. However, it is not really the same reaction which is utilized in this work. The reaction previously used by other authors is obtained when applying a potential below -2 V vs. Ag/Ag+. This reaction have been extensively discussed in the literature [111-118] and are proposed to be lithium intercalation. However, to my knowledge, there is no definite answer. Focus will not be on this "lithium intercalation" reaction.

We have not been able to fully understand what the reaction is that occurring on the ITO electrode in propylene carbonate and lithium perchlorate. Looking at the peaks in Figure 46A it can be seen that the both the reduction peak and the oxidation peak consist of at least two separate peaks each. This suggests that the reactions are more complicated than the examples that was presented in the Theory section. Using equations such as Randle-Sevcik equation is tempting, but one has to keep in mind of where the equations comes from, for which cases they are derived. No quantitative analysis was made on the reactions on ITO.[4] Below I will present some observations and some explanation of how the observations might be interpreted:

1.) Figure 49A. The anodic peak is only present after a cathodic polarization have taken place. This suggests that the species that is reduced at ~-1.5 V is later oxidized at ~1.5 V. If this is a one-step reaction ($O + ne^- \rightarrow R^-$) the high peak separation suggests that the reaction would be highly sluggish (as described in the theory section). Another possibility is that there are EC-reactions occurring ($O + ne^- \rightarrow R^- \rightarrow A$) where the reduction forms a product which chemically reacts and converts to another species (A). Species A are oxidized at the higher potentials. The dashed line shows the "lithium intercalation". This reaction is not used from here and on.

[4] *I tried to squeeze in some of the data I had into Nichols-Shain equations but failed. I asked for help by a real electrochemist, but were promptly told that you cannot use these equations if you have multiple reactions with perhaps a chemical step In between.*

2.) Figure 49B. The reaction is not present after oxygen have been removed from the electrolyte. By adding oxygen, the reaction is again observed. Adding water have limited influence of the reduction but an increase in oxidation peak are observed with oxygen present. An oxidation current is present when water is added without oxygen at ~2 V. This suggests that the reaction is a reduction of oxygen.

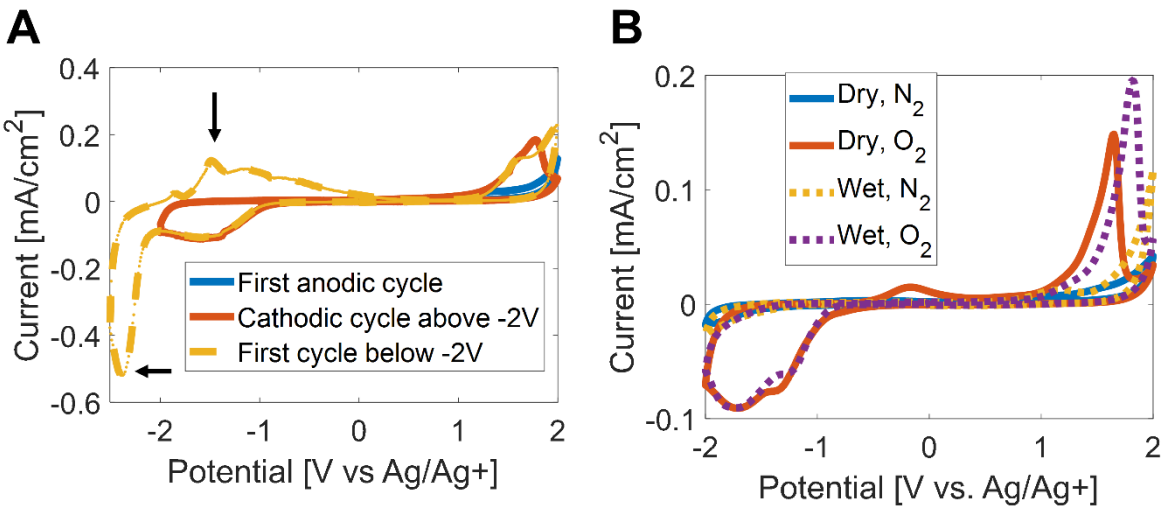

Figure 49 A) The first anodic sweep displays no oxidation peak. If reduction occurs prior to the oxidation sweep a peak is observed. Sweeping below -2 V vs. Ag/Ag+ display the "lithium-intercalation" reaction which are discussed elsewhere. This reaction is pointed out by the arrows. B) Deoxygenated (N_2) electrolyte does not exhibit the reduction peak. When water is added (~8000 ppm) an increase in oxidation current can be observed at around +2 V. Dry electrolyte had 200-400 ppm water content. Scan rate is 100 mV/s and electrolyte used is $LiClO_4$-PC 0.1 M for both A) and B)

3.) Figure 50A. Changing the cation from lithium tertbutyl ammonium (TBA+) gives a reduction reaction, however, the voltammogram is not identical to the voltammogram with lithium. The reduction current is higher when using the TBA+ cation. The ratio of the oxidation peak to the reduction peak is lower for the TBA+ cation. This suggests that the cation is participating in the reaction.

4.) Figure 50B. The reaction is not selective to ITO surfaces but can also be observed on gold, however the peak separation is larger for ITO. This suggests that the ITO electrode does not participate in the reaction but, however, increase the sluggish behavior. The difference in conductivities between gold and ITO does not fully explain the difference between the two electrodes peak separation. Adding resistors with different resistance in series to an ITO electrode shows that the onset of the reaction remains the same. The slope of the current to the potential is decreasing with increasing resistance.

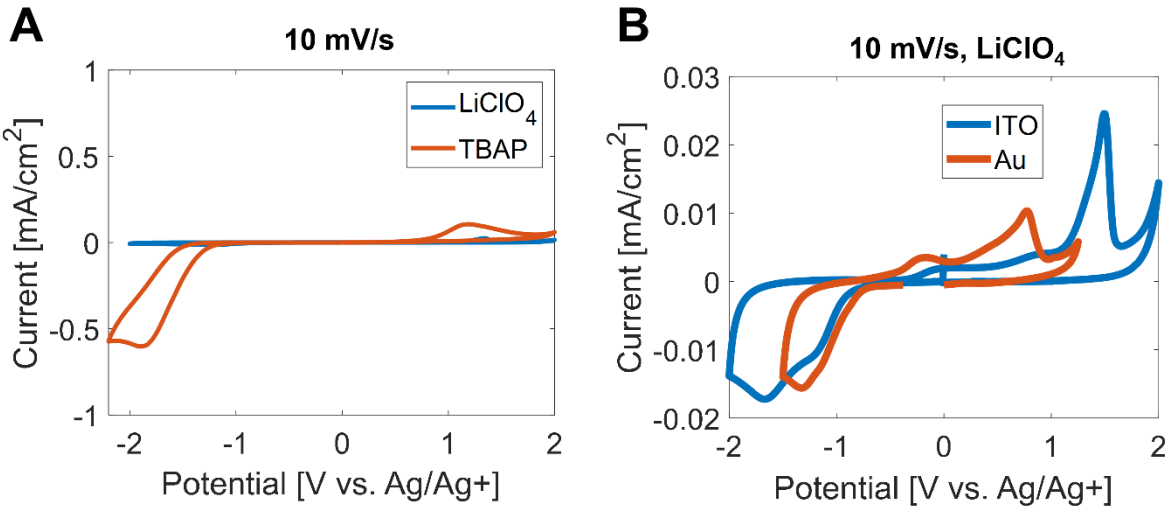

Figure 50 A) Changing the salt from $LiClO_4$ to TBAP alters the voltammogram by increasing the current. B) Similar reactions are found on gold. The scan rate is 10 mV/s for both A) and B) and the solvent was PC.

5.) Figure 51A. EQCMD suggests that something is deposited on the ITO electrode during reduction when the lithium salt is used. No deposition occurs when TBA+ is used even though it gives a higher current. Deposition was also present on a gold electrode when reducing with the salt containing lithium.

6.) Figure 51B. Similar reaction can be seen by changing the solvent from propylene carbonate to acetonitrile. This suggests that the solvent is not participating in the reaction.

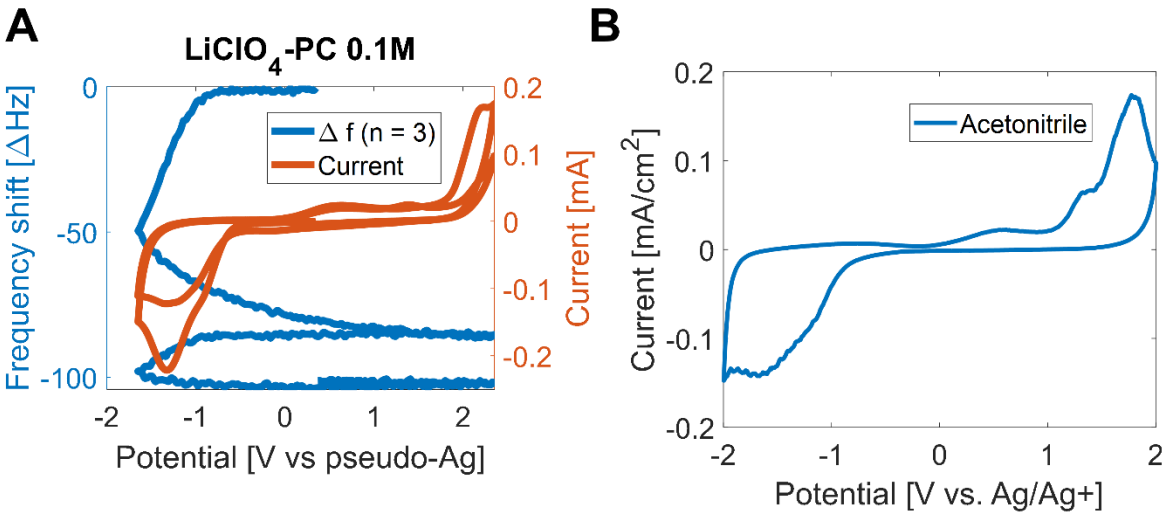

Figure 51 A) ITO in EQCMD with $LiClO_4$-PC 0.1 M. Right axis (red) shows the current (CV). Left axis shows the frequency shift which decreases when the current increases indicating a deposition. Scan rate is 100 mV/ B) Similar voltammograms are observed when changing the solvent from PC to acetonitrile. Scan rate is 100 mV/s and salt used is $LiClO_4$ 0.1 M.

7.) Figure 52A. Multiple reduction sweeps with lithium salt (0 V → -2 V → 0 V → -2 V) only give a reduction current the first cycle. The reduction cycles after are significantly lower. This suggests that the electrode have been passivated.

8.) Figure 52B. After the electrode have undergone one reduction cycle, no more reduction can occur as described above. If an anodic sweep occurs the oxidation peak is obtained. If a reduction cycle is performed after the anodic cycle the reduction peak is once again obtained. This suggests that the oxidation peak is removing the passivating species.

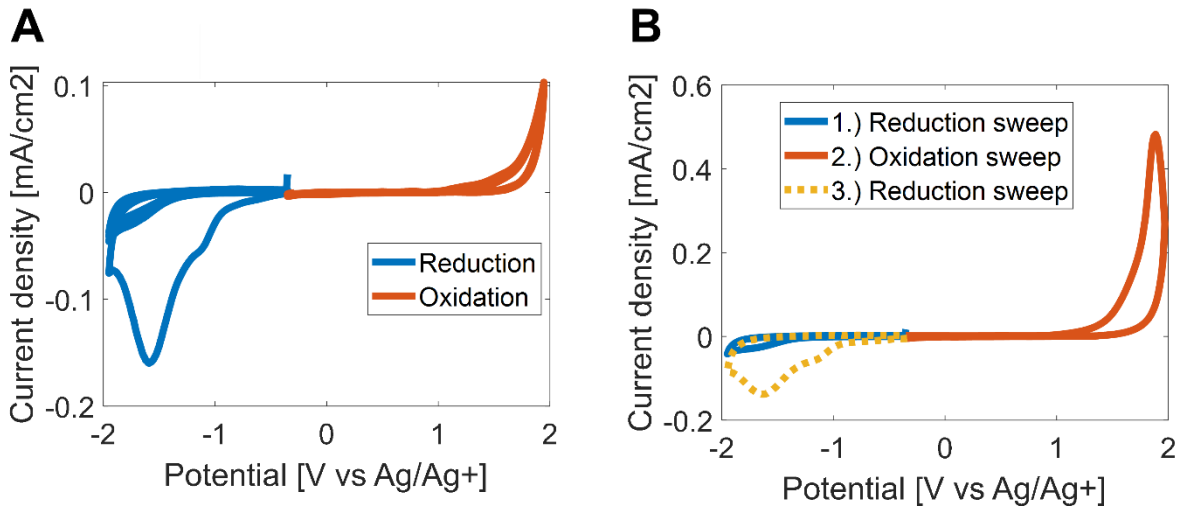

Figure 52 A) Multiple reduction cycles. Only the first cycle exhibits the reduction peak(s). No oxidation peak occurs without first performing a reduction cycle. B) 1.) No reduction peak visible if reduction already have been performed. The electrode is passivated 2.) Sweeping anodically removes the passivating species. 3.) The, now, unpassivated, electrode can once again exhibit reduction. Both A) and B) used a scan rate is 100 mV/s and $LiClO_4$ -PC 0.1 M in an open beaker.

9.) Figure 53A. Multiple sweeps of reduction and oxidation diminish the current. If sweeping within the span of -1.5 V to +1.5 V the current goes down to micro ampere per centimeter. This is probably because not high enough oxidation potentials are used to depassivate the electrode. If sweeping between -1.5 V to +2 V a current of 50 micro ampere per centimeter is still present. Sweeping between -2 V and +2 V an additional peak at around -1 V have spawned after 1000 cycles. Sweeping between -2.5 V and +2 V (Figure 53B) the "lithium intercalation" reaction can be seen but with lower currents than for cycle 1 (Figure 49A, dashed curve).

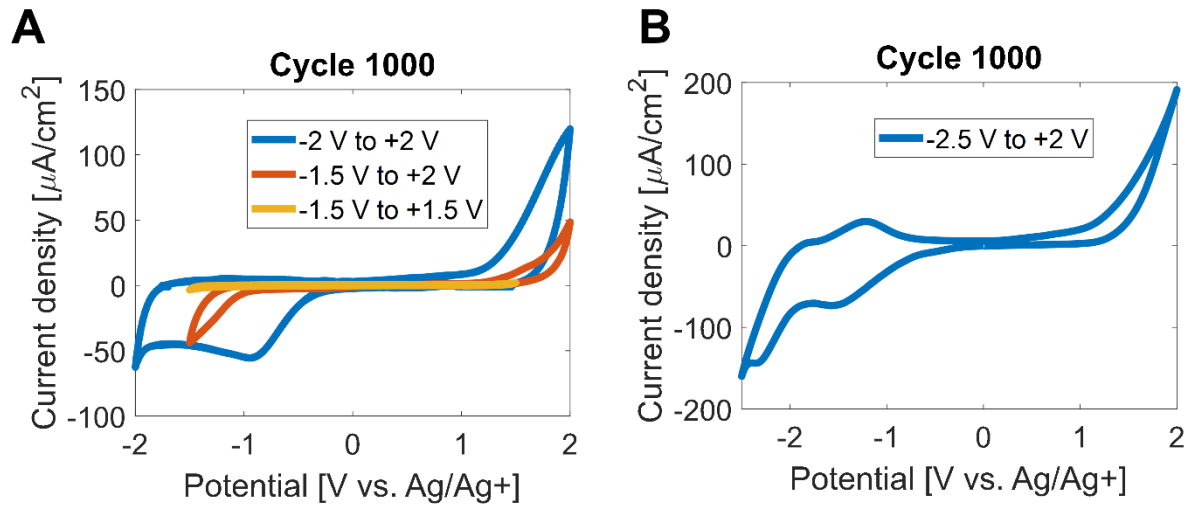

Figure 53 Voltammogram after 1000 cycles. The various curves are within different potential spans. A) shows -1.5 V to +1.5 V, -1.5 V to +2 V, and -2 V to +2 V. B) shows -2.5 V to +2 V.

Previous literature suggests that when oxygen reduction occurs on noble metals, such as gold, in the present of lithium ions, a passivating lithium containing coating is formed on the electrode. This does not occur when tetrabutylammonium (TBA+) salts are used [119]. This is one of the most probable explanations that we currently have.

As a final remark of this project, I will present some data that I was unable to reproduce in a controlled environment (flow cell). By adding water to the electrolyte (propylene carbonate and lithium perchlorate) and performing the electrochemical experiments (cyclic voltammetry) in an open beaker, and additional peak at around -1 V vs. Ag/Ag+ occurred. This reduction peak was only observed after a high enough anodic polarization occurred (~ +2 V vs. Ag/Ag+). In an open beaker, 800 cycles were able to be cycled. Figure 54A shows voltammogram of when water is added in the electrolyte in an open beaker. Additional peaks form at -1.3 V and +2 V vs. Ag/Ag+ (indicated with arrows).

Figure 54B shows the cyclic voltammograms of the polymer PProDOT-Me_2 on gold as working electrode and ITO as counter electrode in the flow cell. Comparing TBAP and $LiClO_4$ we see that the reduction peak of the device is at lower potentials for TPAB than for $LiClO_4$. This is because the oxidation peak is at lower potentials for TBAP (the reduction potential for the device is corresponding to the oxidation peak for the ITO since the ITO is the counter electrode). Using the wet electrolyte and the reaction in Figure 54A displayed similar voltammograms as for the “original” $LiClO_4$ reaction. Figure 54C shows that the three cases exhibit hysteresis with slightly different voltages where the onset of either decline or incline in the reflection starts.

With this I want to communicate that it is not selective to use the reaction using $LiClO_4$-PC with oxygen on ITO described in this section for introducing the necessary hysteresis required for the passive matrix. If a CV exhibit the right characteristic with a “diode-like” shape and large peak separation it could be incorporated. Hopefully, these results could inspire other researchers to find the most suitable counter electrode reaction to be used for an electrochromic passive matrix.

4.3.3 Final remarks regarding matrix configurations

The engineering issues with the active matrix were a challenge. Contacting individual electrodes were a cumbersome project which gave low yield. Nanofabrication on flexible substrate was not straight forward and required many steps. However, we proved that you could use a commercial flexible TFT-array to build our metasurfaces on top. Polymerization could be performed on top of the metasurfaces and switched. Electropolymerized could be performed on individual pixels, this opens up to use different polymers for different pixels e.g. PProDOP on blue pixels for higher contrast. Unfortunately, the storage capacitor was of no use to reduce the switch time. I believe that TFT-arrays made for OLEDs would be the next step to try, this because they can withstand higher currents by utilizing two transistors.

Because of the slow updating time of the passive matrix, I do not believe that it can be made into any high-end products. However, since it is easy to fabricate, I believe that it could be incorporated into low end products. These products could be smart windows or sunglasses.

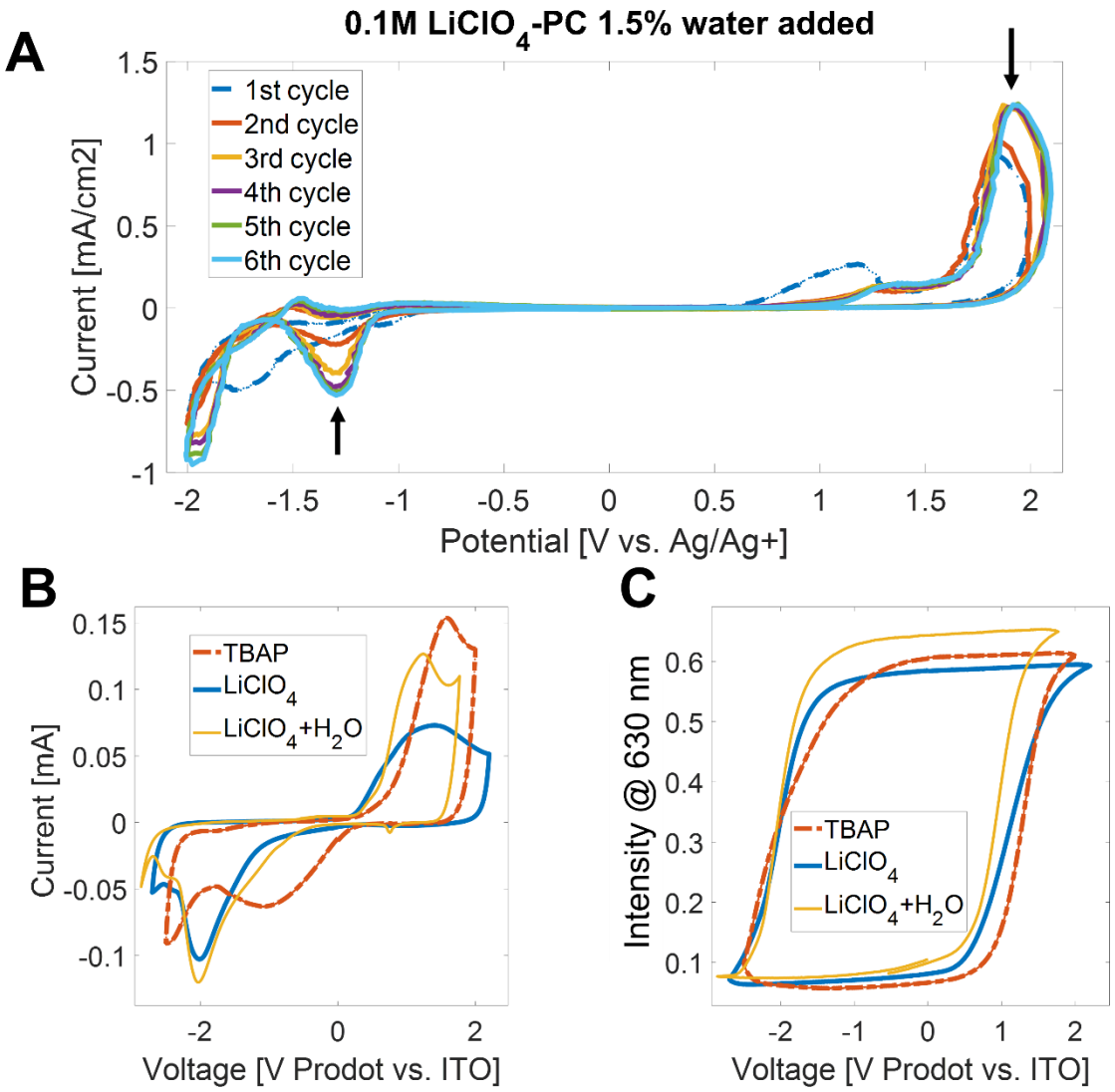

Figure 54 A) Adding water into the electrolyte ($LiClO_4$-PC 0.1 M) added a reduction peak with cycles. B) Different electrolytes used with PProDOT-Me_2 on gold as working electrode and ITO as counter electrode. C) Hysteresis is present in for the three different electrolytes.

5 Conclusion and future outlook

To summarize: out of the polymers we tried, PProDOT-Me_2 seems to be the most suitable polymer as shutter on top of red and green pixels since it exhibited high contrast. PProDOP has higher blue contrast and is more suitable for blue pixels. WO_3 has higher contrast than any polymer tested for all pixels, red, green, and blue. However, the switching time of polymers is one order of magnitude faster than WO_3 and can even reach video speeds [84].

Comparing WO_3 and the polymer PT34bT for building dynamic cavities, the inorganic option gives better uniformity, though it provides a narrower range of colors. Locally, one pixel with PT34bT could, with high reflection, produce any color. WO_3 cavities require 2 pixels to give the full color range but the cavities are significantly slower when switching [3]. By using electrodeposited WO_3 we managed to decrease the switching time. These two designs (PT34bT and WO_3) represent a step forward from the current three-subpixel systems, although some improvements would still be necessary such as using a second electrochromic layer to adjust the reflectivity of the pixel.

The red, green, and blue metasurfaces could also be fabricated on top of commercially available active matrices, creating an RGB-subpixel configuration. On these matrices, PProDOT-Me_2 could be polymerized and individual pixels could be switched ON and OFF. In addition, we constructed a 3x3 passive matrix, where ITO is used as counter electrode. This was possible since an oxygen reduction reaction is likely occurring in the non-aqueous electrolyte on the ITO counter electrode. This reaction creates non-linearities (threshold behavior) in the voltage-current relation and an electrochromic device that allows for passive matrix configurations.

To conclude, a total of three goals were set and all were partially accomplished. Higher contrasts compared to previous work were achieved on colored pixels by changing the electrochromic material. Pixels that changed their color were made from both organic and inorganic materials. Active and passive matrices were used to construct pixelated devices. However, these were baby steps and we still don't have magical Harry Potter paper in color. Could it be produced in the future? Maybe. The science is in place and with some additional engineering work based upon this work, there is a good chance of success.

The question is how good is this technology and would it work for commercialization? For the subpixel configuration without electrochromics, the whitest white will still be around 30-40%. This is good enough but a monopixel system would be ideal. Switch time is still a problem. Video speed requires the full image to update at least 24 times a second. If a passive matrix can update row-by-row, this puts the condition on the individual material to update within 0.2 ms. This is far faster than what is achievable today. The passive matrix configuration can, however, be made very cheaply, at least cheaper than an active matrix configuration. This technology could be used in electrochromic windows, to electronically alter the transparent region size by changing the opacity of different areas.

To create a display with faster switching time, an active matrix configuration must be used. A capacitor must be incorporated into the active matrix that is large enough to sustain charge injection into the material while the other rows are addressed. By making a customized TFT-backplane for electrochromics, this could be achieved.

For high-end products, there is still the big elephant in the room - life time. There is a loss of contrast with cycle number that is seemingly unavoidable. For low-end, cheap products it might not be an issue with devices that only work for 1'000'000 switches. As an example, if a digital clock were made from

the material it would work for more than 11 days straight if updated every second. In our group, we demonstrated the year 2019 that this could be extended 10 times [84] to 110 days or 4 months, or 13 hours of video (25 Hz). In 2002 the lifetime was 1 000 000 switches. 19 years later, the lifetime was 10 times increased. Hopefully, we don't have to wait 20 more years to see 100 million switches which would be 130 hours of video.

Even though the final paragraphs of this thesis end in a rather melancholic tone, I still believe that the technology (and our achievements) will find its place sooner or later. As stated in the Introduction, structural colors and plasmonics is a field on the rise. Even more so together with electrochromics. I believe that the will of having better reflective displays, with “better” meaning either cheaper or higher optical performance, is still ongoing.

6 Acknowledgments

I would want to thank the Swedish Foundation for Strategic Research (SSF) for funding. I would like to thank my supervisor, Andreas Dahlin, my co-supervisor, Per Rudquist, and my first examiner, Christian Müller, for the constructive discussions. Thank as well to my second examiner Ergang Wang. I would like to acknowledge my former colleagues, Philip Holgersson and Felix Karlsson, at RDOT. I would also want to acknowledge Peter Andersson Ersman for all his help regarding electrochromism and displays and Ioannis Petsagkourakis for help regarding conjugated polymers. I would like to thank all my colleagues in the Dahlin group, both present and former. John Andersson and Gustav Ferrand Drake helped tremendously with my experience with the SPR instrument and the modeling. And I would like to thank my family for their support. My mom, Anna-Karin Sandberg, and my dad Peter Olsson, my brothers Ludvig Olsson and Gustav Olsson. Thanks to Magnus Neuendorf and Lena Neuendorf for all the help, especially for letting me stay with you here in Göteborg :) Thanks to my friends, wherever you currently might be. Thanks to all the people at the department that make it such an enjoyable workplace. Especially thank Lotta Pettersson for handling all of my annoying small purchases. Andreas Schaefer for helping me with XPS and letting me come see the machine. Thanks to former teachers, especially Lena Fredriksson and Fredrik Olsson. Especially thanks to Marika Gugole, my (probable) future wife.

Göteborg, May, 2023

7 Bibliography

[1] P. F. Bai *et al.*, "REVIEW OF PAPER-LIKE DISPLAY TECHNOLOGIES (Invited Review)," *Progress In Electromagnetics Research,* vol. 147, pp. 95-116, 2014, doi: 10.2528/pier13120405.

[2] M. Omodani, "10.1: Invited Paper: What is Electronic Paper? The Expectations," *SID Symposium Digest of Technical Papers,* vol. 35, no. 1, p. 128, 2004, doi: 10.1889/1.1825751.

[3] M. Gugole, O. Olsson, S. Rossi, M. P. Jonsson, and A. Dahlin, "Electrochromic Inorganic Nanostructures with High Chromaticity and Superior Brightness," *Nano Letters,* 2021, doi: 10.1021/acs.nanolett.1c00904.

[4] J. Heikenfeld, P. Drzaic, J.-S. Yeo, and T. Koch, "Review Paper: A critical review of the present and future prospects for electronic paper," *Journal of the Society for Information Display,* vol. 19, no. 2, p. 129, 2011, doi: 10.1889/jsid19.2.129.

[5] H. Zang *et al.*, "44-1: Distinguished Paper: Electrophoretic Display Comprising Black, White, Red, and Yellow Particles," *SID Symposium Digest of Technical Papers,* vol. 53, no. 1, pp. 549-552, 2022, doi: 10.1002/sdtp.15546.

[6] E. Huitema and I. French, "E Ink's Technicolor Moment: The Road to Color E-Paper Took Two Decades," *IEEE Spectrum,* vol. 59, no. 2, pp. 30-35, 2022, doi: 10.1109/mspec.2022.9706404.

[7] B. Comiskey, J. D. Albert, H. Yoshizawa, and J. Jacobson, "An electrophoretic ink for all-printed reflective electronic displays," *Nature,* vol. 394, no. 6690, pp. 253-255, 1998, doi: 10.1038/28349.

[8] Y. Lu, B. Tang, G. Yang, Y. Guo, L. Liu, and A. Henzen, "Progress in Advanced Properties of Electrowetting Displays," *Micromachines,* vol. 12, no. 2, p. 206, 2021, doi: 10.3390/mi12020206.

[9] R. A. Hayes and B. J. Feenstra, "Video-speed electronic paper based on electrowetting," *Nature,* vol. 425, no. 6956, pp. 383-385, 2003, doi: 10.1038/nature01988.

[10] H. Holding. "Applications and Industries." https://www.heraeus.com/en/hep/applications_hep/applications_overview_hep/applications_hep_1.html (accessed 19-04-2023.

[11] R. J. Mortimer, "Electrochromic Materials," *Annual Review of Materials Research,* vol. 41, no. 1, pp. 241-268, 2011, doi: 10.1146/annurev-matsci-062910-100344.

[12] R. J. Mortimer, "Organic electrochromic materials," *Electrochimica Acta,* vol. 44, no. 18, pp. 2971-2981, 1999, doi: 10.1016/s0013-4686(99)00046-8.

[13] S. Kinoshita, S. Yoshioka, and J. Miyazaki, "Physics of structural colors," *Reports on Progress in Physics,* vol. 71, no. 7, p. 076401, 2008.

[14] A. Kristensen *et al.*, "Plasmonic colour generation," *Nature Reviews Materials,* vol. 2, no. 1, p. 16088, 2017, doi: 10.1038/natrevmats.2016.88.

[15] S. Kinoshita, *Structural Colors In The Realm Of Nature*. Singapore, SINGAPORE: World Scientific Publishing Company, 2008.

[16] K. Xiong, D. Tordera, M. P. Jonsson, and A. B. Dahlin, "Active control of plasmonic colors: emerging display technologies," *Reports on Progress in Physics,* vol. 82, no. 2, p. 024501, 2019, doi: 10.1088/1361-6633/aaf844.

[17] S. Mukherjee *et al.*, "A first demonstration and analysis of the biprimary color system for reflective displays," *Journal of the Society for Information Display,* vol. 22, no. 2, pp. 106-114, 2014, doi: 10.1002/jsid.225.

[18] *Handbook of Visual Display Technology*. Springer-Verlag Berlin Heidelberg, 2012.

[19] E. Hecht, *Optics*, 5. ed., Global Edition ed. Pearson Education, 2017.

[20] S. Rossi and M. P. Jonsson, "Highly reflective optical nanocavities for structural coloration by combining broadband absorber and Fabry–Pérot effects," *Journal of Optics,* vol. 23, no. 1, 2020, doi: 10.1088/2040-8986/abccfe.

[21] S. A. Maier, *Plasmonics: fundamentals and applications*. Springer Science & Business Media, 2007.

[22] D. J. Griffith, "Introduction to Electrodynamics 4th Edition," ed: Pearson Education, 2012.

[23] Y. Kim, S. Cha, J.-H. Kim, J.-W. Oh, and J.-M. Nam, "Electrochromic response and control of plasmonic metal nanoparticles," *Nanoscale,* 2021, doi: 10.1039/d1nr01055g.

[24] W. L. Barnes, A. Dereux, and T. W. Ebbesen, "Surface plasmon subwavelength optics," *Nature,* vol. 424, no. 6950, pp. 824-830, 2003, doi: 10.1038/nature01937.

[25] J. Homola, "Surface Plasmon Resonance Sensors for Detection of Chemical and Biological Species," *Chemical Reviews,* vol. 108, no. 2, pp. 462-493, 2008, doi: 10.1021/cr068107d.

[26] J. Weiner, "The physics of light transmission through subwavelength apertures and aperture arrays," *Reports on Progress in Physics,* vol. 72, no. 6, 2009, doi: 10.1088/0034-4885/72/6/064401.

[27] A. B. Dahlin, M. Mapar, K. Xiong, F. Mazzotta, F. Höök, and T. Sannomiya, "Plasmonic Nanopores in Metal-Insulator-Metal Films," *Advanced Optical Materials,* vol. 2, no. 6, pp. 556-564, 2014, doi: 10.1002/adom.201300510.

[28] J. Junesch, T. Sannomiya, and A. B. Dahlin, "Optical Properties of Nanohole Arrays in Metal–Dielectric Double Films Prepared by Mask-on-Metal Colloidal Lithography," *ACS Nano,* vol. 6, no. 11, pp. 10405-10415, 2012, doi: 10.1021/nn304662e.

[29] K. Xiong *et al.*, "Plasmonic Metasurfaces with Conjugated Polymers for Flexible Electronic Paper in Color," *Advanced Materials,* vol. 28, no. 45, pp. 9956-9960, 2016, doi: 10.1002/adma.201603358.

[30] K. Xiong *et al.*, "Switchable Plasmonic Metasurfaces with High Chromaticity Containing Only Abundant Metals," *Nano Letters,* vol. 17, no. 11, pp. 7033-7039, 2017, doi: 10.1021/acs.nanolett.7b03665.

[31] A. J. Bard and L. R. Faulkner, *Electrochemical Methods: Fundamentals and Applications*. John Wiley & Sons, Incorporated, 2001.

[32] S. W. Boettcher *et al.*, "Potentially Confusing: Potentials in Electrochemistry," *ACS Energy Letters,* vol. 6, no. 1, pp. 261-266, 2021, doi: 10.1021/acsenergylett.0c02443.

[33] L.-Q. Chen, "Chemical potential and Gibbs free energy," *MRS Bulletin,* vol. 44, no. 7, pp. 520-523, 2019, doi: 10.1557/mrs.2019.162.

[34] R. Memming, *Semiconductor electrochemistry*. John Wiley & Sons, 2015.

[35] R. G. Compton and C. E. Banks, *Understanding voltammetry*. World Scientific, 2018.

[36] S. Trasatti, "The absolute electrode potential: an explanatory note (Recommendations 1986)," *Pure and Applied Chemistry,* vol. 58, no. 7, pp. 955-966, 1986, doi: doi:10.1351/pac198658070955.

[37] R. G. Compton, E. Kätelhön, K. R. Ward, and E. Laborda, *Understanding voltammetry: simulation of electrode processes*. World Scientific, 2014.

[38] A. J. Coffman, J. Lu, and J. E. Subotnik, "A grid-free approach for simulating sweep and cyclic voltammetry," *The Journal of Chemical Physics,* vol. 154, no. 16, p. 161101, 2021, doi: 10.1063/5.0044156.

[39] "The Nobel Prize in Chemistry 2000," ed. Nobel Prize Outreach AB 2023.

[40] D. N. Batchelder, "Colour and chromism of conjugated polymers," *Contemporary Physics,* vol. 29, no. 1, pp. 3-31, 1988, doi: 10.1080/00107518808213749.

[41] A. Köhler and H. Bässler, *Electronic processes in organic semiconductors: An introduction*. John Wiley & Sons, 2015.

[42] M. Heydari Gharahcheshmeh and K. K. Gleason, "Texture and nanostructural engineering of conjugated conducting and semiconducting polymers," *Materials Today Advances,* vol. 8, p. 100086, 2020, doi: 10.1016/j.mtadv.2020.100086.

[43] J. Clayden, N. Greeves, and S. Warren, *Organic chemistry*. Oxford university press, 2012.

[44] J. Roncali, "Molecular Engineering of the Band Gap of π-Conjugated Systems: Facing Technological Applications," *Macromolecular Rapid Communications,* vol. 28, no. 17, pp. 1761-1775, 2007, doi: 10.1002/marc.200700345.

[45] O. Bubnova and X. Crispin, "Towards polymer-based organic thermoelectric generators," *Energy & Environmental Science,* vol. 5, no. 11, p. 9345, 2012, doi: 10.1039/c2ee22777k.

[46] R. Hoffmann, "How Chemistry and Physics Meet in the Solid State," *Angewandte Chemie International Edition in English,* vol. 26, no. 9, pp. 846-878, 1987, doi: 10.1002/anie.198708461.

[47] A. O. Patil, A. J. Heeger, and F. Wudl, "Optical properties of conducting polymers," *Chemical Reviews,* vol. 88, no. 1, pp. 183-200, 1988, doi: 10.1021/cr00083a009.

[48] A. J. Heeger, "Semiconducting polymers: the Third Generation," *Chemical Society Reviews,* vol. 39, no. 7, p. 2354, 2010, doi: 10.1039/b914956m.

[49] J.-L. Bredas, "Mind the gap!," *Mater. Horiz.,* vol. 1, no. 1, pp. 17-19, 2014, doi: 10.1039/c3mh00098b.

[50] J. M. Hollas, *Modern spectroscopy*. John Wiley & Sons, 2004.

[51] F. C. Spano, "The Spectral Signatures of Frenkel Polarons in H- and J-Aggregates," *Accounts of Chemical Research,* vol. 43, no. 3, pp. 429-439, 2010, doi: 10.1021/ar900233v.

[52] A. L. Dyer, E. J. Thompson, and J. R. Reynolds, "Completing the Color Palette with Spray-Processable Polymer Electrochromics," *ACS Applied Materials & Interfaces,* vol. 3, no. 6, pp. 1787-1795, 2011, doi: 10.1021/am200040p.

[53] P. M. Beaujuge and J. R. Reynolds, "Color Control in π-Conjugated Organic Polymers for Use in Electrochromic Devices," *Chemical Reviews,* vol. 110, no. 1, pp. 268-320, 2010, doi: 10.1021/cr900129a.

[54] J. L. Bredas and G. B. Street, "Polarons, bipolarons, and solitons in conducting polymers," *Accounts of Chemical Research,* vol. 18, no. 10, pp. 309-315, 1985, doi: 10.1021/ar00118a005.

[55] K. Lee, S. Cho, S. Heum Park, A. J. Heeger, C.-W. Lee, and S.-H. Lee, "Metallic transport in polyaniline," *Nature,* vol. 441, no. 7089, pp. 65-68, 2006, doi: 10.1038/nature04705.

[56] I. Zozoulenko, A. Singh, S. K. Singh, V. Gueskine, X. Crispin, and M. Berggren, "Polarons, Bipolarons, And Absorption Spectroscopy of PEDOT," *ACS Applied Polymer Materials,* vol. 1, no. 1, pp. 83-94, 2019, doi: 10.1021/acsapm.8b00061.

[57] S. W. Feldberg, "Reinterpretation of polypyrrole electrochemistry. Consideration of capacitive currents in redox switching of conducting polymers," *Journal of the American Chemical Society,* vol. 106, no. 17, pp. 4671-4674, 1984, doi: 10.1021/ja00329a004.

[58] J. R. Heinze, B. A. Frontana-Uribe, and S. Ludwigs, "Electrochemistry of Conducting Polymers—Persistent Models and New Concepts†," *Chemical Reviews,* vol. 110, no. 8, pp. 4724-4771, 2010, doi: 10.1021/cr900226k.

[59] P. Shiri, D. Neusser, C. Malacrida, S. Ludwigs, and L. G. Kaake, "Mixed Ion-Carrier Diffusion in Poly(3-hexyl thiophene)/Perchlorate Electrochemical Systems," *The Journal of Physical Chemistry C,* vol. 125, no. 1, pp. 536-545, 2021, doi: 10.1021/acs.jpcc.0c09527.

[60] A. V. Volkov *et al.*, "Understanding the Capacitance of PEDOT:PSS," *Advanced Functional Materials,* vol. 27, no. 28, p. 1700329, 2017, doi: 10.1002/adfm.201700329.

[61] T. F. Otero, H.-J. Grande, and J. Rodríguez, "Reinterpretation of Polypyrrole Electrochemistry after Consideration of Conformational Relaxation Processes," *The Journal of Physical Chemistry B,* vol. 101, no. 19, pp. 3688-3697, 1997, doi: 10.1021/jp9630277.

[62] B. J. West, T. F. Otero, B. Shapiro, and E. Smela, "Chronoamperometric Study of Conformational Relaxation in PPy(DBS)," *The Journal of Physical Chemistry B,* vol. 113, no. 5, pp. 1277-1293, 2009, doi: 10.1021/jp8058245.

[63] X. Wang, B. Shapiro, and E. Smela, "Development of a Model for Charge Transport in Conjugated Polymers," *The Journal of Physical Chemistry C,* vol. 113, no. 1, pp. 382-401, 2009, doi: 10.1021/jp802941m.

[64] E. Smela, "Microfabrication of PPy microactuators and other conjugated polymer devices," *Journal of micromechanics and microengineering,* vol. 9, no. 1, p. 1, 1999.

[65] T. F. Otero, "Electroactive macromolecular motors as model materials of ectotherm muscles," *RSC Advances,* vol. 11, no. 35, pp. 21489-21506, 2021, doi: 10.1039/d1ra02573b.

[66] P. Camurlu, "Polypyrrole derivatives for electrochromic applications," *RSC Advances,* vol. 4, no. 99, pp. 55832-55845, 2014, doi: 10.1039/c4ra11827h.

[67] E. P. Knott, M. R. Craig, D. Y. Liu, J. E. Babiarz, A. L. Dyer, and J. R. Reynolds, "A minimally coloured dioxypyrrole polymer as a counter electrode material in polymeric electrochromic window devices," vol. 22, no. 11, p. 4953, 2012, doi: 10.1039/c2jm15057c.

[68] M. A. Invernale, V. Seshadri, D. M. D. Mamangun, Y. Ding, J. Filloramo, and G. A. Sotzing, "Polythieno[3,4-b]thiophene as an optically transparent ion-storage layer," *Chemistry of Materials,* Article vol. 21, no. 14, pp. 3332-3336, 2009, doi: 10.1021/cm900843b.

[69] A. Kumar, D. M. Welsh, M. C. Morvant, F. Piroux, K. A. Abboud, and J. R. Reynolds, "Conducting Poly(3,4-alkylenedioxythiophene) Derivatives as Fast Electrochromics with High-Contrast Ratios," *Chemistry of Materials,* vol. 10, no. 3, pp. 896-902, 1998, doi: 10.1021/cm9706614.

[70] I. Schwendeman *et al.*, "Enhanced Contrast Dual Polymer Electrochromic Devices," *Chemistry of Materials,* vol. 14, no. 7, pp. 3118-3122, 2002, doi: 10.1021/cm020050y.

[71] J. Hwang, D. B. Tanner, I. Schwendeman, and J. R. Reynolds, "Optical properties of nondegenerate ground-state polymers: Three dioxythiophene-based conjugated polymers," *Physical Review B,* vol. 67, no. 11, 2003, doi: 10.1103/physrevb.67.115205.

[72] P. Schottland *et al.*, "Poly(3,4-alkylenedioxypyrrole)s: Highly Stable Electronically Conducting and Electrochromic Polymers," *Macromolecules,* vol. 33, no. 19, pp. 7051-7061, 2000, doi: 10.1021/ma000490f.

[73] X. Li, K. Perera, J. He, A. Gumyusenge, and J. Mei, "Solution-processable electrochromic materials and devices: roadblocks and strategies towards large-scale applications," *Journal of Materials Chemistry C,* vol. 7, no. 41, pp. 12761-12789, 2019, doi: 10.1039/c9tc02861g.

[74] B. Winther-Jensen, J. Chen, K. West, and G. Wallace, "Vapor Phase Polymerization of Pyrrole and Thiophene Using Iron(III) Sulfonates as Oxidizing Agents," *Macromolecules,* vol. 37, no. 16, pp. 5930-5935, 2004, doi: 10.1021/ma049365k.

[75] P. Andersson, R. Forchheimer, P. Tehrani, and M. Berggren, "Printable All-Organic Electrochromic Active-Matrix Displays," *Advanced Functional Materials,* vol. 17, no. 16, pp. 3074-3082, 2007, doi: 10.1002/adfm.200601241.

[76] R. Brooke *et al.*, "Infrared electrochromic conducting polymer devices," *Journal of Materials Chemistry C,* vol. 5, no. 23, pp. 5824-5830, 2017, doi: 10.1039/c7tc00257b.

[77] G. Sabouraud, S. Sadki, and N. Brodie, "The mechanisms of pyrrole electropolymerization," *Chemical Society Reviews,* vol. 29, no. 5, pp. 283-293, 2000, doi: 10.1039/a807124a.

[78] M. Zhou and J. Heinze, "Electropolymerization of Pyrrole and Electrochemical Study of Polypyrrole. 2. Influence of Acidity on the Formation of Polypyrrole and the Multipathway Mechanism," *The Journal of Physical Chemistry B,* vol. 103, no. 40, pp. 8443-8450, 1999, doi: 10.1021/jp990161t.

[79] C. G. Granqvist, "Electrochromic tungsten oxide films: Review of progress 1993–1998," *Solar Energy Materials and Solar Cells,* vol. 60, no. 3, pp. 201-262, 2000, doi: 10.1016/s0927-0248(99)00088-4.

[80] P. Tehrani, A. Kanciurzewska, X. Crispin, N. Robinson, M. Fahlman, and M. Berggren, "The effect of pH on the electrochemical over-oxidation in PEDOT:PSS films," *Solid State Ionics,* vol. 177, no. 39-40, pp. 3521-3527, 2007, doi: 10.1016/j.ssi.2006.10.008.

[81] H. Tang, L. Zhu, Y. Harima, and K. Yamashita, "Chronocoulometric determination of doping levels of polythiophenes: influences of overoxidation and capacitive processes," *Synthetic Metals,* vol. 110, no. 2, pp. 105-113, 2000, doi: 10.1016/s0379-6779(99)00269-6.

[82] X. Wang *et al.*, "Mechanical breathing in organic electrochromics," *Nature Communications,* vol. 11, no. 1, 2020, doi: 10.1038/s41467-019-14047-8.

[83] W. Lu, "Use of Ionic Liquids for pi -Conjugated Polymer Electrochemical Devices," *Science,* vol. 297, no. 5583, pp. 983-987, 2002, doi: 10.1126/science.1072651.

[84] K. Xiong, O. Olsson, J. Svirelis, C. Palasingh, J. Baumberg, and A. Dahlin, "Video Speed Switching of Plasmonic Structural Colors with High Contrast and Superior Lifetime," *Advanced Materials,* p. 2103217, 2021, doi: 10.1002/adma.202103217.

[85] B. Bao *et al.*, "Digital Electrochemistry for On-Chip Heterogeneous Material Integration," *Advanced Materials,* vol. 33, no. 26, p. 2101272, 2021, doi: 10.1002/adma.202101272.

[86] N. Leventis, "Characterization of 3 × 3 Matrix Arrays of Solution-Phase Electrochromic Cells," vol. 145, no. 4, p. L55, 1998, doi: 10.1149/1.1838413.

[87] D. Eric Shen, A. M. Österholm, and J. R. Reynolds, "Out of sight but not out of mind: the role of counter electrodes in polymer-based solid-state electrochromic devices," *Journal of Materials Chemistry C,* vol. 3, no. 37, pp. 9715-9725, 2015, doi: 10.1039/c5tc01964h.

[88] C. Gu, A.-B. Jia, Y.-M. Zhang, and S. X.-A. Zhang, "Emerging Electrochromic Materials and Devices for Future Displays," *Chemical Reviews,* vol. 122, no. 18, pp. 14679-14721, 2022, doi: 10.1021/acs.chemrev.1c01055.

[89] P. Andersson Ersman, J. Kawahara, and M. Berggren, "Printed passive matrix addressed electrochromic displays," *Organic Electronics,* vol. 14, no. 12, pp. 3371-3378, 2013, doi: 10.1016/j.orgel.2013.10.008.

[90] P. Andersson Ersman, K. Freitag, J. Kawahara, and J. Åhlin, "The rise of electrochromics through dynamic QR codes and grayscale images in screen printed passive matrix addressed displays," *Scientific Reports,* vol. 12, no. 1, 2022, doi: 10.1038/s41598-022-14792-9.

[91] G. Beni, "Theory of Electrochemical Memory: Application to Short-Circuit Memory in Electrochromic Displays," *Journal of The Electrochemical Society,* vol. 127, no. 10, pp. 467C-477C, 1980, doi: 10.1149/1.2129401.

[92] G. Beni and L. M. Schiavone, "Matrix-addressable electrochromic display cell," *Applied Physics Letters,* vol. 38, no. 8, pp. 593-595, 1981, doi: 10.1063/1.92466.

[93] A. E. Aliev and H. W. Shin, "Image diffusion and cross-talk in passive matrix electrochromic displays," vol. 23, no. 5, pp. 239-247, 2002, doi: 10.1016/s0141-9382(02)00052-5.

[94] M. O. M. Edwards, "Passive-matrix addressing of viologen–TiO[sub 2] displays," vol. 86, no. 7, p. 073507, 2005, doi: 10.1063/1.1865334.

[95] T. Smith and J. Guild, "The C.I.E. colorimetric standards and their use," *Transactions of the Optical Society,* vol. 33, no. 3, pp. 73-134, 1931, doi: 10.1088/1475-4878/33/3/301.

[96] C. Oleari, *Standard Colorimetry : Definitions, Algorithms and Software*. New York, UNITED KINGDOM: John Wiley & Sons, Incorporated, 2016.

[97] K. Yuan, Yan, Hui-min, Jin, Shang-zhong, "The design of color spectrophotometer based on diffuse illumination and compatible SCE/SCI geometric condition," presented at the Proc. SPIE 9046, 2013 International Conference on Optical Instruments and Technology: Optoelectronic Measurement Technology and Systems, 2013. [Online]. Available: https://dx.doi.org/10.1117/12.2036508.full.

[98] H. Wynberg and D. J. Zwanenburg, "Thieno[3,4-b]thiophene. The third thiophthene," *Tetrahedron Letters,* vol. 8, no. 9, pp. 761-764, 1967, doi: 10.1016/s0040-4039(00)71557-7.

[99] G. Emilsson, R. L. Schoch, P. Oertle, K. Xiong, R. Y. H. Lim, and A. B. Dahlin, "Surface plasmon resonance methodology for monitoring polymerization kinetics and morphology changes of brushes—evaluated with poly(N-isopropylacrylamide)," *Applied Surface Science,* vol. 396, pp. 384-392, 2017/02/28/ 2017, doi: https://doi.org/10.1016/j.apsusc.2016.10.165.

[100] I. Reviakine, D. Johannsmann, and R. P. Richter, "Hearing What You Cannot See and Visualizing What You Hear: Interpreting Quartz Crystal Microbalance Data from Solvated Interfaces," *Analytical Chemistry,* vol. 83, no. 23, pp. 8838-8848, 2011, doi: 10.1021/ac201778h.

[101] G. N. Meloni, "Building a Microcontroller Based Potentiostat: A Inexpensive and Versatile Platform for Teaching Electrochemistry and Instrumentation," *Journal of Chemical Education,* vol. 93, no. 7, pp. 1320-1322, 2016, doi: 10.1021/acs.jchemed.5b00961.

[102] M. Gugole *et al.*, "Comparison of Electrodeposited and Sputtered Tungsten Trioxide Films for Inorganic Electrochromic Nanostructures," *ACS Applied Optical Materials,* vol. 1, no. 2, pp. 558-568, 2023, doi: 10.1021/acsaom.2c00133.

[103] G. A. Sotzing and K. Lee, "Poly(thieno[3,4-b]thiophene): A p- and n-dopable polythiophene exhibiting high optical transparency in the semiconducting state," *Macromolecules,* Article vol. 35, no. 19, pp. 7281-7286, 2002, doi: 10.1021/ma020367j.

[104] E. Smela and N. Gadegaard, "Surprising Volume Change in PPy(DBS): An Atomic Force Microscopy Study," *Advanced Materials,* vol. 11, no. 11, pp. 953-957, 1999, doi: https://doi.org/10.1002/(SICI)1521-4095(199908)11:11<953::AID-ADMA953>3.0.CO;2-H.

[105] J. Kim and Y.-H. Choi, "Differential Angle Scanning Surface Plasmon Resonance Detection," *2018 IEEE SENSORS,* pp. 1-4, 2018.

[106] A. Baba, J. Lübben, K. Tamada, and W. Knoll, "Optical Properties of Ultrathin Poly(3,4-ethylenedioxythiophene) Films at Several Doping Levels Studied by In Situ Electrochemical Surface Plasmon Resonance Spectroscopy," *Langmuir,* vol. 19, no. 21, pp. 9058-9064, 2003, doi: 10.1021/la034848n.

[107] N. Granqvist, H. Liang, T. Laurila, J. Sadowski, M. Yliperttula, and T. Viitala, "Characterizing Ultrathin and Thick Organic Layers by Surface Plasmon Resonance Three-Wavelength and Waveguide Mode Analysis," vol. 29, no. 27, pp. 8561-8571, 2013, doi: 10.1021/la401084w.

[108] C. A. Triana, C. G. Granqvist, and G. A. Niklasson, "Electrochromism and small-polaron hopping in oxygen deficient and lithium intercalated amorphous tungsten oxide films," *Journal of Applied Physics,* vol. 118, no. 2, p. 024901, 2015, doi: 10.1063/1.4926488.

[109] G. Cai *et al.*, "Ultra-large optical modulation of electrochromic porous WO3film and the local monitoring of redox activity," *Chemical Science,* vol. 7, no. 2, pp. 1373-1382, 2016, doi: 10.1039/c5sc03727a.

[110] J. Eaves-Rathert, E. Kovalik, C. F. Ugwu, B. R. Rogers, C. L. Pint, and J. G. Valentine, "Dynamic Color Tuning with Electrochemically Actuated TiO₂ Metasurfaces," *Nano Letters,* vol. 22, no. 4, pp. 1626-1632, 2022, doi: 10.1021/acs.nanolett.1c04613.

[111] J. S. E. M. Svensson and C. G. Granqvist, "No visible electrochromism in high-quality e-beam evaporated In2O3:Sn films," *Applied Optics,* vol. 24, no. 15, pp. 2284-2285, 1985/08/01 1985, doi: 10.1364/AO.24.002284.

[112] S. F. Cogan, E. J. Anderson, T. D. Plante, and R. D. Rauh, "Electrochemical investigation of electrochromism in transparent conductive oxides," *Applied Optics,* vol. 24, no. 15, pp. 2282-2283, 1985/08/01 1985, doi: 10.1364/AO.24.002282.

[113] A. Corradini, A. M. Marinangeli, and M. Mastragostino, "Ito as counter-electrode in a polymer based electrochromic device," *Electrochimica Acta,* vol. 35, no. 11-12, pp. 1757-1760, 1990, doi: 10.1016/0013-4686(90)87076-e.

[114] M. Székely *et al.*, "Electrochemical behavior of tin oxide in the presence of lithium ion in acetonitrile," *Journal of Electroanalytical Chemistry,* vol. 391, no. 1-2, pp. 69-75, 1995, doi: 10.1016/0022-0728(95)03959-k.

[115] M. Székely *et al.*, "Behaviour of a fluorine-doped tin oxide electrode: a study by quartz crystal microbalance in propylene carbonate," *Journal of Electroanalytical Chemistry,* vol. 401, no. 1-2, pp. 89-93, 1996, doi: 10.1016/0022-0728(95)04292-x.

[116] P. M. M. C. Bressers and E. A. Meulenkamp, "The Electrochromic Behavior of Indium Tin Oxide in Propylene Carbonate Solutions," *Journal of The Electrochemical Society,* vol. 145, no. 7, pp. 2225-2231, 1998, doi: 10.1149/1.1838624.

[117] Z. Wang and X. Hu, "Structural and electrochemical characterization of 'open-structured' ITO films," vol. 392, no. 1, pp. 22-28, 2001, doi: 10.1016/s0040-6090(01)01012-4.

[118] S. Macher, M. Rumpel, M. Schott, U. Posset, G. A. Giffin, and P. Löbmann, "Avoiding Voltage-Induced Degradation in PET-ITO-Based Flexible Electrochromic Devices," *ACS Applied Materials & Interfaces,* vol. 12, no. 32, pp. 36695-36705, 2020, doi: 10.1021/acsami.0c07860.

[119] D. Aurbach, M. Daroux, P. Faguy, and E. Yeager, "The electrochemistry of noble metal electrodes in aprotic organic solvents containing lithium salts," *Journal of Electroanalytical Chemistry and Interfacial Electrochemistry,* vol. 297, no. 1, pp. 225-244, 1991, doi: 10.1016/0022-0728(91)85370-5.